Fusion of airborne laser scanning and hyperspectral data for predicting forest characteristics at different spatial scales

Kombinasjon av flybåren laserscanning og hyperspektrale data for prediksjon av skoglige egenskaper på ulik romlig skala

Philosophiae Doctor (PhD) Thesis

Kaja Kandare

Faculty of Environmental Sciences and Natural Resource Management,
Norwegian University of Life Sciences

Ås 2017

Norwegian University
of Life Sciences

Thesis number: 2017:53
ISSN: 1894-6402
ISBN: 978-82-575-1452-5

PhD supervisors

Dr. Hans Ole Ørka
Faculty of Environmental Sciences and Natural Resource Management
Norwegian University of Life Sciences
P.O. Box 5003, NMBU, NO-1432 Ås, Norway

Dr. Michele Dalponte
Department of Sustainable Agro-Ecosystems and Bioresources
Research and Innovation Centre, Fondazione Edmund Mach
Via E. Mach 1, 38010 San Michele all'Adige (TN), Italy

Professor Erik Næsset
Faculty of Environmental Sciences and Natural Resource Management
Norwegian University of Life Sciences
P.O. Box 5003, NMBU, NO-1432 Ås, Norway

Evaluation committee

Dr. Valerie A. Thomas
Department of Forest Resources and Environmental Conservation
Virginia Polytechnic Institute and State University
307A Cheatham Hall, Blacksburg, VA 24061, USA

Dr. Petteri Packalén
School of Forest Sciences
University of Eastern Finland
P.O. Box 111, FI-80101 Joensuu, Finland

Professor Hans Fredrik Hoen
Faculty of Environmental Sciences and Natural Resource Management
P.O. Box 5003, NMBU, NO-1432 Ås, Norway

Preface

This thesis has been submitted to the Faculty of Environmental Sciences and Natural Resource Management, Norwegian University of Life Sciences, as a part of my PhD studies. The approval of this thesis, academic training, trial lecture, and public defense are four main components to obtain the Doctor of Philosophy degree. My doctoral studies were funded with support from Fondazione Edmund Mach.

I would not have succeeded to produce this thesis without strong scientific backing of my main-supervisor Dr. Hans Ole Ørka and co-supervisor Dr. Michele Dalponte throughout my PhD studies. They both helped me to design my PhD project, showed me how to organize the scientific work, and guided me continuously until the objectives were achieved. Thank you for always being around and ready for my thoughts and discussions. I also thank my co-supervisor Prof. Erik Næsset for his good suggestions, ideas, and comments on my work.

My sincere thanks go to Damiano Gianelle, Samantha Riccadonna, Pietro Franceschi and other colleges at the Foundation Edmund Mach, Trento for their scientific support. I am also grateful to all the co-authors of the articles and scientific advice.

I am grateful to all fellow colleagues and friends in Italy and Norway for their advice, discussions, ideas, encouragements, and their company during my PhD. I am especially thankful to my friends Viktor Strimbu and Urska Vrhovsek for their moral support.

I am grateful to my loving mother Franciska Kandare and father Srecko Kandare for their continued support. Most importantly, my heartfelt thanks goes to my partner Miha Ilovar, who always encouraged and waited for me to accomplish the mission.

Kaja Kandare,
May 2017, Trento

Contents

Preface iii

Abstract vii

List of papers ix

Synopsis 1

1 Introduction 3

2 Background 7

2.1 Airborne laser scanning (ALS) data 7

2.2 Airborne hyperspectral data 9

2.3 ITC approach and delineation algorithm 11

2.4 Semi-ITC approach 13

2.5 ABA approach 13

2.6 Fusion of ALS and hyperspectral data 14

2.7 Forest characteristics investigated in this thesis 15

3 Material 15

3.1 Study areas 15

3.1.1 Pellizzano 16

3.1.2 Våler 16

3.2 Field data 18

3.2.1 Pellizzano 18

3.2.2 Våler 18

3.3 ALS and hyperspectral data 19

3.3.1 Pellizzano 19

3.3.2 Våler 19

4 Methods 20

5 Major findings 22

5.1 Quantification of influence of forest structure and ALS point cloud density on established ITC delineation algorithm (Paper I) 22

5.2 Improvement of site index maps using ITC approach together with fused ALS and hyperspectral data (Paper II) 22

5.3 Evaluation of the performance of three remotely sensed-based forest inventory approaches to assess how different spatial details influenced the predictions of species-specific volume using fused ALS and hyperspectral data (Paper III) 23

5.4 Investigate the benefits of ALS and hyperspectral data, separately and fused, to predict forest structural measures (Paper VI) 24

6 Discussion 24

6.1 Fusion of ALS and hyperspectral data (Papers II, III, IV) 24

6.2 Exploring different spatial scales in the prediction of forest characteristics (Papers I, II, III) 27

7 Conclusion and further perspectives 30

References 31

APPENDIX: Papers I - IV

Abstract

Forests can be characterized by many attributes such as mean height, volume, diameter at breast height (DBH), age, tree species distribution, and different indices describing productivity and diversity. All these characteristics can be estimated using a wide range of remote sensing data from aerial photography and airborne laser scanning (ALS) to spaceborne or airborne multispectral or hyperspectral sensors, etc. Remote sensing is a science to obtain information of objects without making any physical contact with it, typically from aircraft or satellites. In particular, this thesis focused on two remotely sensed data sources that at the moment seem to be the most promising for abovementioned purposes: ALS and airborne hyperspectral data. Their combined use or fusion can be beneficial as they provide a complementary information for characterizing forest attributes. ALS and hyperspectral technologies provide very high spatial resolution allowing us to map the forest attributes at a very high spatial detail. This can be useful for certain applications but increasing the spatial detail does not always improve the accuracy of the predictions. Indeed, many predicted forest characteristics can be explored at many spatial scales, e.g. from tree to stand. Thus, the major objective of this thesis was to evaluate the potential of fusing ALS and hyperspectral data for the prediction of forest characteristics and to evaluate the benefits of different spatial details in the prediction of such characteristics. The fusion of ALS and hyperspectral data and the spatial scale exploration were carried out simultaneously in this thesis, and in particular it started with a focus on the spatial scale (development of a new ITC delineation algorithm) and it finished with a focus only on data fusion (prediction of forest structural diversity measures).

The ALS and hyperspectral data were fused at two different levels, product and variable-level fusion. The product-level fusion was used for the prediction of the site index and species-specific volume, while the variable-level fusion was used for total and species-specific volume, as well as structural diversity measures. For the evaluation of different spatial details in the prediction of forest characteristics we considered three remotely sensed-based inventory approaches, namely the individual tree crown (ITC) approach, the semi-ITC approach, and the area-based approach (ABA). In order to apply the ITC and semi-ITC approaches, the individual tree delineation algorithm was needed and developed based on the ALS point cloud. The forest characteristics evaluated in this thesis were: individual tree attributes (such as tree height, DBH, stem volume, age, and species), forest attributes (such as site index, total and species-specific volume), and forest structural diversity measures.

The ITC approach allowed an accurate determination of the height, species, DBH, and stem volume, while the age was subject to a greater error. The ITC approach for site index determination in combination with ALS and hyperspectral data was found to be an efficient and a stable procedure and it reached similar accuracy as in the existing site index maps based on field surveys. For species-specific volume, the ITC approach reached high accuracies but there were also large systematic errors for minority species. For majority species, the semi-ITC approach resulted in slightly higher accuracies and smaller systematic errors compared to ABA. In all three approaches, ALS and hyperspectral data were

important to provide higher accuracies. The fusion of ALS and hyperspectral data for forest structural diversity measures did not improve their accuracy but produced accuracy levels comparable to the models built on ALS data alone, except for one measure. In these experiments, ALS data showed the best predictions for the majority of the structural diversity measures taken into account.

To conclude, the ITC and semi-ITC approaches can provide higher spatial detail of the predicted forest characteristics. This information can also be aggregated to coarser scales, e.g. stands. The use of ITC and semi-ITC approaches has a potential in different forestry and ecology applications, where the accuracy of the semi-ITC also showed the capacity in operational forest applications. The fusion of ALS and hyperspectral data improves the predictions of forest characteristics, such as volumes and site index, while for some forest structural diversity measures the fusion did not improve the accuracy of results. Fusion of such data, especially for structural diversity measures has to be further explored.

List of papers

I. Kandare, K., Ørka, H. O., Chan, J. C. W., & Dalponte, M. (2016). Effects of forest structure and airborne laser scanning point cloud density on 3D delineation of individual tree crowns. *European Journal of Remote Sensing*, 49, 337–359. http://doi.org/10.5721/EuJRS20164919

II. Kandare, K., Ørka, H. O., Dalponte, M., Næsset, E., & Gobakken, T. (2017). Individual tree crown approach for predicting site index in boreal forests using airborne laser scanning and hyperspectral data. *International Journal of Applied Earth Observation and Geoinformation*, 60, 72–82. http://doi.org/10.1016/j.jag.2017.04.008

III. Kandare, K., Dalponte, M., Ørka, H., Frizzera, L., & Næsset, E. (2017). Prediction of species-specific volume using different inventory approaches by fusing airborne laser scanning and hyperspectral data. *Remote Sensing*, 9(5). http://doi.org/10.3390/rs9050400

IV. Kandare, K., Riccadonna, S., Franceschi, P., Ørka, H. O., Dalponte, M., (manuscript). Fusion of airborne laser scanning and hyperspectral data for assessing forest structural diversity indices

Synopsis

1 Introduction

Forest structure can be characterized by many biophysical attributes such as canopy cover, stem density, basal area, mean height, volume, diameter at breast height (DBH), age, biomass, and tree species distribution (Dalponte et al., 2014; Hakkenberg et al., 2016; Hernández-Stefanoni et al., 2014; Listopad et al., 2015; M Maltamo et al., 2009). Additionally, such forest characteristics are a key element for retrieving information on site productivity, forest structural diversity, richness of wildlife communities, wildfire behavior, etc. (Guo et al., 2017; Hill and Hinsley, 2015; Kandare et al., 2017b; McElhinny et al., 2005; Riaño, 2003). Thus, accurate and reliable measurements of forest characteristics are important for sustainable forest management to enable forest managers, silviculturists, and ecologists to make sound decisions in a variety of applications.

Silvicultural practices and natural events such as landslides, wildfires, drought, and insect outbreaks alter stand composition and structure. Therefore, frequent updates of forest attributes are requested. Nowadays, remote sensing data are commonly used to describe, predict, and assess forests attributes and they can provide important knowledge to support national forest inventories (McRoberts and Tomppo, 2007) and for conservation monitoring (Nagendra et al., 2013). Furthermore, the remote sensing technologies, such as aerial photography, spaceborne or airborne laser scanning, spaceborne or airborne multispectral and hyperspectral images, and synthetic aperture radar (SAR), enable observation of forest areas at different temporal and geographical scales (Eitel et al., 2016; Fassnacht et al., 2016; Latifi et al., 2015; White et al., 2016; Yu et al., 2015). Among all the available remote sensing data, this thesis focuses on airborne laser scanning (ALS) and airborne hyperspectral data. Airborne sensors were shown to be effective in covering large areas with high detail. Among the mentioned sensors, ALS and airborne hyperspectral data are at the moment the most interesting sources for characterizing forests. In particular, ALS is a key source providing a three-dimensional (3D) point cloud, which appears as dense xyz coordinates (Figure 1). ALS data have shown to produce accurate estimates compared to other remote sensing techniques for forest biophysical attributes (e.g. volume, height, DBH, crown area, and stem density) (Hollaus et al., 2006; Holmgren, 2004; Kankare et al., 2013; Næsset, 2002; Næsset and Økland, 2002; Wing et al., 2012; Yu et al., 2015). For identifying tree species, airborne hyperspectral images (Figure 2) are a very promising data source due to their ability to detect subtle variations in the chemical and structural properties of the tree canopy. In such images, radiance data are available for many narrow contiguous bands (>50), from the visible to the near-infrared part of the spectrum. Due to its high spectral resolution, hyperspectral imagery was found to be superior for the classification of tree species compared to multispectral imagery

(Dalponte et al., 2012; Ørka et al., 2013). Currently, the fusion of ALS and hyperspectral data sources is the most promising approach to improve the accuracy of models predicting species-specific biophysical attributes and various forest characteristics, i.e. forest structural diversity (Ørka et al., 2013; Torabzadeh et al., 2014).

In forestry and ecology studies, sample plots are generally established in order to relate field and remote sensing data. Field data collection is carried using sample plots distributed over an area of interest, and can follow different strategies (e.g. stratified sampling, random sampling, etc.). After co-registering sample plots and remote sensing data, several metrics or variables can be extracted from ALS and hyperspectral data for each sample plot. Subsequently, these variables are used to construct statistical relationships with field-observed forest attributes. The relationships, typically in the form of regression models, are then used to predict forest attributes for a grid-cell size of the same size as the sample plots. Such approach refers to the area-based approach (ABA) (Næsset, 2002).

To increase the spatial detail, individual trees can be detected within a sample plot and forest characteristics can be provided for each tree. Such approach is called the individual tree crown (ITC) approach and it was introduced by Hyyppä and Inkinen (1999). Based on an ALS point cloud or a spectral image, crown segments, often referred to as ITCs, are detected and delineated applying a segmentation algorithm (Eysn et al., 2015; Ke and Quackenbush, 2011; Wang et al., 2016). Each crown segment is matched with one field-observed tree as the ITC approach presumes that one crown segment contains exclusively one field-observed tree. For each crown segment, various ALS- and spectral-derived variables are extracted, such as ALS maximum height, crown area, spectral mean band values and spectral indices. Based on these variables, the biophysical attributes, such as species, volume, age, and DBH can be predicted for each crown segment, and can be aggregated to any grid-cell size or other scales, e.g. to a forest stand. The detection accuracy of the ITC approach is usually measured with omission error (failure to detect a tree or segmenting multiple trees into a single crown segment) and commission error (detecting an object that is not a tree or splitting a single tree into multiple crown segments). Omission error usually leads to underprediction of the forest attributes. This is a common problem as delineation algorithms tend to not detect all the trees within an area of interest. To reduce these errors, the semi-ITC approach has been proposed (Breidenbach et al., 2010), which is equivalent to the ITC approach -regarding the delineation algorithm and remote sensing variables extraction- but it has a different matching procedure. In contrast to the ITC approach, the semi-ITC approach allows a crown segment to contain, beside none and one, also multiple field-observed trees. Forest characteristics for each crown segment are obtained by relating field measurements of trees and remote sensing variables of crown segments to develop prediction models. The work presented in this thesis combines ALS and hyperspectral data by

adopting the three aforementioned inventory approaches (ABA, ITC, and semi-ITC) for the prediction of various forest characteristics.

State of the art remote sensing data acquired from airborne platforms are characterized by a high spatial resolution (<1 m), which can improve the spatial scale of forest characteristics' predictions on maps (with the spatial scale of interest either being an individual tree, a stand, or a region). If the spatial detail of forest characteristics estimations improve different communities, ecologists, forest managers, and forest users are able to use this enhanced information in their activities related to natural resource policy and planning, forest management and conservation, biodiversity, and ecology.

Several forest characteristics (tree heights, tree positions, tree species, DBH, stem volume, site index, and forest structural diversity measures) should be investigated, and innovative inventory approaches should be explored to evaluate whether the increase of spatial detail is possible. In particular, the development of an ITC delineation method would allow to obtain refined maps at a smaller grid size, if the ITC and semi-ITC approaches are able to provide accurate predictions of forest characteristics. Moreover, the comparison among the ITC, semi-ITC, and ABA approaches at the grid-cell level should be further investigated to evaluate the accuracy of forest characteristics obtained with each approach. In many studies, forest characteristics are generally predicted with only one type of remotely sensed data. Thus, the synergy among different data sources appears to be a key step to achieve greater accuracy in the prediction of forest characteristics. In particular, ALS and hyperspectral data provide complementary and independent information: one related to the forest 3D structure and one to the spectral characteristics of the forest. In this context, the efficiency of such data synergy needs to be further investigated.

The major objectives of this thesis were to evaluate the potential of fusing ALS and airborne hyperspectral data (Papers II, III, IV) for the prediction of forest attributes and to explore different spatial levels in the prediction of biophysical attributes (Papers I, II, III). The specific objectives were: 1) to establish a 3D ITC delineation method and to quantify the influence of forest structure and airborne laser scanning point cloud density on the ITC delineation algorithm (Paper I), 2) to improve the existing site index maps by applying the developed ITC delineation method together with fused ALS and hyperspectral data (Paper II), 3) to predict species-specific volume using fused ALS and hyperspectral data in order to analyze the performance of three remotely sensed-based forest inventory approaches to assess how different spatial details influenced the results (Paper III), 4) to predict forest structural diversity with ALS and hyperspectral data, separately and fused, in order to investigate the benefits of each data source (Paper IV). The illustration of relationship between papers, and major and specific objectives is summarized in Figure 3.

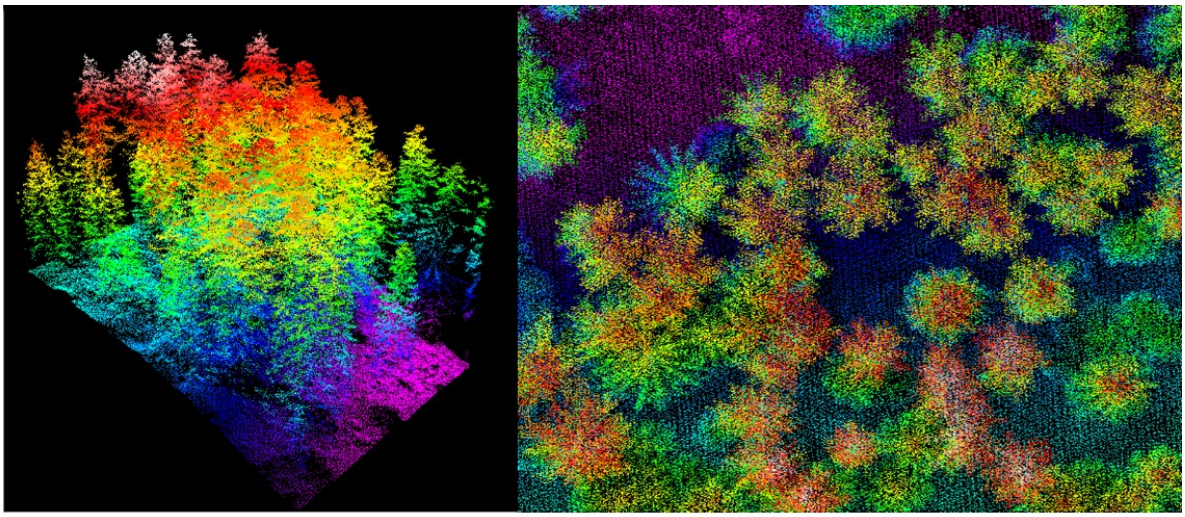

Figure 1: Example of ALS point cloud in forest area.

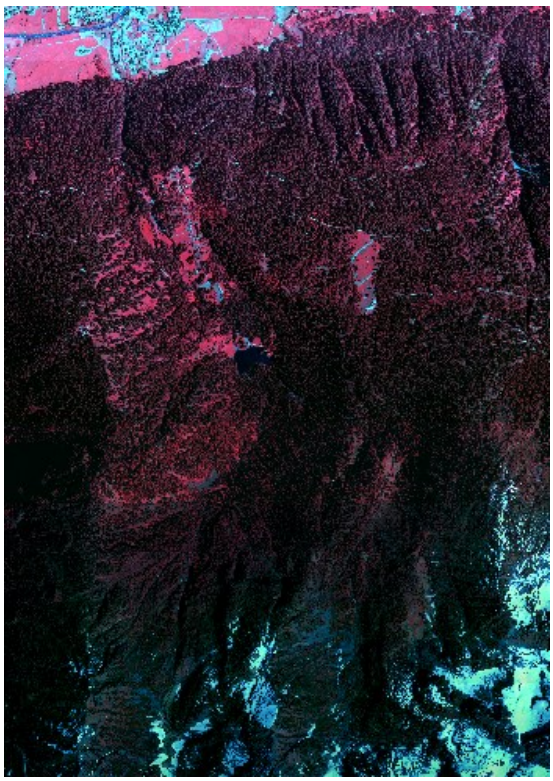

Figure 2: Example of hyperspectral image over forest area.

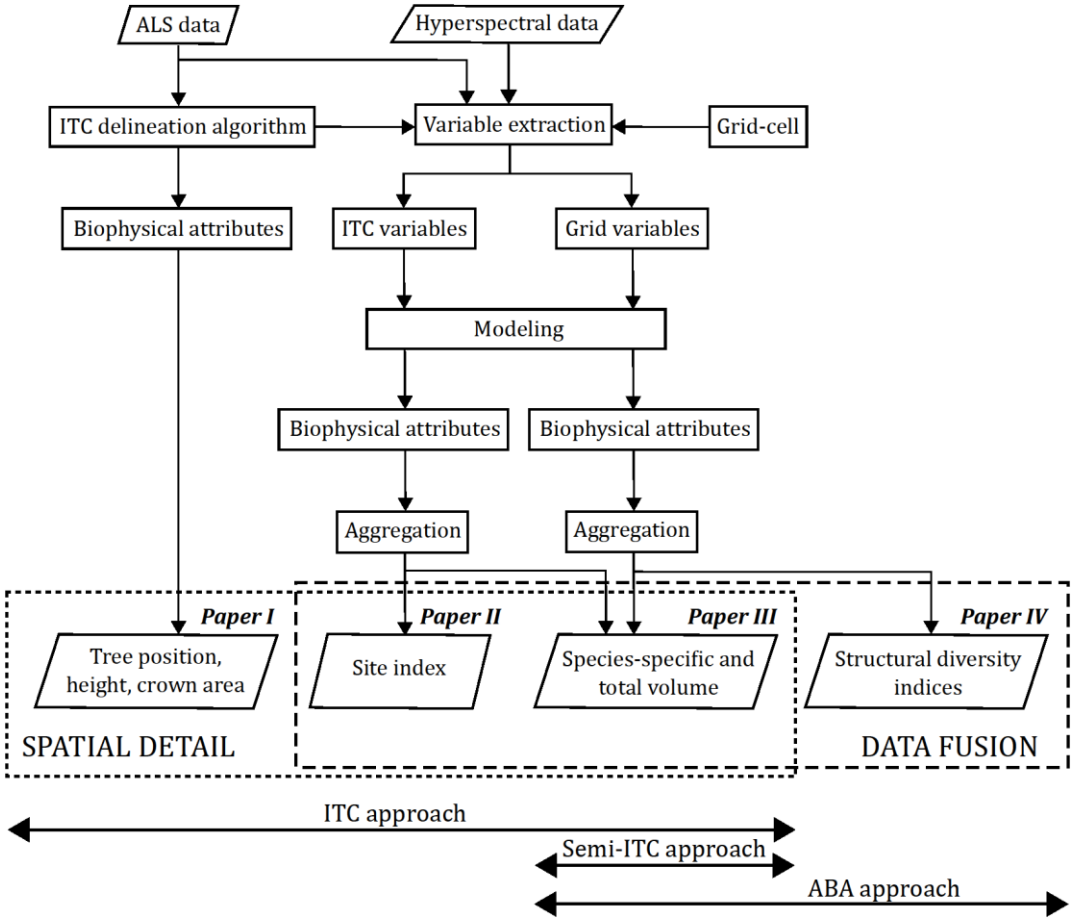

Figure 3: Flowchart explaining the connection between papers and objectives united in the current thesis.

2 Background

2.1 Airborne laser scanning (ALS) data

ALS is a method of adopting active laser sensor mounted on aircrafts which use the light detection and ranging (LiDAR) technology. LiDAR systems used in forestry mostly operate in the near-infrared region (e.g. 1064 nm), although some sensors also operate in the shortwave-infrared or green bands (e.g. Optech Titan sensor), for example to penetrate water and detect bottom features. LiDAR technology consists of an emitter and a receiver. The sensor emits many thousands of individual pulses of, i.e. near-infrared, light per second (Baltsavias, 1999). Each pulse penetrates partly into and possibly through the vegetation cover, and when the pulse reaches a target surface (e.g. branch, leave or ground), part of its energy is reflected back to the receiver. Most of the LiDAR devices used for ALS are time-of-flight LiDARs, and they measure the elapsed time between the emission of a pulse and the arrival of the reflection of that pulse at the sensor's receiver. Knowing the speed of the light and time of the pulse travel, the range is computed (Wehr and Lohr, 1999). From the range, the angle at which the pulse was "fired" (i.e. scan angle), and the absolute location of the LiDAR device the three dimensional (3D)

coordinates (x, y, z) of the target object are computed. The position and orientation of the LiDAR device is continuously recorded along the flight path with a global positioning system (GPS) and an inertial measurement unit (IMU), which allow direct georeferencing. As the LiDAR device can measure for example 300,000 pulses per second, the resulting product is a densely-spaced cloud of highly accurate georeferenced elevation points often called ALS point cloud (Figure 1). In addition to the coordinates, information on the intensity of the backscattered pulse is usually recorded with the LiDAR system.

Each LiDAR system can have different specifications and settings related to the wavelength, power, pulse duration and repetition rate, beam size and divergence angle, the specifics of the scanning mechanism, and the information recorded for each pulse (Wehr and Lohr, 1999). Each emitted pulse can record the range and intensity of various objects along the pulse path and within the area illuminated by the light - footprint. According to the type of information recorded by the LiDAR system, two categories of sensors are distinguished, discrete return and full-waveform. The first can record up to five echoes, i.e. returns per pulse, which represent discrete objects in the path of the laser backscatter. The latter records the time-varying intensity of the returned pulse energy and captures the entire pulse trace. Both sensor types can operate with small (<1 m) or large (>10 m) footprint size. For example, forest inventory sample plot or a single tree can be characterized by a small footprint size, since such size of footprint allows high spatial resolution and can resolve the canopy structure up to a single tree. The vertical and horizontal accuracy can vary between 5-30 cm and 20-80 cm, respectively (Hohenthal et al., 2011). Data derived from a large footprint size are generally at a coarser resolution and can be used to characterize canopy structure of larger areas. The vertical and horizontal accuracy vary between 18-35 cm and 100-250 cm, respectively (Hohenthal et al., 2011).

The ALS technology is widely used in the surveying community to collect high precision 3D survey data. As LiDAR sensors provide a 3D representation of forest structure, it is possible to accurately assess forest biophysical attributes, such as height, basal area, volume, biomass, and canopy structure (Ferraz et al., 2016; Holmgren, 2004; Lee and Lucas, 2007; Lefsky et al., 1999; Næsset and Økland, 2002; Ozdemir and Donoghue, 2013; Varvia et al., 2016), and to provide high-resolution topographic maps (Jung et al., 2013; Tonolli et al., 2010; Valbuena et al., 2013). In addition, ALS data are used to estimate yields (Dash et al., 2015) and carbon stocks (Li et al., 2014; Stephens et al., 2012) of forest stands to ensure a sustainable supply of timber products, and to formulate silvicultural strategies (Coops, 2015; Pedersen et al., 2012). Moreover, ALS-based geometric reconstruction of forest stands also enables to manage wildland fire (Morsdorf et al., 2004), to monitor urban trees (Holopainen et al., 2013) and habitats (Hill and Hinsley, 2015), and to assess the assemblages of beetles (Müller and Brandl, 2009).

2.2 Airborne hyperspectral data

Hyperspectral remote sensing combines imaging and spectroscopy into a single system, also called imaging spectroscopy. Hyperspectral sensors are passive systems that collect and record through a detector the electromagnetic energy that is reflected or emitted by the surface of the objects. Hyperspectral imagery is created using an electro-optical sensor, which defines the range of angles through which incident light travel termed as "field of view". All objects within the field of view are imaged with the detector that records the spatial data and spectra of an object (i.e. radiance). The radiance is the amount of light the instrument detects and that is emitted by the object being observed.

Airborne hyperspectral sensors can be classified into four groups: whiskbroom (point scan), pushbroom (line scan), tunable filter (wavelength scan), and snapshot, and the first two are the most commonly used in remote sensing applications. Whiskbroom hyperspectral imagers are based on a single hyperspectral detector that collects the spectral signature of a single pixel at a time. The detector moves along a scanning line that is perpendicular to the flight line. The opposite is true for the pushbroom technology, also known as line scanning, where a series of many detectors, aligned perpendicularly to the flight line, scans the ground along a line parallel to the flight line. On the platforms, the IMU and GPS systems are used to correct the geometry of the data and relate each pixel in the output imagery to a location on the ground. Hyperspectral data used in this thesis were based on airborne platforms and the pushbroom spectral scanning concept.

Each hyperspectral image consists of pixels, with spatial information collected in the xy-plane, and a spectral information represented in the z-direction. The image spatial resolution is defined by the pixel size, and it could be smaller than 1 m when mounted on airborne platforms. For all the objects captured in the image, the spectral signatures are measured in a large number of narrow spectral bands from the visible to the shortwave infrared part of the spectrum. The number of bands can vary from several tens to hundreds of bands, with narrow bandwidth, usually between 5 to10 nm. The band width may be larger in the near infrared or shortwave infrared wavelength range. The greater is the number of bands, the higher is the level of spectral detail in the hyperspectral images, which gives better capability to see the unseen. Thus, each pixel contains a unique spectral signature, which can be used by the processing techniques to identify and characterize particular objects or materials within a scene. Different objects, for example different tree species, have different spectral signatures (Figure 4). The spectrum is a plot of wavelength versus radiance or reflectance. For example, the spectral signature of trees in the near infrared bands can be different due to species type, plant stress, and canopy state.

When the radiance is processed in order to compensate for the atmospheric effects and the solar illumination, reflectance can be obtained (Schaepman-Strub et al., 2006). In this context, the quality of the atmospheric correction algorithms directly impacts further data post-processing and exploitation. However, it was demonstrated that for certain applications the atmospheric correction process is not necessary and is not strictly required (Schaepman-Strub et al., 2006). Due to illumination effects, the time of acquisition is very important, and the ideal time interval is between 10:00 a.m. and 2:00 p.m. as this provides better illumination and a favorable angle of incidence, or sun angle (Borengaser et al., 2008).

The major advantage of the hyperspectral sensors is that their narrow bandwidths allow a high spectral resolution, which provides more detailed information on the spectral characteristics of the target respect to the wide bands used by the multispectral sensors (Dalponte et al., 2013). Additionally, hyperspectral data have been found to be more efficient in tree species classification than multispectral data (Dalponte et al., 2012; Ørka et al., 2013). The main disadvantages of hyperspectral data are that the processing of the information is more difficult and that the acquisition constraints are higher than with the multispectral data.

Many studies found that hyperspectral data are useful to provide information on vegetation types, tree and canopy phenology, physiology, foliar biochemistry content of forest canopies, and spectral signatures for selected tree species (Asner, 2008; Asner et al., 2017; Kokaly et al., 2009; Ustin et al., 2004).

In the forestry and ecology domains, hyperspectral data are powerful in tree species classification and plat traits prediction, which is needed by a wide variety of applications. These applications include forest inventories (van Aardt and Wynne, 2007), biodiversity and wildlife-habitat assessment and monitoring (Clawges et al., 2008; Shang and Chisholm, 2014), hazard and stress management (Fassnacht et al., 2014, 2012), monitoring of invasive species (Boschetti et al., 2007), wildlife habitat mapping (Santos et al., 2010), disturbances in the vitality of forests (Lausch et al., 2016, 2013), changes of plant communities and ecosystems (Asner et al., 2015), floodplain vegetation prediction (Geerling et al., 2007), and forest trait diversity mapping (Asner et al., 2017). Tree species information is as well as important to predict species-specific forest biophysical attributes (Kandare et al., 2017b; Ørka et al., 2013).

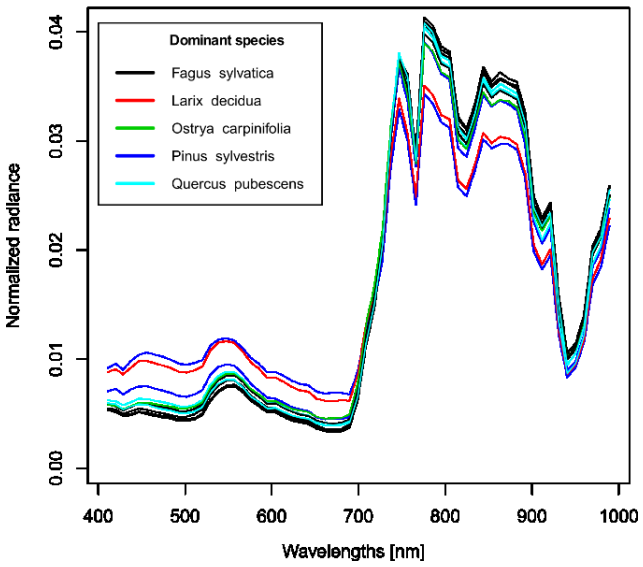

Figure 4: Example of spectral signatures of different tree species.

2.3 ITC approach and delineation algorithm

Individual trees are the smallest unit on which the forest management is carried out within the tree level forest inventory (Maltamo et al., 2014). The idea is to base the inventory on the characterization of individual trees in the area of interest. The first step of the tree level inventories is to detect and delineate individual tree crowns, also referred to as crown segments. For the delineation of tree crowns, ALS data were found superior to passive optical data as they are less affected by occlusions and shading (Voss and Sugumaran, 2008), and it is also possible to reach higher delineation and detection quality with ALS data (Dalponte et al., 2015b, 2014). For each delineated crown segment, the biophysical attributes, such as tree height, crown area, DBH, stem volume, and age, can be extracted or modelled (Ferraz et al., 2016; Kandare et al., 2016). When crown segments are co-registered with the hyperspectral data, hyperspectral variables can also be obtained as the aggregation of the digital value of the pixels within each crown segment as first order statistics (e.g. mean, variance, skewness, and kurtosis)(Kandare et al., 2017a). Moreover, forest attributes can be modelled by relating field observations with ALS and/or hyperspectral variables calculated for each crown segment. The most common point-based ALS variables computed for each crown segment based on height are: percentiles, mean, maximum, minimum, coefficient of variation, standard deviation, variance, skewness, and kurtosis (Breidenbach et al., 2010; Næsset and Økland, 2002; Ørka et al., 2013; Yu et al., 2010). In addition, crown projection area and crown density metrics computed as cumulative proportional densities for different height thresholds (Næsset and Økland, 2002; Yu et al., 2011). All these ALS variables can be calculated for the first, intermediates, and/or last returned LiDAR pulses. Some forest characteristics can be obtained without modelling. For instance, tree height and crown area can

be directly extracted from each crown segment by maximum ALS point (z) and the projection of x and y coordinates of ALS points on horizontal plane, respectively (Kaartinen and Hyyppä, 2008; Morsdorf et al., 2004; Næsset and Økland, 2002; Yu et al., 2011, 2010). The obtained biophysical attributes of each crown segment can be further aggregated to any grid-cell size.

One of the first delineation algorithm was proposed by Hyyppä and Inkinen (1999). In the last two decades, numerous delineation algorithms were developed (Duncanson et al., 2014; Ene et al., 2012; Kandare et al., 2016; Persson et al., 2002; Reitberger et al., 2009; Solberg et al., 2006; Strîmbu and Strîmbu, 2015). Some of them are based on 2D canopy height model, 3D ALS points, or the combination of both. The evolution of such a great number of delineation algorithms emerged as there is no such method that would be applicable in different forest types (e.g. boreal, tropical, temperate deciduous forests) and conditions (e.g. structure, productive capacity, cover) governed by a variety of different management regimes (Kaartinen et al., 2012; Wang et al., 2016). Moreover, the performance of the delineation algorithm is quantitatively validated by different detection accuracy measures: omission error, commission error, detection rate, and accuracy index. The omission error is accounting for the number of field-observed trees that were not detected by the delineation algorithm (Equation 1). This kind of error occurs especially in dense forests, when trees grow close to each other and are consequently segmented as one crown segment. When a delineation algorithm detects a crown segment that is not matched with any field-observed trees, it leads to the omission error (Equation 2). This usually happens when tree crowns are big and the algorithm split one tree into two or more crown segments. The detection rate indicates the rate of correctly delineated field-observed trees (Equation 3). The accuracy index considers both omission and commission errors into a single metric (Equation 4).

$$Omission\ error = \frac{N_{ITC} - C_M}{N_F} 100\% \qquad \textit{Equation 1}$$

$$Commission\ error = \frac{C_{NM}}{N_{ITC}} 100\% \qquad \textit{Equation 2}$$

$$Detection\ rate = \frac{C_M}{N_F} 100\% \qquad \textit{Equation 3}$$

$$Accuracy\ indec = 100\% - (Omission\ error + Commission\ error) \qquad \textit{Equation 4}$$

In Equations 1-4, N_{ITC} is the number of delineated crown segments, N_F the actual number of field-observed trees, C_M is the number of correctly matched, and C_{NM} is the number of crown segments without a match with a field tree. To obtain C_M and C_{NM} values, a matching procedure is conducted, following various thresholds for permitted horizontal and/or vertical distance between field-observed trees and crown segments (Eysn et al., 2015; Wang et al., 2016).

2.4 Semi-ITC approach

The semi-ITC approach is equivalent to the ITC approach regarding the ITC delineation algorithm and the computation of the ALS and hyperspectral variables. They are distinguished by the matching procedure (Kandare et al., 2017a). In the common matching procedure of the ITC approach, the rule is that only one field tree can be matched with one crown segment, if not a field tree remains unmatched. Differently, in the semi-ITC approach more than one field tree can be matched with one crown segment (Breidenbach et al., 2010). Furthermore, all field trees must be matched with the closest crown segment. With such matching procedure, the omission and commission errors are substantially reduced in the following prediction models (Breidenbach et al., 2010; Kandare et al., 2017a). Subsequently, field measurements of biophysical attributes from accurately georeferenced sample plots are related to the remote sensing variables of crown segments taken from exactly the same area, and prediction models are developed. The predicted values of forest attributes are provided for trees within a sample plot area. Moreover, the prediction models can be exploited to predict the forest attributes of interest at any grid-cell size by aggregation of predicted attributes. According to the literature, the semi-ITC method has never been used in an application context and only a few studies exist (Breidenbach et al., 2010; Kandare et al., 2017a; Ørka et al., 2013; Rahlf et al., 2015).

2.5 ABA approach

In the majority of the forest management purposes assisted by ALS data, the area based approach (ABA) is used (Næsset et al., 2004). This approach was introduced by Næsset (2002). In the ABA, forest attributes are predicted for each element (e.g. grid cell) of a population with the size of each element being equal to the area of the sample plots. For each sample plot several remote sensing variables are extracted, for which predictive relationships with field-observed forest attributes are constructed. Furthermore, the prediction models can be utilized to predict the forest attributes of interest where the smallest grid-cell size is equal to the size of the sample plots. Typical ALS variables used in this approach are the height metrics (percentiles, mean, maximum, minimum, coefficient of variation, standard deviation, variance, skewness, and kurtosis) and the canopy density metrics (Næsset, 2004; Packalén et al., 2012). The canopy density variables can be calculated as the proportions of laser echoes above each defined height threshold in relation to the total number of echoes. All these variables can be computed for all echoes' categories. The hyperspectral variables can be computed as the average value of first order statistics for pixels within a grid-cell or sample plot (Kandare et al., 2017a). Additionally, variables can be computed from vegetation indices (Luo et al., 2017) or grey level co-occurrence matrices (e.g. contrast, energy, and correlation) (Meng et al., 2016; Packalén et al., 2012).

Currently, the ABA is the most used approach for operational forest inventories due to less demanding collection of the field data, and it can work quite well also at very low ALS point density (e.g. < 3 pulses m^{-2}).

2.6 Fusion of ALS and hyperspectral data

In order to fulfil the requirements for a comprehensive forest ecosystem characterization some complex forest characteristics cannot be accurately determined by one remote sensing system alone (Zhang, 2010). In such cases, the fusion of the complementary remote sensing data could offer a good solution to retrieve robust assessments. Due to accurate 3D measurements of forest structure and spectral measurements, specifically rich on information for biophysical and chemical canopy properties, obtained by ALS and airborne hyperspectral data, respectively, the fusion of both data systems has become very promising for evaluating forest characteristics (Fassnacht et al., 2016; Luo et al., 2017). Although, such fusion can be complicated due to the differences in the measured physical quantities (elevation vs radiance), geometry of data acquisition (3D points vs 2D image) and sources of illumination (laser vs solar radiation). Data fusion, sometimes also called data combination or integration, can be employed by 1) empirical or statistical, 2) physical, or 3) hybrid approaches (Torabzadeh et al., 2014). The most straightforward is the statistical approach, which will be the main focus in the current thesis, based on predictive models e.g. generalized linear models, ordinary least squares, k-nearest neighbor algorithm, support vector machines, etc.

One of the first attempts exploring the fusion of ALS and hyperspectral data in forestry domain was carried out in 2004 (Gillespie et al., 2004), followed by other studies assessing and producing landcover maps (Asner et al., 2008; Dalponte et al., 2012; Hill and Thomson, 2005; Koetz et al., 2008), above ground biomass (Anderson et al., 2008; Clark et al., 2011; Dalponte et al., 2015b; Luo et al., 2017; Swatantran et al., 2011; Vaglio Laurin et al., 2014), volume (Kandare et al., 2017a), species composition (Dalponte et al., 2008; Jones et al., 2010; Koetz et al., 2008; Richter et al., 2016), etc. mostly in tropical and temperate forests. These studies were carried out mostly in tropical and temperate forests, and there is a need to test data fusion over a wider range of forest cover and types. Among this studies, only a few were conducted on temperate forests in the Alps and boreal forest types (Dalponte et al., 2014, 2012; Ørka et al., 2013).

The statistical data fusion approaches used in this thesis could be categorized into 1) product-level, where separate processing chains for ALS and hyperspectral data are conducted to compute biophysical attributes, i.e. tree species with hyperspectral and volume by ALS, and then the attributes are fused to provide species-specific volume; and 2) variable-level, where both ALS and hyperspectral variables are combined into empirical models to predict biophysical attributes, i.e. species-specific volume. The product-level fusion is more common for the ITC approach and

the variable-level fusion for semi-ITC and ABA approaches. ITC and semi-ITC approaches allow to obtain accurate biophysical attributes at tree level thanks to the delineation algorithm. When ALS and hyperspectral data are co-registered, both ALS and spectral variables are computed for each crown segment. For the ITC approach, spectral information per crown enables to preform tree species classification resulting in high accuracies (Dalponte et al., 2013, 2008). Fusing species information with ALS-derived forest attributes per each crown segment, results can be obtained in species-specific forest attributes such as volume, basal area, and stem density, which are valuable information for forest managers. With the semi-ITC approach, the classification of tree species per crown is not possible because crown segments can contain one or more tree species. Thus with semi-ITC and ABA approaches only species proportions within a segment/grid can be predicted.

2.7 Forest characteristics investigated in this thesis

Based on biophysical attributes, such as tree age, species, position, DBH, and height, many forest characteristics, such as site index or structural diversity measured can be obtained. Site index is a very common quantitative measure and widely accepted method of forest site productivity defined as expected height of the trees at a given base age (e.g. 70 years) for certain tree species in area of interest (Skovsgaard and Vanclay, 2008). In order to ensure a sustainable supply of timber products and to formulate silvicultural strategies the reliable site index estimates are important. Forest structural diversity can be described by variability in spatial arrangement of trees, tree dimensions, and mingling of different tree species (Aguirre et al., 2003; McElhinny et al., 2005; Pommerening, 2002). These characteristics, called structural diversity measures, can be quantified through, e.g. diameter differentiation index, Gini coefficient of basal area, uniform angle index, mean nearest neighbors, Shannon's index, species mingling index, etc. (Meng et al., 2016; Neumann and Starlinger, 2001; Pommerening, 2006). Structural diversity measures are crucial in order to gain a better understanding of forest ecosystems as they express the sustainability of management practices for economic as well as environmental purposes. Moreover, information of structural diversity is also important to describe forest health, to model animal and forest plant species behavior, and to predict forest fire behaviors (Lausch et al., 2016; Martinuzzi et al., 2009; Morsdorf et al., 2004).

3 Material

3.1 Study areas

In the current thesis, two study areas were used: 1) a temperate forest in the municipality of Pellizzano in the Italian Alps (46°17′22′′N, 10°46′05′′E, 900–2220 m above sea level) (Figure 5);

and 2) a boreal forest in the Våler municipality in south-eastern Norway (59°30′N 10°55′E, 70–120 m above sea level) (Figure 6).

3.1.1 Pellizzano

The Pellizzano study area extends on 3200 ha. The forest is dominated by Norway spruce (*Picea abies* (L.) Karst.), with the presence of other coniferous species (e.g., larch (*Larix decidua* Mill.), silver fir (*Abies alba* Mill.)) and broadleaves species (e.g., rowan (*Sorbus aucuparia* L.), common hazel (*Corylus avellana* L.), silver birch (*Betula pendula* Roth), and sycamore maple (*Acer pseudoplatanus* L.)). At higher altitudes, the forest is sparse, whereas at lower altitudes, the forest structure is more complex, varying from a one-to multi-layer forest with patches of mixed and homogeneous tree species composition. The area has been managed since 1950 with silvicultural plans implemented every 10 years. Selective logging is done with the help of cableway focusing on the productive forest area, especially Norway spruce, and trees are harvested according to their stem diameter.

3.1.2 Våler

The Våler study area cover 853 ha. The dominant species are Norway spruce (*Picea abies* (L.) Karst.) and Scots pine (*Pinus sylvestris* L.). Younger stands have large proportions of deciduous species dominated by birch trees (*Betula pubescens* Ehrh.). The active forest management in the forest area is directed towards the timber production with clear-cuts and shelterwood cutting applied at the end of the rotation depending on the site fertility. For the former harvest method, the regeneration is achieved by plantation, and for the latter by natural regeneration after selective logging.

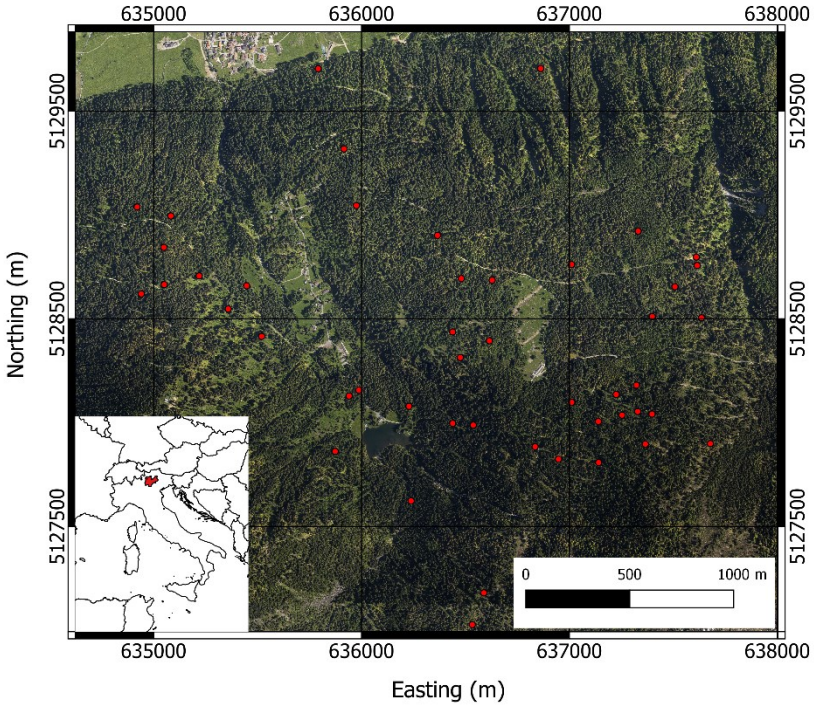

Figure 5: Map of the Pellizzano study area. The red dots are indicating the field plots.

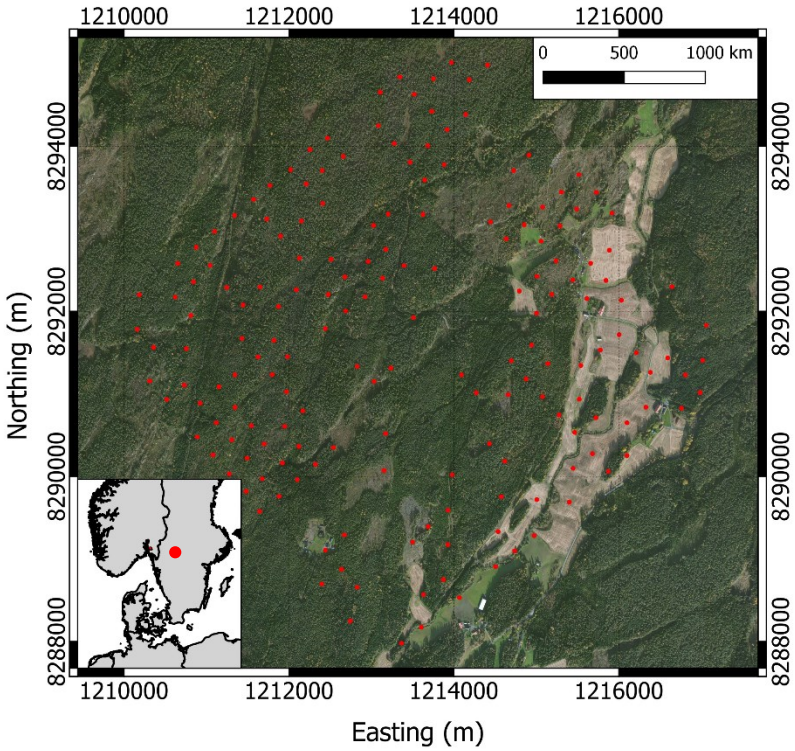

Figure 6: Map of the Våler study area. The red dots are indicating the field plots.

3.2 Field data

3.2.1 Pellizzano

During the summers of 2013 and 2015, 47 circular sample plots were surveyed. The size of the sample plots was 700 m^2. The center location of each plot was determined with a GPS and global navigation satellite system (GLONASS) measurements, resulting in a positional error of less than 1 m. For all trees within the sample plot, the location was recorded as a polar coordinates to the center of the plot (azimuth and range). In addition, DBH along two orthogonal directions and tree species were recorded. Tree height on two-thirds of randomly selected trees was measured using a Vertex III hypsometer. Tree heights of the remaining trees were predicted with allometric equations (Scrinzi et al., 2010). Dead or damaged trees were excluded. The tree species observed for the 1888 trees were: 72.9% Norway spruce, 7.9% rowan, 7.1% larch, 1.7% silver birch, 1.3% silver fir, 1.3% common hazel, 1.2% sycamore maple, and the rest were other minority broadleaves.

3.2.2 Våler

In 2010, 153 systematically distributed circular sample plots were inventoried. The size of each plot was 400 m^2. For all trees inside the plots with DBH above 4 cm the tree position, tree species, and DBH were recorded. Tree height was measured only on selected sample trees, approximately for 10 trees per plot. The polar tree coordinates were established by using measurements of distance and angle from the plot center. These measurements were carried out with a tape measure and a compass with a sight. The plot center was measured using differential GPS and GLONASS receiver. Out of 9414 recorded trees, 52% were spruce, 25% were pine, and 23% were broadleaves.

In July 2013, 96 of the forest inventory plots dominated either by spruce or pine were revisited to measure data for site index determination. Out of 384 recorded trees, 58% were spruce and 42% were pine trees. In each plot, the four largest trees according to DBH of the dominant species were selected as sample trees, which corresponds as closely as possible to the definition of the dominant trees, i.e., the 100 largest trees per ha (Rennolls, 1978), given the limited plot size of 400 m^2. For each sample tree, the position, height, and DBH were recorded. For further age analyses, core samples of two dominant trees per plot were taken at 1.3 m height. In the laboratory, the age was obtained by counting growth rings on the core samples. The ring widths were measured manually with the LINTABTM 6 tree-ring measurement station and the TSAP-WinTM software for tree-ring measurement.

3.3 ALS and hyperspectral data

3.3.1 Pellizzano

ALS data were acquired between 7th and 9th September, 2012 with a Riegl LMS-Q680i laser scanner. The system, mounted on a Multi Mission Aircraft, was optimized to measure canopy structure with a flying speed of about 51 m s^{-2} at an altitude of 660 m above ground level. The pulse repetition frequency was 400 kHz with a 60° field of view and the overlap for each stripe was at least 30%. The result of the scanning was an ALS point cloud (x, y, z) with a mean point density of 48 pulses m^{-1} for the first returns. The scanner recorded up to five returns for each laser pulse. The data vendor generated a digital terrain model (DTM) with TerraScan software with a spatial resolution of 0.5 m. Furthermore, ALS point cloud was normalized to obtain a canopy height above ground by subtracting the DTM elevations from the z values of the ALS pulses.

Hyperspectral data were acquired on 13th June 2013 with an AISA Eagle II sensor with a spatial resolution of 1 m. Twenty-one images were acquired between 12:00 a.m. and 1:12 p.m. and mosaicked in order to create a uniform image. The minimum overlap among the images was 20%. Each image was characterized by 65 spectral bands acquired between 403.1 nm and 995.3 nm with a spectral resolution of 9 nm. Non-vegetated areas were removed by filtering out pixels with a normalized difference vegetation index (NDVI) below 0.5. To reduce minor differences in reflectance occurring between different images, the value of each pixel was normalized dividing it by the sum of the (original) values of the same pixel along all the bands (Yu et al., 1999).

3.3.2 Våler

ALS and airborne hyperspectral data were simultaneously acquired over the study area on 9th September 2011. The flying altitude was 1500 m above ground level. Twenty-one flight lines were flown between 10:48 a.m. and 2:22 p.m., having sun zenith angle between 59° and 61°. ALS data were acquired using the Leica ALS70 system with a pulse repetition frequency of 180 kHz. The system recorded up to five returns per pulse and the average pulse density was 2.4 pulses m^{-2}.

Hyperspectral data were acquired using the HySpex VNIR-1600 sensor with spatial resolution of 0.5 m. The images consisted of 80 bands between 410 nm and 990 nm with 7.2 nm spectral resolution. All the hyperspectral images were acquired in non-nadir conditions regarding the field plots. Hyperspectral data were orthorectified using a DTM derived from ALS data by the data vendor. To minimize co-registration problems the vendor also applied a transformation based on tree top detection in the two datasets. In the pre-processing, the

hyperspectral images were atmospherically corrected using the QUAC algorithm (Bernstein et al., 2005). Afterwards, the value of each pixel was normalized with respect to the sum of the values of the same pixel in all the bands to reduce a minor difference in reflectance occurring between the different images (Yu et al., 1999).

4 Methods

In this thesis, the fusion is employed by a statistic approach, which is based on predictive models, such as generalized linear models, k-nearest neighbor algorithm, support vector machines (SVM) classifier etc. The statistic approach was investigated on product and variable-level, using exploratory data analysis, parametric and non-parametric machine learning algorithms for modeling and different statistical tests (Table 1). The detection accuracy of the delineation algorithm was evaluated with omission error (OE), commission error (CE), and accuracy index (AI). The model accuracy for the forest characteristics was evaluated in terms of the root mean square error (RMSE) and the coefficient of determination (r2) computed as the square value of Pearson correlation coefficient. The systematic error was assessed with the mean differences (MD). For the ITC approach, the tree species classification accuracy was validated with the overall accuracy (OA), kappa coefficient (KA), and the producer's and user's accuracies derived from the confusion matrix. The reliability of the predicted forest characteristics was tested by means of the cross-validation technique.

Table 1: Summary of exploratory data analysis, machine learning algorithms for modeling, test statistics, and accuracy measures applied in Papers I, II, III, and IV.

	Paper I	**Paper II**	**Paper III**	**Paper IV**
Exploratory data analysis	Parameters tuning and sensitivity analysis	/	/	/
Machine learning algorithms	K-means clustering	Linear regression, Poisson regression, SVM classification	Linear and non-linear regression, k-nearest neighbors, SVM classification	Partial least square regression
Test statistics	Two-sided Mann-Whitney-Wilcoxon test	/	Wilcoxon signed rank test, Friedman test, Conover post-hoc analysis	Permutation test
Accuracy assessment	OE, CE, AI, RMSE, MD, r^2	OE, CE, OA, KA, producer's accuracy, RMSE, MD, standard deviation of the differences, r^2	OE, CE, OA, KA, producer's and user's accuracies, RMSE, MD, r^2	RMSE, MD, q^2

The ITC delineating algorithm was based on a K-means clustering applied on horizontal slices followed by vertical merging based on overlapping among clusters. In addition, the effects

of different forest structures (characterized by mean DBH, number of stems per hectare, mean nearest neighbor distance, and Gini coefficient of basal area) and point cloud densities (50, 30, 20, 10, 6 and 4 pulses m^{-2}) on the ITC delineation algorithm were analysed in terms of omission and commission errors. To test if the differences among accuracies obtained with different point cloud densities and original data were significant, a two-sided Mann-Whitney-Wilcoxon test was carried out. For each crown segment, biophysical attributes (tree height, crown area, and crown position) were extracted at the ITC level and aggregated at the plot level (Paper I).

The same ITC delineation algorithm was applied in the study of Paper II. Moreover, once the crown segments were delineated, they were co-registered with the hyperspectral data in order to obtain ALS and hyperspectral variables for each delineated crown segment. These variables were used to predict forest attributes at the ITC level. Tree species were predicted with SVM classifier and used to predict age per species with Poisson regression using ALS and hyperspectral variables, while stem height and DBH were predicted with ALS variables fitting species-specific linear models. The models were validated using a 10-fold cross validation approach. Subsequently, these biophysical attributes were used to compute dominant height, species, and age for each sample plot in order to determine the site index at grid level (Paper II).

The species-specific volume was predicted with ITC, semi-ITC, and ABA approaches. For the ITC approach, hyperspectral variables were used to predict tree species with SVM classifier, and ALS variables to predict DBH with non-linear regression models. Knowing the predicted species and DBH, the species-specific volumes were computed based on allometric models. For the semi-ITC and ABA approaches, the statistical relationships between the ALS and hyperspectral variables, and the field-observed species-specific volumes were constructed based on multivariate k most similar neighbor (MSN) method. The ALS and hyperspectral variables were calculated for each crown segment in the semi-ITC approach and for each sample plot in ABA. The species-specific volumes for ITC and semi-ITC were aggregated at the same grid size as ABA in order to compare and evaluate the performance of each approach. Wilcoxon signed rank test was performed to test the significance of the differences between the observed and predicted volumes for each inventory approach. The Friedman test was applied to check the significance of the differences in the distribution of the differences between the observed and predicted species-specific volumes among sample plots for the three inventory approaches. For validating species-specific volumes, leave-one-out (LOO) cross-validation procedure was applied (Paper III).

The ALS (height and density matrices) and hyperspectral variables (1st and 2nd order image statistics) were computed for each sample plot and used in partial least square (PLS) regression models in order to predict six forest structural diversity measures. We checked if the encoded information may be useful for prediction purposes when considering ALS and hyperspectral variables, either alone or fused. The optimal number of latent variables was

selected by minimizing the RMSE of predictions based on a 5-fold cross-validation. The number of ALS and hyperspectral variables was balanced using the correlation threshold, thus, equally weighing the impacts of both kind of variables on the PLS model. A permutation test was applied to test each model's reliability. The model accuracy and systematic error were compared using ALS and hyperspectral data, separately or fused (Paper VI).

5 Major findings

5.1 Quantification of influence of forest structure and ALS point cloud density on established ITC delineation algorithm (Paper I)

With the field measurements and a well-established reference delineation method, the performance of the developed ITC delineation method based on ALS data was evaluated in terms of detection accuracy and tree attributes estimation. Both methods reached similar detection accuracies and both were effective in tree attributes estimation. Forest structure characterized by stem density, distribution of trees, number of stems per hectare, and the evenness expressed by Gini coefficient of basal area, had significant influence on the detection accuracy in terms of omission and commission errors. The omission error was lower (in range of 25%–60%) in plots with a homogeneous forest structure and tree species, and higher (in range of 60%–85%) in plots with a heterogeneous forest structure and tree species. In addition, the forest structure only had a slight effect on the commission error as it was similar for all plots. The point density analysis showed that the detection accuracy, in terms of accuracy index, marginally increased for the point densities from 6 to 50 pulses m^{-2} applying Mann-Whitney-Wilcoxon test. However, the accuracy index of the ITC delineation algorithm was the highest with the original point cloud density at 60 pulses m^{-2} and significantly different from the other point cloud densities.

5.2 Improvement of site index maps using ITC approach together with fused ALS and hyperspectral data (Paper II)

Plot level-derived biophysical attributes via ITC approach using ALS and hyperspectral data provided a reliable input for the determination of site index. ALS variables obtained for each crown segment were important for the height and DBH modeling, while the fused ALS and hyperspectral variables were important for tree species and age modeling. The selection of the dominant crown segments derived from ITC delineation algorithm from which the inputs for the site index were computed, did not affect the accuracy of the predicted site index. The prediction accuracies of dominant height and species were high (RMSE = 1.12 m and kappa accuracy = 0.85) in contrast to errors related to age (RMSE = 34.01 years). The RMSE for site indices was 4.30 m when all biophysical attributes (dominant height, tree species, and age) were predicted from the

remote sensing data and 1.18 m when only the age was taken from the field measurements. Age prediction based on remotely sensed data is still a challenging task, especially in mixed age stands. The site index determination based on ITC delineation at the variable-level fusion was stable and efficient for the site index determination.

5.3 Evaluation of the performance of three remotely sensed-based forest inventory approaches to assess how different spatial details influenced the predictions of species-specific volume using fused ALS and hyperspectral data (Paper III)

Three remotely sensed-based forest inventory approaches were compared (ITC, semi-ITC and ABA approach). The fusion for the first approach was conducted on the product-level, and for the others at the variable-level. The hyperspectral data were important in the ITC approach for the classification of tree species, and ALS data for the DBH and height prediction which together allowed the predictions of species-specific models. For the semi-ITC and ABA approaches, ALS and hyperspectral variables were combined into *k*-mean nearest neighbor models. The ITC approach performed better according to relative RMSE for the volumes of minority species but in general resulted in larger systematic errors (relative mean differences of the mean) compared to the semi-ITC and ABA approaches. The ABA approach resulted in relatively high accuracies and small systematic errors for the dominant species and vice versa for the minority species. For majority species, the semi-ITC performed slightly better compared to the ABA, resulting in higher accuracies and smaller systematic errors. The total volume of the ITC, semi-ITC, and ABA resulted in relative RMSEs of 25.31%, 17.41%, and 30.95% of the mean and relative mean differences of 21.59%, 0.27%, and 2.69% of the mean, respectively. The results indicated that the semi-ITC outperformed the two other inventory approaches, considering the greatest balance between accuracies and the systematic errors. The Friedman's test demonstrated that the pairs of the inventory approaches (ITC vs. semi-ITC, ITC vs. ABA, semi-ITC vs. ABA) were significantly different ($p \leq 0.05$) from each other for the total and species-specific volumes, except for the pair of semi-ITC vs ABA, where the Norway spruce and larch volumes were not statistically significant. For the ITC approach, hyperspectral variables were important for tree species identification, while ALS data were important for ITC delineation in order to extract crown segment height and crown area for predicting DBH. Both species and DBH, were considered as inputs for volume prediction. In the semi-ITC and ABA approaches, the ALS and hyperspectral variables were both important for volume modeling.

5.4 Investigate the benefits of ALS and hyperspectral data, separately and fused, to predict forest structural measures (Paper VI)

Six types of measures of forest structural diversity that describe the variability of tree sizes (Gini coefficient of basal area and diameter differentiation index), the spatial distribution of tree positions (mean nearest neighbor distance and uniform angle index), and the tree species diversity (Shannon's index and species mingling index) were considered. The forest structural diversity measures were predicted with ALS and hyperspectral data, alone and combined, where the data fusion was conducted at variable-level. None of the structural diversity measures based on hyperspectral data passed the permutation test meaning that the predictions were not different from a random prediction. The uniform angle index was the only one that was not predictable with any remote sensing data combination. Fused data improved the prediction performances of the diameter differentiation index only, when obtained as a combination of ALS and 2nd order image statistics on hyperspectral data. Compared to predictions based on ALS data, the predictions based on fused data reached higher relative RMSE for 5% and variance explained by model was higher for 28%. The fusion of ALS and hyperspectral data did not improve any other structural diversity measures, but produced accuracy levels comparable to the structural diversity measures derived from ALS data alone. In this experiment, ALS data showed the best predictions for the majority of the structural diversity measures taken into account.

6 Discussion

6.1 Fusion of ALS and hyperspectral data (Papers II, III, IV)

ALS and hyperspectral data were fused to provide species information, total and species-specific volume, height, DBH, age, site index, and structural diversity measures at different fusion levels. In particular, the fusion in Papers II and III was conducted at product-level, while in Papers II, III, and IV at variable-level (see Table 2). In the same order, the aforementioned forest characteristics will be discussed.

Tree species are characterized by different plant chemical and physical properties, which results in differing levels of reflectance (amplitude). Such differences significantly affect the reflectance spectrum shape (Fassnacht et al., 2016). These differences in reflectance from the visible to the shortwave infrared part of the spectrum are therefore the main drivers to discriminate species. Moreover, tree species also have different architecture of crowns (e.g. conical, rounded), branching, and foliage (Coops et al., 2007). Thus, the hyperspectral and ALS data can be considered the most promising combination for discriminating tree species and to outperform other data fusions, e.g. fusion of ALS and multispectral data (Dalponte et al., 2012;

Ørka et al., 2013). In Paper II, such fusion was proved to be suitable in distinguishing tree species, especially for spectrally similar tree species. Similar was confirmed in the study of Dalponte et al. (2012). The classification accuracy was higher for the dominant species as they were more representative in samples compared to the minority species. This was also showed by Ørka et al. (2013). The species accuracy obtained in Paper II, was in line with the study of Dalponte et al. (2015a) conducted on the same study area. Moreover, the fusion of ALS and hyperspectral data was shown as a powerful basis for the discrimination of tree species also in other studies conducted on different study areas (Alonzo et al., 2014; Dalponte et al., 2014).

Using different inventory approaches to characterize the species composition was demonstrated with the combined use of ALS and hyperspectral data, and higher accuracies were achieved compared to other data fusions (Ørka et al., 2013). Moreover, many methods have been proposed for fusing ALS data with aerial photographs or airborne multispectral images (Breidenbach et al., 2010; Packalén and Maltamo, 2006; Vauhkonen et al., 2012) in order to predict species-specific volumes. According to the existing literature, in Paper III, the first attempt to fuse the ALS and hyperspectral data were investigated in order to provide species-specific volumes with three different inventory approaches. With the ITC approach, stem volume was predicted based on ALS data, and the species were classified based on hyperspectral data. Both coupled together enable to provide species-specific volume representing product-level fusion. In contrast, in the semi-ITC and ABA approaches, both ALS and hyperspectral variables were used for modeling total and species-specific volumes, and the fusion was conducted at a variable-level. The fusion of such complementary data at product- and variable-level provided the predictions with high accuracies. The results obtained in Paper III were in line with the study of Breidenbach et al. (2010) but we have to consider that both studies were applied to different forest types.

In Paper II, the fusion at the product-level was found important for the species-specific models of height and DBH. The age was modeled by fusing data on variable-level. Both ALS and hyperspectral variables were found important. In addition, the site index was determined by applying product-level fusion which was based on the abovementioned forest characteristics, and the results showed high potential to improve existing site index maps in an objective and automatic way. The fusion of ALS and hyperspectral data was found powerful to predict age, which was overpredicted in younger (< 60 years) and underpredicted in older (> 60 years) stands. The reasons of the importance of the fusion of ALS and hyperspectral data is two sided. First, with the aging, the canopy structure (Ishii and McDowell, 2002), plant chemical properties, and the leaf morphology (Roberts et al., 1997) are changing. Thus, changes in reflectance are measured by hyperspectral sensors. Dye et al. (2011) demonstrated that the hyperspectral data were suitable to predict age in young stands. Furthermore, the better the site productivity is and the higher the tree age is, the higher the tree can grow. Thus, it was demonstrated that ALS data

can provide good age predictability (Racine et al., 2014). However, such relationship between ALS heights and age is usually strong in stands with smaller age variability or in even-aged stands. In the study area used in Paper II, the stands were mixed-age and the age-structure relationship in such stands is more ambiguous, since the strength of the relationship becomes asymptotic with aging. These was also confirmed by Ung et al. (2001) and Sharma et al. (2011). However, the accuracy of age predictions vary considerably between different studies, using only ALS or spectral data, and it seems to be strongly effected by forest management strategies, and forest structure and type (M. Maltamo et al., 2009; Niemann, 1995; Pretzsch, 2009; Racine et al., 2014).

In Paper IV, structural diversity measures describing tree size variation, spatial pattern of trees, and tree species diversity were predicted by ALS and hyperspectral data alone and both together fused at variable-level. According to the existing literature in relation to the forest structural diversity of biophysical attributes, the fusion of ALS and hyperspectral data was mostly explored for the estimation of the stem density and above ground biomass (Anderson et al., 2008; Latifi et al., 2012; Luo et al., 2017; Vaglio Laurin et al., 2014) and less for the structural diversity measures explored in Paper IV. The ALS variables provided the most effective information amongst the entire data source combinations, while the hyperspectral variables contributed only slightly to describe the variation beyond those explained by ALS. Similar was also highlighted by Anderson et al. (2008). Thus, data fusion generally did not contribute to the accuracy increase for structural diversity measures accounted in this study. Image texture refers to the spatial variation and arrangement of the pixels of which any image is composed. It could be that the distribution of trees and the tree species were similar among the sample plots, therefore hyperspectral variables did not make high contribution to the fused models. In many studies, the variables calculated from grey level co-occurrence matrix, which was derived from spectral images, were demonstrated as good variables in distinguishing spatial pattern in remote sensing imagery analysis, and they were mostly used for classification purposes (Franklin et al., 2001; Murray et al., 2010; Ouma et al., 2008) and less for modelling purposes (Gallardo-Cruz et al., 2012; Meng et al., 2016). To explain why fusion in Paper IV did not increase the accuracy of structural diversity measures, more research should be carried out in similar forest conditions, especially for modeling purposes.

From the processing point of view, the disadvantage of data fusion is that ALS and hyperspectral data require the co-registration of datasets, and any uncertainty at this stage could influence the accuracy of the final products (Torabzadeh et al., 2014). The advantage of such data fusion, when both sensors are combined on the same platform, is higher geometric accuracy for data fusion and highly compatible datasets, also proved for similar data fusions (St-Onge et al., 2008). In addition, when both sensors are mounted on a platform of the same mission, the cost is

reduced. For mapping purposes, Jones et al. (2010) proved that ALS and hyperspectral data fusion was superior to aerial photograph interpretation in terms of accuracy and cost.

Considering the achieved accuracies in Papers II, III, and IV it can be seen that in most cases fused data obtain higher accuracies than ALS and hyperspectral data only.

Table 2: Fusion levels of predicted forest characteristics with ALS and hyperspectral data in Papers II, III, and IV.

	Paper II	**Paper III**	**Paper IV**
Product level	Height, DBH, Site index	Species-specific volume with ITC approach	/
Variables level	Tree species and age	Total and species-specific volume with semi-ITC and ABA approaches	Structural diversity measures

6.2 Exploring different spatial scales in the prediction of forest characteristics (Papers I, II, III)

The extraction and prediction of different forest characteristics (species information, age, total volume, species-specific volume, and structural diversity measures) at different spatial scales were investigated in Papers I, II, and III (see Table 3). With the ITC approach, all papers produced information with the highest spatial scale, the tree. Papers II and III provided information on the grid-cell scale using the ABA, while Paper II also considered the tree group scale using the semi-ITC. First, the ITC delineation algorithm and the point density is discussed, continued with the forest characteristics obtained with the ITC, semi-ITC, and ABA approaches.

Low point density ALS data provide limited possibilities to detect and delineate co-dominant and subordinate trees, i.e., the intermediate and suppressed trees. In this regard, ALS point cloud with density above 5 pulses per m^{-2} (Peuhkurinen et al., 2011) already allows development of delineation methods to better distinguish individual tree crowns. In many studies, it was assumed that the higher the point density, the better the detection and delineation of trees. This was shown to be particularly true in structurally complex and dense forests (Wang et al., 2016). In a few studies (Kaartinen et al., 2012; Wang et al., 2016; Yao et al., 2014), different point densities were tested, up to 8 and 20 pulses per m^{-2}. Kaartinen et al. (2012) and Yao et al. (2014) reported that there were no significant improvements in performances of the ITC delineation algorithms, at least for those datasets with a point density larger than 10 pulses per m^{-2}. Additionally, in both studies, the ITC delineation algorithms were mostly developed on 2D canopy height models. Thus, in such 2D delineation methods after a certain point density the information seemed to be saturated and the detection accuracy could not improve (Wang et al., 2016). With a different perspective, Wang et al. (2016) also considered delineation algorithms based on 3D ALS points and reported that such algorithms performed better with higher

densities. However, the range of point densities considered in the abovementioned studies is too small to make any conclusions. One of the objectives in Paper I was to test if a high point density can improve the detection and delineation accuracy of the developed delineation algorithm based on 3D ALS points. This study was the first to evaluate point densities above 20 pulses considering point densities up to 60 pulses per m^{-2}. It was demonstrated that the detection accuracy increased with higher point densities, but it achieved marginal improvements when the point density expanded from 10 to 50 pulses per m^{-2}. This is in line with earlier research that have found that the detection accuracy did not change between 10 and 20 pulses per m^{-2}. However, with 60 pulses per m^{-2} the detection accuracy was significantly different compared to other point densities. Thus, a 3D delineation algorithm seems to be able to provide higher spatial detail using the high point density data. The optimal point density most probably depends on tree size, structure, and stand density of the forest. In Paper I, it was found that the detection accuracy was higher in more sparse and single layered forest. Thus, to detect the dominant trees the lower point densities could be used. This is in line with the suggestions of Wang et al. (2016) indicating that ALS data with point density between 2 to 5 pulses m^{-2} may already provide satisfactory results for the applications where the main focus is to obtain characteristics of dominant trees.

High point density could also affect the prediction accuracy of the forest characteristics related to the detected crown segments. Kaartinen et al. (2012) found out that the use of different point densities marginally improved the accuracy of the extracted tree heights, tree positions, and crown areas. Unfortunately, there are no studies that tested such effect on higher point densities. In addition, most studies were conducted on point densities below 8 pulses m^{-2} and were carried out at plot level (Manuri et al., 2017; Ruiz et al., 2014; Tesfamichael et al., 2010). In Paper I, attributes extracted from a 3D and a 2D algorithms were compared, and it emerged that they were quite similar between the algorithms. Moreover, the 2D method provided better estimates from the crown area.

The ITC and semi-ITC approaches can provide detailed forest characteristics, such as age, DBH, species, volume, etc. for each crown segment (Breidenbach et al., 2010; M Maltamo et al., 2009; Yu et al., 2010). However, the accuracy of such characteristics depends on the success of the ITC delineation algorithm and its calibration (Kandare et al., 2016; Latifi et al., 2015; Yu et al., 2010). Although the delineation algorithm was applied in Paper II and III, the results are hardly comparable at the tree level, because the characteristics were further aggregated at grid-level. In particular, in Paper II, only the four largest crown segments per plot were used for the calculation of forest characteristics at grid-level (dominant height, species, age, and site index) while in Paper III all delineated crown segments were used. The biggest advantages of the ITC and semi-ITC approaches are that they allow to obtain predictions at the minimum possible scale in a forest, such as a crown segment, and allow better localization of forest characteristic due to the known

tree positions (Paper II, III). Indeed, in Paper II it was demonstrated that through the ITC approach it was possible to obtain site index results at an accuracy similar to the existing site index maps in Norway. We have to keep in mind that site index on the existing maps has one value for each stand while with the ITC approach we are able to provide a more detailed information within a stand. Thus, the proposed approach could provide a means to summarize site index in more homogeneous areas within a stand, even at sub-grid-cell scale.

One of the advantages of ITC approach is also the ability to characterize tree species for each tree with high accuracy since it is assumed that one crown segment is one tree (Paper II and III). While methods such as semi-ITC and ABA assume that there could be many species in the segment or grid, the species information is possible only through proportions of any forest attribute (e.g. species-specific volume) per each crown segment and grid-cell, respectively (Paper III) (Latifi et al., 2015). Knowing the species information for each tree, it is possible to develop species-specific models for any forest attribute, and this is important for forest inventory (Packalén and Maltamo, 2007, 2006). In this regard in Paper III, the ITC approach showed to provide high accuracies for minority species (even if with large systematic errors). This was also showed in a study by Ørka et al. (2013). The aggregated volume at grid-cell was affected by systematic error using ITC approach, while a high accuracy and low systematic error were achieved with the semi-ITC approach (Paper III). In this thesis, it was found that the semi-ITC approach provided prediction accuracies higher or similar to the ABA. This was also reported in earlier studies, comparing the semi-ITC and ABA approaches (Breidenbach et al., 2010; Rahlf et al., 2015). Thus, based on trade-off between RMSEs and mean differences, the volume predictions based on the semi-ITC approach outperformed the other approaches. In addition to the aforementioned species-specific studies, other studies compared predicted forest characteristics with ITC and ABA approaches and obtained comparable, higher or lower accuracies (Coomes et al., 2017; Latifi et al., 2015; Lee et al., 2017; Peuhkurinen et al., 2007; Yu et al., 2010). However, the forest type in Paper I was different from the other studies. Thus, this phenomenon also depend on the forest type, structure and the species present (Latifi et al., 2015).

Which spatial scale information should be provided and which approach is superior depends on the user's needs. In this thesis, the ITC approach provided means to accurate tree species identification, especially for minority species, and was a way to provide site index prediction with good accuracy. The semi-ITC approach seems to be the best choice to provide accurate species-specific attributes. The resulted forest characteristics can be aggregated at any other spatial scale (groups of trees, grids, and stands) with both approaches i.e. as it was done for the volume. This improved the knowledge of within-stand variation at any scale, especially for the minority species (Ørka et al., 2013). The only drawbacks of the ITC approach are the large systematic error unsuitable in operational forest inventories and the high cost of field surveys as

tree positions are needed. The last statement also applies to the semi-ITC approach. However, methods for positioning trees using different methods are under development (Holopainen et al., 2014). In particular, detailed forest information obtained by ITC and semi-ITC can be used for improvements in forest management decisions, for example to optimize selection of silvicultural treatments (Wang et al., 2016), or for future tree-based growth simulations (Lo and Lin, 2013). Knowing the position of each tree can be important for many applications with sound ecological reasons, such as examination of habitat structure, distribution of dead trees (Dobbertin et al., 2001; Gillespie et al., 2008; Polewski et al., 2015), identification of invasive species (Dash et al., 2017), fire management (Morsdorf et al., 2004), and biomass estimation (Hauglin et al., 2013).

Table 3: Forest characteristics predicted in Papers I, II, and III with different spatial scales.

Spatial scale	Paper I	Paper II	Paper III
Tree	Tree positions, crown area, tree heights	Tree species, height, DBH, and age	Species, stem volume
Tree group	/	/	Total and species-specific volume
Grid-cell	/	Dominant, height, species, age, and site index	Total and species-specific volume

7 Conclusion and further perspectives

This thesis demonstrated the potential to improve the prediction of forest characteristics with fusion of complementary 3D ALS and 2D hyperspectral data at different spatial scales. First, the fusion of complementary information derived from ALS and hyperspectral data was shown as a powerful basis for the discrimination of tree species, especially at tree level, which indirectly allows to reach high accuracies for species-specific models, such as height, DBH, volumes, and site index. The age was predicted with a moderate accuracy but there are still many unexplored fusions of ALS and hyperspectral data that could provide higher accuracies. Also, at grid-cell, the fusion of such data contributes to a high accuracy of species-specific forest characteristics for majority species. In contrast to abovementioned forest characteristics, the forest structural diversity measures were the only ones that in general did not gain in accuracy from the variable-level fusion of ALS and hyperspectral data. In addition, there is a huge lack of studies to make any conclusions about the benefits of such data fusion in different forest conditions, and in order to enlighten such data fusion properly, this subject should be further investigated in different environments. The acquisition costs of high-density ALS and the integration of LiDAR technology with hyperspectral sensors on the same platform are expected to decrease due to the technical advances in acquisition equipment. Recently, the hyperspectral ALS sensors have been developed

with a high potential to be used as a future single-sensor solution for forest studies and mapping. However, they are still in the development stage and have not reached full maturity yet. Second, the evaluation of different spatial scales, via ITC and semi-ITC approaches, reached high accuracies for the site index, and total and species-specific volume determination, respectively. The accuracies of both forest characteristics were comparable with the ones obtained in the field and used in practice. Thus, the ITC and semi-ITC approaches have a high potential to map any forest characteristic to any scale that would help silviculturists and ecologists in their applications to facilitate their field work. In addition, the ITC approach was a successful method for the determination of the species-specific volume of minority species, but it resulted in too large systematic errors for all species to support forest inventories in contrast to the semi-ITC and ABA approaches. The advantage of the ITC and semi-ITC approaches, when large sample plots are observed, is that they can improve the estimation of certain forest characteristics as they directly take into account the variability within a forest stand. From such approaches, ecologists and silviculturists could profit greater knowledge to better model wildfires, monitor wildlife habitats, map aboveground carbon stock, describe growth dynamics, and formulate silvicultural strategies. As such approaches are more expensive due to more extensive field work, the combination of ABA and semi-ITC methods could further pave the way also for operational forest inventories by combining detection of individual trees in structurally complex and heterogeneous stands, with the ABA approach in homogeneous stands. Further studies are needed to examine the complementarity of different remotely sensed-based inventory approaches to obtain more knowledge about their benefits in different disciplines over larger areas.

References

Aguirre, O., Hui, G., Von Gadow, K., Jiménez, J., 2003. An analysis of spatial forest structure using neighbourhood-based variables. For. Ecol. Manage. 183, 137–145. doi:10.1016/S0378-1127(03)00102-6

Alonzo, M., Bookhagen, B., Roberts, D.A., 2014. Urban tree species mapping using hyperspectral and lidar data fusion. Remote Sens. Environ. 148, 70–83. doi:10.1016/j.rse.2014.03.018

Anderson, J.E., Plourde, L.C., Martin, M.E., Braswell, B.H., Smith, M.L., Dubayah, R.O., Hofton, M.A., Blair, J.B., 2008. Integrating waveform lidar with hyperspectral imagery for inventory of a northern temperate forest. Remote Sens. Environ. 112, 1856–1870. doi:10.1016/j.rse.2007.09.009

Asner, G., 2008. Hyperspectral remote sensing of canopy chemistry, physiology, and biodiversity in tropical rainforests, in: Hyperspectral Remote Sensing of Tropical and Sub-Tropical Forests. CRC Press, pp. 261–296. doi:10.1201/9781420053432.ch12

Asner, G.P., Knapp, D.E., Kennedy-Bowdoin, T., Jones, M.O., Martin, R.E., Boardman, J., Hughes, R.F., 2008. Invasive species detection in Hawaiian rainforests using airborne imaging spectroscopy and LiDAR. Remote Sens. Environ. 112, 1942–1955. doi:10.1016/j.rse.2007.11.016

Asner, G.P., Martin, R.E., Anderson, C.B., Knapp, D.E., 2015. Quantifying forest canopy traits: Imaging spectroscopy versus field survey. Remote Sens. Environ. 158, 15–27. doi:10.1016/j.rse.2014.11.011

Asner, G.P., Martin, R.E., Knapp, D.E., Tupayachi, R., Anderson, C.B., Sinca, F., Vaughn, N.R., Llactayo, W., 2017. Airborne laser-guided imaging spectroscopy to map forest trait diversity and guide conservation. Science (80-.). 355, 385–389. doi:10.1126/science.aaj1987

Baltsavias, E.P., 1999. Airborne laser scanning: basic relations and formulas. ISPRS J. Photogramm. Remote Sens. 54, 199–214. doi:10.1016/S0924-2716(99)00015-5

Bernstein, L.S., Adler-Golden, S.M., Sundberg, R.L., Levine, R.Y., Perkins, T.C., Berk, A., Ratkowski, A.J., Felde, G., Hoke, M.L., 2005. A new method for atmospheric correction and aerosol optical property retrieval for VIS-SWIR multi- and hyperspectral imaging sensors: QUAC (QUick Atmospheric Correction), in: International Geoscience and Remote Sensing Symposium (IGARSS). pp. 3549–3552. doi:10.1109/IGARSS.2005.1526613

Borengaser, M., Hungate, W.S., Watkins, R., 2008. Hyperspectral remote sensing-Principles and aplications. CRC Press Taylor & Francis Group, Boca Raton.

Boschetti, M., Boschetti, L., Oliveri, S., Casati, L., Canova, I., 2007. Tree species mapping with airborne hyper-spectral MIVIS data: the Ticino Park study case. Int. J. Remote Sens. 28, 1251–1261. doi:10.1080/01431160600928542

Breidenbach, J., Næsset, E., Lien, V., Gobakken, T., Solberg, S., 2010. Prediction of species specific forest inventory attributes using a nonparametric semi-individual tree crown approach based on fused airborne laser scanning and multispectral data. Remote Sens. Environ. 114, 911–924. doi:10.1016/j.rse.2009.12.004

Clark, M.L., Roberts, D.A., Ewel, J.J., Clark, D.B., 2011. Estimation of tropical rain forest aboveground biomass with small-footprint lidar and hyperspectral sensors. Remote Sens. Environ. 115, 2931–2942. doi:10.1016/j.rse.2010.08.029

Clawges, R., Vierling, K., Vierling, L., Rowell, E., 2008. The use of airborne lidar to assess avian species diversity, density, and occurrence in a pine/aspen forest. Remote Sens. Environ. 112, 2064–2073. doi:10.1016/j.rse.2007.08.023

Coomes, D.A., Dalponte, M., Jucker, T., Asner, G.P., Banin, L.F., Burslem, D.F.R.P., Lewis, S.L., Nilus, R., Phillips, O.L., Phua, M.-H., Qie, L., 2017. Area-based vs tree-centric approaches to mapping forest carbon in Southeast Asian forests from airborne laser scanning data. Remote Sens. Environ. 194, 77–88. doi:10.1016/j.rse.2017.03.017

Coops, N.C., 2015. Characterizing Forest Growth and Productivity Using Remotely Sensed Data. Curr. For. Reports 195–205. doi:10.1007/s40725-015-0020-x

Coops, N.C., Hilker, T., Wulder, M.A., St-Onge, B., Newnham, G., Siggins, A., Trofymow, J.A. (Tony), 2007. Estimating canopy structure of Douglas-fir forest stands from discrete-return LiDAR. Trees 21, 295–310. doi:10.1007/s00468-006-0119-6

Dalponte, M., Bruzzone, L., Gianelle, D., 2008. Fusion of hyperspectral and LIDAR remote sensing data for classification of complex forest areas. IEEE Trans. Geosci. Remote Sens. 46, 1416–1427. doi:10.1109/TGRS.2008.916480

Dalponte, M., Bruzzone, L., Gianelle, D., 2012. Tree species classification in the southern Alps based on the fusion of very high geometrical resolution multispectral/hyperspectral images and LiDAR data. Remote Sens. Environ. 123, 258–270. doi:10.1016/j.rse.2012.03.013

Dalponte, M., Ene, L.T., Marconcini, M., Gobakken, T., Næsset, E., 2015a. Semi-supervised SVM for individual tree crown species classification. ISPRS J. Photogramm. Remote Sens. 110, 77–87.

doi:10.1016/j.isprsjprs.2015.10.010

Dalponte, M., Ørka, H.O., Ene, L.T., Gobakken, T., Næsset, E., 2014. Tree crown delineation and tree species classification in boreal forests using hyperspectral and ALS data. Remote Sens. Environ. 140, 306–317. doi:10.1016/j.rse.2013.09.006

Dalponte, M., Ørka, H.O., Gobakken, T., Gianelle, D., Næsset, E., 2013. Tree species classification in boreal forests with hyperspectral data. IEEE Trans. Geosci. Remote Sens. 51, 2632–2645. doi:10.1109/TGRS.2012.2216272

Dalponte, M., Reyes, F., Kandare, K., Gianelle, D., 2015b. Delineation of individual tree crowns from ALS and hyperspectral data: a comparison among four methods. Eur. J. Remote Sens. 48, 365–382. doi:10.5721/EuJRS20154821

Dash, J., Pearse, G., Watt, M., Paul, T., 2017. Combining airborne laser scanning and aerial imagery enhances echo classification for invasive conifer detection. Remote Sens. 9, 156. doi:10.3390/rs9020156

Dash, J.P., Marshall, H.M., Rawley, B., 2015. Methods for estimating multivariate stand yields and errors using k-NN and aerial laser scanning. Forestry 88, 237–247. doi:10.1093/forestry/cpu054

Dobbertin, M., Baltensweiler, A., Rigling, D., 2001. Tree mortality in an unmanaged mountain pine (Pinus mugo var. uncinata) stand in the Swiss National Park impacted by root rot fungi. For. Ecol. Manage. 145, 79–89. doi:10.1016/S0378-1127(00)00576-4

Duncanson, L.I., Cook, B.D., Hurtt, G.C., Dubayah, R.O., 2014. An efficient, multi-layered crown delineation algorithm for mapping individual tree structure across multiple ecosystems. Remote Sens. Environ. 154, 378–386. doi:10.1016/j.rse.2013.07.044

Dye, M., Mutanga, O., Ismail, R., 2011. Examining the utility of random forest and AISA Eagle hyperspectral image data to predict Pinus patula age in KwaZulu-Natal, South Africa. Geocarto Int. 26, 275–289. doi:10.1080/10106049.2011.562308

Eitel, J.U.H., Höfle, B., Vierling, L.A., Abellán, A., Asner, G.P., Deems, J.S., Glennie, C.L., Joerg, P.C., LeWinter, A.L., Magney, T.S., Mandlburger, G., Morton, D.C., Müller, J., Vierling, K.T., 2016. Beyond 3-D: The new spectrum of lidar applications for earth and ecological sciences. Remote Sens. Environ. 186, 372–392. doi:10.1016/j.rse.2016.08.018

Ene, L., Næsset, E., Gobakken, T., 2012. Single tree detection in heterogeneous boreal forests using airborne laser scanning and area-based stem number estimates. Int. J. Remote Sens. 33, 5171–5193. doi:10.1080/01431161.2012.657363

Eysn, L., Hollaus, M., Lindberg, E., Berger, F., Monnet, Jean-Matthieu Dalponte, M., Kobal, M., Pellegrini, M., Lingua, E., Mongus, D., Pfeifer, N., 2015. A benchmark of lidar based single tree detection methods using heterogeneous forest data from the Alpine space. Forests 6, 1721–1747. doi:10.3390/f6051721

Fassnacht, F.E., Latifi, H., Koch, B., 2012. An angular vegetation index for imaging spectroscopy data—Preliminary results on forest damage detection in the Bavarian National Park, Germany. Int. J. Appl. Earth Obs. Geoinf. 19, 308–321. doi:10.1016/j.jag.2012.05.018

Fassnacht, F.E., Latifi, H., Stereńczak, K., Modzelewska, A., Lefsky, M., Waser, L.T., Straub, C., Ghosh, A., 2016. Review of studies on tree species classification from remotely sensed data. Remote Sens. Environ. 186, 64–87. doi:10.1016/j.rse.2016.08.013

Fassnacht, F.E., Neumann, C., Forster, M., Buddenbaum, H., Ghosh, A., Clasen, A., Joshi, P.K., Koch, B., 2014. Comparison of feature reduction algorithms for classifying tree species with hyperspectral data on three central European test sites. IEEE J. Sel. Top. Appl. Earth Obs.

Remote Sens. 7, 2547–2561. doi:10.1109/JSTARS.2014.2329390

Ferraz, A., Saatchi, S., Mallet, C.M., Jacquemoud, S., Gonçalves, G., Silva, C.A., Soares, P., Tomé, M., Pereira, L., 2016. Airborne lidar estimation of aboveground forest biomass in the absence of field inventory. Remote Sens. 8, 1–18. doi:10.3390/rs8080653

Franklin, S.E., Maudie, A.J., Lavigne, M.B., 2001. Using spatial co-occurrence texture to increase forest structure and species composition classification accuracy. Photogramm. Eng. Remote Sens. 67, 849–855.

Gallardo-Cruz, J.A., Meave, J.A., González, E.J., Lebrija-Trejos, E.E., Romero-Romero, M.A., Pérez-García, E.A., Gallardo-Cruz, R., Hernández-Stefanoni, J.L., Martorell, C., 2012. Predicting tropical dry forest successional attributes from space: Is the key hidden in image texture? PLoS One 7, 38–45. doi:10.1371/journal.pone.0030506

Geerling, G.W., Labrador-Garcia, M., Clevers, J.G.P.W., Ragas, a. M.J., Smits, A. J.M., 2007. Classification of floodplain vegetation by data fusion of spectral (CASI) and LiDAR data. Int. J. Remote Sens. 28, 4263–4284. doi:10.1080/01431160701241720

Gillespie, T.W., Brock, J., Wright, C.W., 2004. Prospects for quantifying structure, floristic composition and species richness of tropical forests. Int. J. Remote Sens. 25, 707–715. doi:10.1080/01431160310001598917

Gillespie, T.W., Foody, G.M., Rocchini, D., Giorgi, A.P., Saatchi, S., 2008. Measuring and modelling biodiversity from space. Prog. Phys. Geogr. 32, 203–221. doi:10.1177/0309133308093606

Guo, X., Coops, N.C., Tompalski, P., Nielsen, S.E., Bater, C.W., John Stadt, J., 2017. Regional mapping of vegetation structure for biodiversity monitoring using airborne lidar data. Ecol. Inform. 38, 50–61. doi:10.1016/j.ecoinf.2017.01.005

Hakkenberg, C.R., Song, C., Peet, R.K., White, P.S., Rocchini, D., 2016. Forest structure as a predictor of tree species diversity in the North Carolina Piedmont. J. Veg. Sci. 27, 1151–1163. doi:10.1111/jvs.12451

Hauglin, M., Dibdiakova, J., Gobakken, T., Næsset, E., 2013. Estimating single-tree branch biomass of Norway spruce by airborne laser scanning. ISPRS J. Photogramm. Remote Sens. 79, 147–156. doi:10.1016/j.isprsjprs.2013.02.013

Hernández-Stefanoni, J.L., Dupuy, J.M., Johnson, K.D., Birdsey, R., Tun-Dzul, F., Peduzzi, A., Caamal-Sosa, J.P., Sánchez-Santos, G., López-Merlín, D., 2014. Improving species diversity and biomass estimates of tropical dry forests using airborne LiDAR. Remote Sens. 6, 4741–4763. doi:10.3390/rs6064741

Hill, R. A., Thomson, A. G., 2005. Mapping woodland species composition and structure using airborne spectral and LiDAR data. Int. J. Remote Sens. 26, 3763–3779. doi:10.1080/01431160500114706

Hill, R., Hinsley, S., 2015. Airborne lidar for woodland habitat quality monitoring: Exploring the significance of lidar data characteristics when modelling organism-habitat relationships. Remote Sens. 7, 3446–3466. doi:10.3390/rs70403446

Hohenthal, J., Alho, P., Hyyppa, J., Hyyppa, H., 2011. Laser scanning applications in fluvial studies. Prog. Phys. Geogr. 35, 782–809. doi:10.1177/0309133311414605

Hollaus, M., Wagner, W., Eberhöfer, C., Karel, W., 2006. Accuracy of large-scale canopy heights derived from LiDAR data under operational constraints in a complex alpine environment. ISPRS J. Photogramm. Remote Sens. 60, 323–338. doi:10.1016/j.isprsjprs.2006.05.002

Holmgren, J., 2004. Prediction of tree height, basal area and stem volume in forest stands using

airborne laser scanning. Scand. J. For. Res. 19, 543–553. doi:10.1080/02827580410019472

Holopainen, M., Kankare, V., Vastaranta, M., Liang, X., Lin, Y., Vaaja, M., Yu, X., Hyyppä, J., Hyyppä, H., Kaartinen, H., Kukko, A., Tanhuanpää, T., Alho, P., 2013. Tree mapping using airborne, terrestrial and mobile laser scanning - A case study in a heterogeneous urban forest. Urban For. Urban Green. 12, 546–553. doi:10.1016/j.ufug.2013.06.002

Holopainen, M., Vastaranta, M., Hyyppä, J., 2014. Outlook for the next generation's precision forestry in Finland. Forests 5, 1682–1694. doi:10.3390/f5071682

Hyyppä, J., Inkinen, M., 1999. Detecting and estimating attributes for single trees using laser scanner. Photogramm. J. Finl. 16, 27–42.

Ishii, H., McDowell, N., 2002. Age-related development of crown structure in coastal Douglas-fir trees. For. Ecol. Manage. 169, 257–270. doi:10.1016/S0378-1127(01)00751-4

Jones, T.G., Coops, N.C., Sharma, T., 2010. Assessing the utility of airborne hyperspectral and LiDAR data for species distribution mapping in the coastal Pacific Northwest, Canada. Remote Sens. Environ. 114, 2841–2852. doi:10.1016/j.rse.2010.07.002

Jung, J., Pekin, B.K., Pijanowski, B.C., 2013. Mapping open space in an old-growth, secondary-growth, and selectively-logged tropical rainforest using discrete return LIDAR. IEEE J. Sel. Top. Appl. Earth Obs. Remote Sens. 6, 2453–2461. doi:10.1111/j.1472-4642.2012.00928.x

Kaartinen, H., Hyyppä, J., 2008. EuroSDR/ISPRS Project, Commission II "Tree Extraction," Final Report. Dubline, Irland.

Kaartinen, H., Hyyppä, J., Yu, X., Vastaranta, M., Hyyppä, H., Kukko, A., Holopainen, M., Heipke, C., Hirschmugl, M., Morsdorf, F., Næsset, E., Pitkänen, J., Popescu, S., Solberg, S., Wolf, B.M., Wu, J.-C., 2012. An international comparison of individual tree detection and extraction using airborne laser scanning. Remote Sens. 4, 950–974. doi:10.3390/rs4040950

Kandare, K., Dalponte, M., Ørka, H., Frizzera, L., Næsset, E., 2017a. Prediction of species-specific volume using different inventory approaches by fusing airborne laser scanning and hyperspectral data. Remote Sens. 9, 400. doi:10.3390/rs9050400

Kandare, K., Ørka, H.O., Chan, J.C.W., Dalponte, M., 2016. Effects of forest structure and airborne laser scanning point cloud density on 3D delineation of individual tree crowns. Eur. J. Remote Sens. 49, 337–359. doi:10.5721/EuJRS20164919

Kandare, K., Ørka, H.O., Dalponte, M., Næsset, E., Gobakken, T., 2017b. Individual tree crown approach for predicting site index in boreal forests using airborne laser scanning and hyperspectral data. Int. J. Appl. Earth Obs. Geoinf. 60, 72–82. doi:10.1016/j.jag.2017.04.008

Kankare, V., Vastaranta, M., Holopainen, M., Räty, M., Yu, X., Hyyppä, J., Hyyppä, H., Alho, P., Viitala, R., 2013. Retrieval of forest aboveground biomass and stem volume with airborne scanning LiDAR. Remote Sens. 5, 2257–2274. doi:10.3390/rs5052257

Ke, Y., Quackenbush, L.J., 2011. A review of methods for automatic individual tree-crown detection and delineation from passive remote sensing. Int. J. Remote Sens. 32, 4725–4747. doi:10.1080/01431161.2010.494184

Koetz, B., Morsdorf, F., van der Linden, S., Curt, T., Allgöwer, B., 2008. Multi-source land cover classification for forest fire management based on imaging spectrometry and LiDAR data. For. Ecol. Manage. 256, 263–271. doi:10.1016/j.foreco.2008.04.025

Kokaly, R.F., Asner, G.P., Ollinger, S. V., Martin, M.E., Wessman, C.A., 2009. Characterizing canopy biochemistry from imaging spectroscopy and its application to ecosystem studies. Remote Sens. Environ. 113, S78–S91. doi:10.1016/j.rse.2008.10.018

Latifi, H., Fassnacht, F.E., Koch, B., 2012. Forest structure modeling with combined airborne hyperspectral and LiDAR data. Remote Sens. Environ. 121, 10–25. doi:10.1016/j.rse.2012.01.01

Latifi, H., Fassnacht, F.E., Müller, J., Tharani, A., Dech, S., Heurich, M., 2015. Forest inventories by LiDAR data: A comparison of single tree segmentation and metric-based methods for inventories of a heterogeneous temperate forest. Int. J. Appl. Earth Obs. Geoinf. 42, 162–174. doi:10.1016/j.jag.2015.06.008

Lausch, A., Erasmi, S., King, D., Magdon, P., Heurich, M., 2016. Understanding forest health with remote sensing - Part I—A review of spectral traits, processes and remote-sensing characteristics. Remote Sens. 8, 1029. doi:10.3390/rs8121029

Lausch, A., Heurich, M., Gordalla, D., Dobner, H.-J., Gwillym-Margianto, S., Salbach, C., 2013. Forecasting potential bark beetle outbreaks based on spruce forest vitality using hyperspectral remote-sensing techniques at different scales. For. Ecol. Manage. 308, 76–89. doi:10.1016/j.foreco.2013.07.043

Lee, A.C., Lucas, R.M., 2007. A LiDAR-derived canopy density model for tree stem and crown mapping in Australian forests. Remote Sens. Environ. 111, 493–518. doi:10.1016/j.rse.2007.04.018

Lee, J., Coomes, D., Schonlieb, C.-B., Cai, X., Lellmann, J., Dalponte, M., Malhi, Y., Butt, N., Morecroft, M., 2017. A graph cut approach to 3D tree delineation, using integrated airborne LiDAR and hyperspectral imagery.

Lefsky, M.A., Cohen, W.B., Acker, S.A., Parker, G.G., Spies, T.A., Harding, D., 1999. Lidar remote sensing of the canopy structure and biophysical properties of Douglas-fir western hemlock forests. Remote Sens. Environ. 70, 339–361. doi:10.1016/S0034-4257(99)00052-8

Li, M., Im, J., Quackenbush, L.J., Liu, T., 2014. Forest biomass and carbon stock quantification using airborne LiDAR data: A case study over Huntington wildlife forest in the Adirondack park. IEEE J. Sel. Top. Appl. Earth Obs. Remote Sens. 7, 3143–3156. doi:10.1109/JSTARS.2014.2304642

Listopad, C.M.C.S., Masters, R.E., Drake, J., Weishampel, J., Branquinho, C., 2015. Structural diversity indices based on airborne LiDAR as ecological indicators for managing highly dynamic landscapes. Ecol. Indic. 57, 268–279. doi:10.1016/j.ecolind.2015.04.017

Lo, C.-S., Lin, C., 2013. Growth-competition-based stem diameter and volume modeling for tree-level forest inventory using airborne LiDAR data. IEEE Trans. Geosci. Remote Sens. 51, 2216–2226. doi:10.1109/TGRS.2012.2211023

Luo, S., Wang, C., Xi, X., Pan, F., Peng, D., Zou, J., Nie, S., Qin, H., 2017. Fusion of airborne LiDAR data and hyperspectral imagery for aboveground and belowground forest biomass estimation. Ecol. Indic. 73, 378–387. doi:10.1016/j.ecolind.2016.10.001

Maltamo, M., Næsset, E., Vauhkonen, J., 2014. Forestry applications of airborne laser scanning, Managing Forest Ecosystems. Springer Netherlands, Dordrecht. doi:10.1007/978-94-017-8663-8

Maltamo, M., Packalén, P., Suvanto, A., Korhonen, K.T., Mehtätalo, L., Hyvönen, P., 2009. Combining ALS and NFI training data for forest management planning: a case study in Kuortane, Western Finland. Eur. J. For. Res. 128, 305–317. doi:10.1007/s10342-009-0266-6

Maltamo, M., Peuhkurinen, J., Malinen, J., Vauhkonen, J., Packalén, P., Tokola, T., 2009. Predicting tree attributes and quality characteristics of scots pine using airborne laser scanning data. Silva Fenn. 43, 507–521.

Manuri, S., Andersen, H., McGaughey, R.J., Brack, C., 2017. Assessing the influence of return density on estimation of lidar-based aboveground biomass in tropical peat swamp forests of Kalimantan, Indonesia. Int. J. Appl. Earth Obs. Geoinf. 56, 24–35. doi:10.1016/j.jag.2016.11.002

Martinuzzi, S., Vierling, L.A., Gould, W. a., Falkowski, M.J., Evans, J.S., Hudak, A.T., Vierling, K.T., 2009. Mapping snags and understory shrubs for a LiDAR-based assessment of wildlife habitat suitability. Remote Sens. Environ. 113, 2533–2546. doi:10.1016/j.rse.2009.07.002

McElhinny, C., Gibbons, P., Brack, C., Bauhus, J., 2005. Forest and woodland stand structural complexity: Its definition and measurement. For. Ecol. Manage. 218, 1–24. doi:10.1016/j.foreco.2005.08.034

McRoberts, R.E., Tomppo, E.O., 2007. Remote sensing support for national forest inventories. Remote Sens. Environ. 110, 412–419. doi:10.1016/j.rse.2006.09.034

Meng, J., Li, S., Wang, W., Liu, Q., Xie, S., Ma, W., 2016. Estimation of forest structural diversity using the spectral and textural information derived from SPOT-5 satellite images. Remote Sens. 8, 24. doi:10.3390/rs8020125

Morsdorf, F., Meier, E., Kötz, B., Itten, K.I., Dobbertin, M., Allgöwer, B., 2004. LIDAR-based geometric reconstruction of boreal type forest stands at single tree level for forest and wildland fire management. Remote Sens. Environ. 92, 353–362. doi:10.1016/j.rse.2004.05.013

Müller, J., Brandl, R., 2009. Assessing biodiversity by remote sensing in mountainous terrain: The potential of LiDAR to predict forest beetle assemblages. J. Appl. Ecol. 46, 897–905. doi:10.1111/j.1365-2664.2009.01677.x

Murray, H., Lucieer, A., Williams, R., 2010. Texture-based classification of sub-Antarctic vegetation communities on Heard Island. Int. J. Appl. Earth Obs. Geoinf. 12, 138–149. doi:10.1016/j.jag.2010.01.006

Næsset, E., 2002. Predicting forest stand characteristics with airborne scanning laser using a practical two-stage procedure and field data. Remote Sens. Environ. 80, 88–99. doi:10.1016/S0034-4257(01)00290-5

Næsset, E., 2004. Practical large-scale forest stand inventory using a small-footprint airborne scanning laser. Scand. J. For. Res. 19, 164–179. doi:10.1080/02827580310019257

Næsset, E., Gobakken, T., Holmgren, J., Hyyppä, H., Hyyppä, J., Maltamo, M., Nilsson, M., Olsson, H., Persson, Å., Söderman, U., 2004. Laser scanning of forest resources: The nordic experience. Scand. J. For. Res. 19, 482–499. doi:10.1080/02827580410019553

Næsset, E., Økland, T., 2002. Estimating tree height and tree crown properties using airborne scanning laser in a boreal nature reserve. Remote Sens. Environ. 79, 105–115. doi:10.1016/S0034-4257(01)00243-7

Nagendra, H., Lucas, R., Honrado, J.P., Jongman, R.H.G., Tarantino, C., Adamo, M., Mairota, P., 2013. Remote sensing for conservation monitoring: Assessing protected areas, habitat extent, habitat condition, species diversity, and threats. Ecol. Indic. 33, 45–59. doi:10.1016/j.ecolind.2012.09.014

Neumann, M., Starlinger, F., 2001. The significance of different indices for stand structure and diversity in forests. For. Ecol. Manage. 145, 91–106. doi:10.1016/S0378-1127(00)00577-6

Niemann, K.O., 1995. Remote-sensing of forest stand age using airborne spectrometer data. Photogramm. Eng. Remote Sensing 61, 1119–1127.

Ørka, H.O., Dalponte, M., Gobakken, T., Næsset, E., Ene, L.T., 2013. Characterizing forest species composition using multiple remote sensing data sources and inventory approaches. Scand. J. For. Res. 28, 677–688. doi:10.1080/02827581.2013.793386

Ouma, Y.O., Tetuko, J., Tateishi, R., 2008. Analysis of co-occurrence and discrete wavelet transform textures for differentiation of forest and non-forest vegetation in very high resolution optical sensor imagery. Int. J. Remote Sens. 29, 3417–3456. doi:10.1080/01431160701601782

Ozdemir, I., Donoghue, D.N.M., 2013. Modelling tree size diversity from airborne laser scanning using canopy height models with image texture measures. For. Ecol. Manage. 295, 28–37. doi:10.1016/j.foreco.2012.12.044

Packalén, P., Maltamo, M., 2006. Predicting the plot volume by tree species using airborne laser scanning and aerial photographs. For. Sci. 52, 611–622.

Packalén, P., Maltamo, M., 2007. The k-MSN method for the prediction of species-specific stand attributes using airborne laser scanning and aerial photographs. Remote Sens. Environ. 109, 328–341. doi:10.1016/j.rse.2007.01.005

Packalén, P., Temesgen, H., Maltamo, M., 2012. Variable selection strategies for nearest neighbor imputation methods used in remote sensing based forest inventory. Can. J. Remote Sens. 38, 557–569. doi:10.5589/m12-046

Pedersen, R.Ø., Bollandsås, O.M., Gobakken, T., Næsset, E., 2012. Deriving individual tree competition indices from airborne laser scanning. For. Ecol. Manage. 280, 150–165. doi:10.1016/j.foreco.2012.05.043

Persson, Å., Holmgren, J., Soderman, U., 2002. Detecting and measuring individual trees using an airborne laser scanner. Photogrametric Eng. Remote Sens. 68, 925–932.

Peuhkurinen, J., Maltamo, M., Malinen, J., Pitkänen, J., Packalén, P., 2007. Preharvest measurement of marked stands using airborne laser scanning. For. Sci. 53, 653–661.

Peuhkurinen, J., Mehtätalo, L., Maltamo, M., 2011. Comparing individual tree detection and the area-based statistical approach for the retrieval of forest stand characteristics using airborne laser scanning in Scots pine stands. Can. J. For. Res. 41, 583–598. doi:10.1139/X10-223

Polewski, P., Yao, W., Heurich, M., Krzystek, P., Stilla, U., 2015. Detection of fallen trees in ALS point clouds using a Normalized Cut approach trained by simulation. ISPRS J. Photogramm. Remote Sens. 105, 252–271. doi:10.1016/j.isprsjprs.2015.01.010

Pommerening, A., 2002. Approaches to quantifying forest structures. Forestry 75, 305–324. doi:10.1093/forestry/75.3.305

Pommerening, A., 2006. Evaluating structural indices by reversing forest structural analysis. For. Ecol. Manage. 224, 266–277. doi:10.1016/j.foreco.2005.12.039

Pretzsch, H., 2009. Forest dynamics, growth and yield: From Measurement to Model. Springer-Verlag Berlin Heidelberg, Berlin. doi:10.1007/978-3-540-88307-4

Racine, E.B., Coops, N.C., St-Onge, B., Begin, J., 2014. Estimating forest stand age from LiDAR-derived predictors and nearest neighbor imputation. For. Sci. 60, 128–136. doi:10.5849/forsci.12-088

Rahlf, J., Breidenbach, J., Solberg, S., Astrup, R., 2015. Forest parameter prediction using an image-based point cloud: A comparison of semi-ITC with ABA. Forests 6, 4059–4071. doi:10.3390/f6114059

Reitberger, J., Schnörr, C., Krzystek, P., Stilla, U., 2009. 3D segmentation of single trees exploiting

full waveform LIDAR data. ISPRS J. Photogramm. Remote Sens. 64, 561–574. doi:10.1016/j.isprsjprs.2009.04.002

Rennolls, K., 1978. "Top Height"; its definition and estimation. Commonw. For. Rev. 57, 215–219.

Riaño, D., 2003. Modeling airborne laser scanning data for the spatial generation of critical forest parameters in fire behavior modeling. Remote Sens. Environ. 86, 177–186. doi:10.1016/S0034-4257(03)00098-1

Richter, R., Reu, B., Wirth, C., Doktor, D., 2016. The use of airborne hyperspectral data for tree species classification in a species-rich Central European forest area. Int. J. Appl. Earth Obs. Geoinf. 52, 464–474. doi:10.1016/j.jag.2016.07.018

Roberts, D.A., Green, R.O., Adams, J.B., 1997. Temporal and spatial patterns in vegetation and atmospheric properties from AVIRIS. Remote Sens. Environ. 62, 223–240. doi:10.1016/S0034-4257(97)00092-8

Ruiz, L.A., Hermosilla, T., Mauro, F., Godino, M., 2014. Analysis of the influence of plot size and LiDAR density on forest structure attribute estimates. Forests 5, 936–951. doi:10.3390/f5050936

Santos, M.J., Greenberg, J.A., Ustin, S.L., 2010. Using hyperspectral remote sensing to detect and quantify southeastern pine senescence effects in red-cockaded woodpecker (Picoides borealis) habitat. Remote Sens. Environ. 114, 1242–1250. doi:10.1016/j.rse.2010.01.009

Schaepman-Strub, G., Schaepman, M.E., Painter, T.H., Dangel, S., Martonchik, J.V., 2006. Reflectance quantities in optical remote sensing—definitions and case studies. Remote Sens. Environ. 103, 27–42. doi:10.1016/j.rse.2006.03.002

Scrinzi, G., Galvagni, D., Marzullo, L., 2010. I nuovi modelli dendrometrici per la stima delle masse assestamentali in Provincia di Trento. Provincia Autonoma di Trento - Servizio Foreste e Fauna, Trento.

Shang, X., Chisholm, L.A., 2014. Classification of Australian native forest species using hyperspectral remote sensing and machine-learning classification algorithms. IEEE J. Sel. Top. Appl. Earth Obs. Remote Sens. 7, 2481–2489. doi:10.1109/JSTARS.2013.2282166

Sharma, R.P., Brunner, A., Eid, T., Øyen, B.H., 2011. Modelling dominant height growth from national forest inventory individual tree data with short time series and large age errors. For. Ecol. Manage. 262, 2162–2175. doi:10.1016/j.foreco.2011.07.037

Skovsgaard, J.P., Vanclay, J.K., 2008. Forest site productivity: A review of the evolution of dendrometric concepts for even-aged stands. Forestry 81, 13–31. doi:10.1093/forestry/cpm041

Solberg, S., Næsset, E., Bollandsås, O.M., 2006. Single tree segmentation using airborne laser scanner data in a structurally heterogeneous spruce forest. Photogramm. Eng. Remote Sens. 72, 1369–1378. doi:0099-1112/06/7212–1369

St-Onge, B., Vega, C., Fournier, R. a., Hu, Y., 2008. Mapping canopy height using a combination of digital stereo-photogrammetry and lidar. Int. J. Remote Sens. 29, 3343–3364. doi:10.1080/01431160701469040

Stephens, P.R., Kimberley, M.O., Beets, P.N., Paul, T.S.H., Searles, N., Bell, A., Brack, C., Broadley, J., 2012. Airborne scanning LiDAR in a double sampling forest carbon inventory. Remote Sens. Environ. 117, 348–357. doi:10.1016/j.rse.2011.10.009

Strîmbu, V.F., Strîmbu, B.M., 2015. A graph-based segmentation algorithm for tree crown extraction using airborne LiDAR data. ISPRS J. Photogramm. Remote Sens. 104, 30–43.

doi:10.1016/j.isprsjprs.2015.01.018

Swatantran, A., Dubayah, R., Roberts, D., Hofton, M., Blair, J.B., 2011. Mapping biomass and stress in the Sierra Nevada using lidar and hyperspectral data fusion. Remote Sens. Environ. 115, 2917–2930. doi:10.1016/j.rse.2010.08.027

Tesfamichael, S.G., Ahmed, F.B., Van Aardt, J.A.N., 2010. Investigating the impact of discrete-return lidar point density on estimations of mean and dominant plot-level tree height in Eucalyptus grandis plantations. Int. J. Remote Sens. 31, 2925–2940. doi:10.1080/01431160903144086

Tonolli, S., Dalponte, M., Vescovo, L., Rodeghiero, M., Bruzzone, L., Gianelle, D., 2010. Mapping and modeling forest tree volume using forest inventory and airborne laser scanning. Eur. J. For. Res. 130, 569–577. doi:10.1007/s10342-010-0445-5

Torabzadeh, H., Morsdorf, F., Schaepman, M.E., 2014. Fusion of imaging spectroscopy and airborne laser scanning data for characterization of forest ecosystems – A review. ISPRS J. Photogramm. Remote Sens. 97, 25–35. doi:10.1016/j.isprsjprs.2014.08.001

Ung, C.H., Bernier, P.Y., Raulier, F., Fournier, R.A., Lambert, M.C., Régnière, J., 2001. Biophysical site indices for shade tolerant and intolerant boreal species. For. Sci. 47, 83–95.

Ustin, S.L., Roberts, D.A., Gamon, J.A., Asner, G.P., Green, R.O., 2004. Using imaging spectroscopy to study ecosystem processes and properties. Bioscience 54, 523. doi:10.1641/0006-3568(2004)054[0523:UISTSE]2.0.CO;2

Vaglio Laurin, G., Chen, Q., Lindsell, J.A., Coomes, D.A., Frate, F. Del, Guerriero, L., Pirotti, F., Valentini, R., 2014. Above ground biomass estimation in an African tropical forest with lidar and hyperspectral data. ISPRS J. Photogramm. Remote Sens. 89, 49–58. doi:10.1016/j.isprsjprs.2014.01.001

Valbuena, R., Maltamo, M., Marti-Fernandez, S., Packalen, P., Pascual, C., Nabuurs, G.J., 2013. Patterns of covariance between airborne laser scanning metrics and Lorenz curve descriptors of tree size inequality. Can. J. Remote Sens. 39. doi:10.5589/m13-012

van Aardt, J.A.N., Wynne, R.H., 2007. Examining pine spectral separability using hyperspectral data from an airborne sensor: An extension of field-based results. Int. J. Remote Sens. 28, 431–436. doi:10.1080/01431160500444772

Varvia, P., Lähivaara, T., Maltamo, M., Packalen, P., Tokola, T., Seppänen, A., 2016. Uncertainty quantification in ALS-based species-specific growing stock volume estimation. IEEE Trans. Geosci. Remote Sens. in process, 1–11. doi:10.1109/TGRS.2016.2628960

Vauhkonen, J., Seppänen, A., Packalén, P., Tokola, T., 2012. Improving species-specific plot volume estimates based on airborne laser scanning and image data using alpha shape metrics and balanced field data. Remote Sens. Environ. 124, 534–541. doi:10.1016/j.rse.2012.06.002

Voss, M., Sugumaran, R., 2008. Seasonal effect on tree species classification in an urban environment using hyperspectral data, LiDAR, and an object-oriented approach. Sensors 8, 3020–3036. doi:10.3390/s8053020

Wang, Y., Hyyppä, J., Liang, X., Kaartinen, H., Yu, X., Lindberg, E., Holmgren, J., Qin, Y., Mallet, C., Ferraz, A., Torabzadeh, H., Morsdorf, F., Zhu, L., Liu, J., Alho, P., 2016. International benchmarking of the individual tree detection methods for modeling 3-D canopy structure for silviculture and forest ecology using airborne laser scanning. IEEE Trans. Geosci. Remote Sens. 54, 5011–5027. doi:10.1109/TGRS.2016.2543225

Wehr, A., Lohr, U., 1999. Airborne laser scanning - an introduction and overview. ISPRS J. Photogramm. Remote Sens. 54, 68–82. doi:10.1016/S0924-2716(99)00011-8

White, J.C., Coops, N.C., Wulder, M.A., Vastaranta, M., Hilker, T., Tompalski, P., 2016. Remote sensing technologies for enhancing forest inventories: A review. Can. J. Remote Sens. 42, 619–641. doi:10.1080/07038992.2016.1207484

Wing, B.M., Ritchie, M.W., Boston, K., Cohen, W.B., Gitelman, A., Olsen, M.J., 2012. Prediction of understory vegetation cover with airborne lidar in an interior ponderosa pine forest. Remote Sens. Environ. 124, 730–741. doi:10.1016/j.rse.2012.06.024

Yao, W., Krull, J., Krzystek, P., Heurich, M., 2014. Sensitivity analysis of 3D individual tree detection from LiDAR point clouds of temperate forests. Forests 5, 1122–1142. doi:10.3390/f5061122

Yu, B., Ostland, I.M., Gong, P., Pu, R.L., 1999. Penalized discriminant analysis of in situ hyperspectral data for conifer species recognition. IEEE Trans. Geosci. Remote Sens. 37, 2569–2577. doi:10.1109/36.789651

Yu, X., Hyyppä, J., Holopainen, M., Vastaranta, M., 2010. Comparison of area-based and individual tree-based methods for predicting plot-level forest attributes. Remote Sens. 2, 1481–1495. doi:10.3390/rs2061481

Yu, X., Hyyppä, J., Karjalainen, M., Nurminen, K., Karila, K., Vastaranta, M., Kankare, V., Kaartinen, H., Holopainen, M., Honkavaara, E., Kukko, A., Jaakkola, A., Liang, X., Wang, Y., Hyyppä, H., Katoh, M., 2015. Comparison of laser and stereo optical, SAR and InSAR point clouds from air- and space-borne sources in the retrieval of forest inventory attributes. Remote Sens. 7, 15933–15954. doi:10.3390/rs71215809

Yu, X., Hyyppä, J., Vastaranta, M., Holopainen, M., Viitala, R., 2011. Predicting individual tree attributes from airborne laser point clouds based on the random forests technique. ISPRS J. Photogramm. Remote Sens. 66, 28–37. doi:DOI: 10.1016/j.isprsjprs.2010.08.003

Zhang, J., 2010. Multi-source remote sensing data fusion: status and trends. Int. J. Image Data Fusion 1, 5–24. doi:10.1080/19479830903561035

Paper I

European Journal of Remote Sensing - 2016, 49: 337-359
doi: 10.5721/EuJRS20164919
Received 04/09/2015 accepted 23/06/2016

European Journal of Remote Sensing
An official journal of the Italian Society of Remote Sensing

www.aitjournal.com

Effects of forest structure and airborne laser scanning point cloud density on 3D delineation of individual tree crowns

Kaja Kandare[1,2]*, Hans Ole Ørka[2], Jonathan Cheung-Wai Chan[1,3] and Michele Dalponte[4]

[1]FoxLab, Joint CNR-FEM Initiative, Fondazione E. Mach,
Via E. Mach 1, 38010, San Michele all'Adige (TN), Italy
[2]Department of Ecology and Natural Resource Management,
Norwegian University of Life Sciences, P.O. Box 5003, N-1432 Ås, Norway
[3]Department of Electronics and Informatics (ETRO), Vrije Universiteit Brussel,
Pleinlaan 2, 1050, Brussels, Belgium
[4]Department of Sustainable Agro-ecosystems and Bioresources, Research and Innovation Centre,
Fondazione E. Mach, Via E. Mach 1, 38010, San Michele all'Adige (TN), Italy
*Corresponding author, e-mail address: kaja.kandare@fmach.it

Abstract
This paper presents a 3D delineation method for airborne laser scanning point cloud. The method is based on an unsupervised clustering technique applied on horizontal slices followed by vertical merging based on overlapping among clusters. On an Alpine forest dataset, we analysed the effects of different forest structures and point cloud densities on tree crown delineation. Forest structure affects mainly the omission error, which eases with homogeneous tree spacing and sizes, while on the commission error forest structure has only slight effect. Delineation accuracy increases with higher point densities where Mann-Whitney-Wilcoxon test shows that accuracy differences between thinned data and original data are statistically significant.
Keywords: 3D delineation, ITC, ALS, point density, forest structure, alpine forest.

Introduction
Airborne laser scanning (ALS) data allows us to analyze large areas and to provide accurate up-to-date information about the composition, distribution and condition of forests. ALS data has become a common data source used for the estimation of forest biophysical attributes at stand level such as mean tree height, basal area (*BA*) and volume per hectare [Næsset, 2002], and also at tree level such as tree height, diameter at breast height (*DBH*) and stem volume [Hyyppä et al., 2001]. Individual trees are the basic and smallest unit on which forest management is carried out. The first processing step for tree-level inventories using ALS data is typically the delineation of individual tree crowns (ITCs). Then, for each ITC, attributes such as tree position, tree height, stem *DBH* and stem volume are estimated

[Hyyppä et al., 2001]. In inventory practice, many attributes have to be estimated at the tree level in order to be useful. Individual tree coordinates, for instance, are needed for harvesting operations and growth predictions [Pedersen et al., 2012]. ITC approaches are used also in operational urban tree mapping, and monitoring [Holopainen et al., 2013]. When combined with multispectral or hyperspectral images, ITC approaches could provide species information for each tree [Ørka et al., 2013]. Other recent works have shown that ITC delineation could provide supplementary information for area-based prediction of forest variables [Hyyppä et al., 2012] with reduce edge-effects [Packalen et al., 2015].

Numerous ITC detection methods for ALS data have been proposed in the last two decades [Hyyppä and Inkinen, 1999; Brandtberg et al., 2003; Solberg et al., 2006; Tang et al., 2007; Ferraz et al., 2012; Duncanson et al., 2014]. The first ITC delineation methods proposed in the literature used a 2D canopy height model (CHM) which is interpolated from the normalized ALS heights. Individual trees were delineated by defining a crown around local maximum. The most common 2D delineation methods are region growing [Hyyppä and Inkinen, 1999; Hyyppä et al., 2001; Solberg et al., 2006], multi-scale techniques [Persson et al., 2002; Brandtberg et al., 2003] or watershed segmentation [Tang et al., 2007; Ene et al., 2012]. However, the majority of these delineation methods can detect only trees that are well visible in the uppermost canopy layer, whereas intermediate and suppressed trees are rarely detected. Furthermore, while these 2D methods provided at times good results, the accuracy of delineated ITCs is strongly dependent on the quality of the CHM [Ene et al., 2012]. Indeed, generating a CHM from an ALS point cloud resulted in loss of information. Alternatively, if higher point density data are available, advanced 3D methods can refine the initial CHM-based delineation. 3D point clouds are often used to characterize a vertical structure of heterogeneous canopies. However, effective processing of high point density data is still a challenging task. Many methods delineated tree crowns by various 3D clustering analysis, namely: K-means [Morsdorf et al., 2004; Gupta et al., 2010], adaptive and agglomerative clustering [Lee et al., 2010; Gupta et al., 2010], mean shift clustering [Ferraz et al., 2012] and ellipsoidal clustering [Lindberg et al., 2014]. Some of these clustering methods were also combined with surface models or CHM. Other 3D delineation methods first generated a preliminary watershed segmentation of the CHM to define tree segments and afterwards separated trees within each segment by normalized cut segmentation [Shi and Malik, 2000] on the ALS point cloud [Reitberger et al., 2009], or by a trough-finding algorithm on the ALS height histogram [Duncanson et al., 2014]. Some delineation methods first delineated tree crowns on the 2D horizontal projection images at different height levels, and then the 'tree' segments delineated from various layers were combined to form 3D tree crowns [Wang et al., 2008; Tang et al., 2013]. Some 3D methods are very particular in their approach [Li et al., 2012; Lähivaara et al., 2014; Lu et al., 2014]. Li et al. [2012] delineated ITCs based on object-oriented classification rules such as tree proximity and shape criteria. Using a prior information on tree shapes Lähivaara et al. [2014] applied Bayesian estimation for 3D delineation. For identifying tree trunk points, Lu et al. [2014] used the ALS intensities and then points belonging to the same tree were defined by topology relationship.

While there are many 3D delineation methods proposed in the literature, they are not all adequately validated as important accuracy measures such as omission and commission errors, or errors are not reported [e.g. Gupta et al., 2010; Tang et al., 2013]. When an ITC

delineation method fail to detect individual trees present, it leads to omission errors. When one tree is split in multiple ITCs, it leads to a commission error. Many 3D methods seem to have a high commission error [Kaartinen et al., 2012; Eysn et al., 2015]. The absence of a well-established or benchmark method is making the comparison of performance among various methods difficult. Furthermore, few methods were tested in different forest conditions in terms of complexity. As forest structure usually affects the performance of delineation, its influence should be described and assessed using measures such as spatial arrangement, size variation of trees and structural diversity [Neumann and Starlinger, 2001; McElhinny et al., 2005; Lexerød and Eid, 2006; O'Hara et al., 2007].

New ALS technologies gather data at very high point density, which allows for development of 3D delineation methods. To our knowledge, no reported studies have analyzed the influence of point density higher than 30 pulses m^{-2} on ITC delineation. In this work, we tested a 3D delineation method for a very high-density ALS point cloud data (approx. 60 pulses m^{-2}). The forests are characterized by different structures: from mixed to pure stands, and from unevenly to evenly aged stands. Using field measurements, we evaluated the performances of the proposed 3D method in terms of delineation accuracy as well as tree attributes estimation. Finally, we qualitatively assessed the proposed method and compared it with a selected popular method (Reference delineation method). It would be important to evaluate the ITC delineation method with respect to various forest structures and point cloud densities. To this end, our objectives are two folds:

i. to understand the effect of forest structure on the delineation performance;
ii. to understand the effect of point density on the delineation performance.

Given the high point density made available to this study, we have the opportunity to assess the saturation of information intrinsic in ALS point cloud density with respect to tree delineation applications. Testing high-density ALS data may shed some light on whether it is worthwhile to acquire expensive high-density data for ITC studies.

Data set description

Study area

The 32 km^2 study area is located in the municipality of Pellizzano (46°17'22''N, 10°46'05''E) in the Italian Alps (Fig. 1). The forest structure is complex, with patches of mixed and pure tree species composition [Dalponte and Coomes, 2016]. Norway spruce (*Picea abies* (L.) H. Karst.) represents around 65% of the total stem volume, European larch (*Larix decidua* Mill.) around 25%, and the remaining 10% consists of other conifers (i.e. Silver fir (*Abies alba* Mill.), Swiss stone pine (*Pinus cembra* L.) and broadleaves (i.e. Silver birch (*Betula pendula* Roth), Common alder (*Alnus glutinosa* (L.) Gaertn.), Sycamore maple (*Acer pseudoplatanus* L.), Rowan (*Sorbus aucuparia* (L.) Crantz)). The topography varies considerably, with altitude ranging between 850 m and 2700 m and some areas characterized by very steep slopes. Vegetation varies from meadows in the higher parts of the study area to very dense forest in the lower parts. The area has been managed since 1950 with silvicultural plans carried out every 10 years. Selective logging is done with the help of cableway focusing on productive wood (e.g. Norway spruce). The harvesting methods are different depending on the forest structure and species present.

Figure 1 - Location of study area in Pellizzano, province of Trento in Italy.

Airborne Laser Scanner data

The data acquisition was carried out between 7th and 9th of September 2012 using a Riegl LMS-Q680i laser scanner. The system mounted on a Multi Mission Aircraft was optimized to measure canopy structure with a flying speed of about 51 m/s at an altitude of 660 m above ground level. The scan frequency was 400 kHz with a 60° field of view and the overlap for each stripe was at least 30%. Up to five returns were recorded for each emitted pulse and the mean point density was approximately 60 pulses m^{-2}. A Digital Terrain Model (DTM) was generated with TerraScan software with a grid size of 0.5 m. ALS point cloud was normalized to obtain a canopy height by subtracting the DTM from the z values of the ALS pulses. Figure 2a shows a common example of field plot and Figure 2b is an example of Norway spruces.

Field data

Field data were collected in the summers of 2013 and 2014. 14 plots were surveyed in forest stands with various structure and topography (mean slope is 20.4° with standard deviation at ± 6.7°). The plot radius was 15 m for six plots and 20 m for the remaining ones. The center location of each plot was measured with a GPS/GLONASS system resulting in a position error of less than 1 m. Furthermore, all trees on the plots were measured and the location was recorded as a reference to the center of the plot (azimuth and range). In total,

735 trees were measured across the plots. For each tree, the *DBH* along two orthogonal directions, the tree species, and the crown area were measured. Crown area was calculated from the field-measured distances north, south, east and west directions from the trunk center to the crown boundary assuming an ellipsoidal shape. Tree heights were measured on 66% of the trees using a Vertex III hypsometer. Tree heights for the remaining 34% trees were estimated with allometric equations [Scrinzi et al., 2010]. The allometric derived heights are overestimated compared to the field measured ones for 1.2 m with a RMSE of 2.35 m. The horizontal and vertical accuracies for an individual tree measurement are within ± 1 m error range. In each plot, only trees with a *DBH* greater than or equal to 5 cm were considered in the analyses. Dead or damaged trees without crown were excluded from further process. The total number of trees across all plots was 685. Table 1 summarizes the field data.

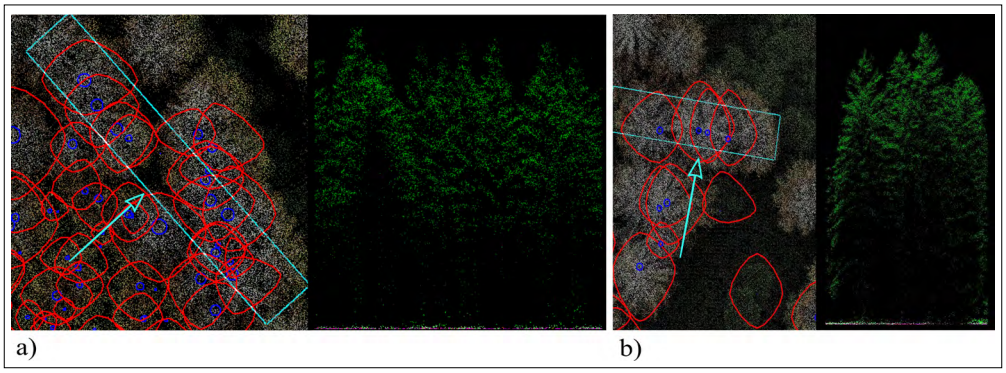

Figure 2 - a) Common plot structure. b) Group of four Norway spruces with five treetops. The last tree in the row has two tops growing from the same stem. On the left side of both figures there is a top view of the ALS point cloud. The light blue rectangles show the area of interest and the arrows show the view direction of the side view on the right side. The top view is overlaid with the field-measured stem positions marked with blue circles, and the field-measured tree crowns marked with red polygons. Polygons without stem position are bushes.

Table 1 - Summary of the field measurements at both tree and plot levels. *DBH* = Diameter at Breast Height (1.30 m), *BA* = basal area.

		Minimum	Maximum	Mean
Tree level	*DBH* [cm]	5.0	89.0	32.3
	Tree height [m]	2.5	39.8	21.5
	Crown area [m^2]	0.03	123.70	17.06
	Number of stems/plot	11	132	49
Plot level	Mean *DBH* [cm]	21.7	58.1	36.7
	Number of stems/ha	127	1050	502
	Gini coefficient of *BA*	0.19	0.65	0.46
	BA [m^2/ha]	35.7	77.8	55.0

Methods

3D delineation method

Figure 3 summarizes the four steps of the proposed 3D delineation method. In the preprocessing, the ALS point cloud with *X, Y, Z* coordinates is normalized and the ALS points with normalized *Z* coordinates (height) lower than 1.5 m are not used to avoid negative effects due to terrain objects and herbaceous vegetation. The point cloud is horizontally sliced. Within each slice, points are spatially clustered through several steps. The processes and parameters are described in detail in the following subsections.

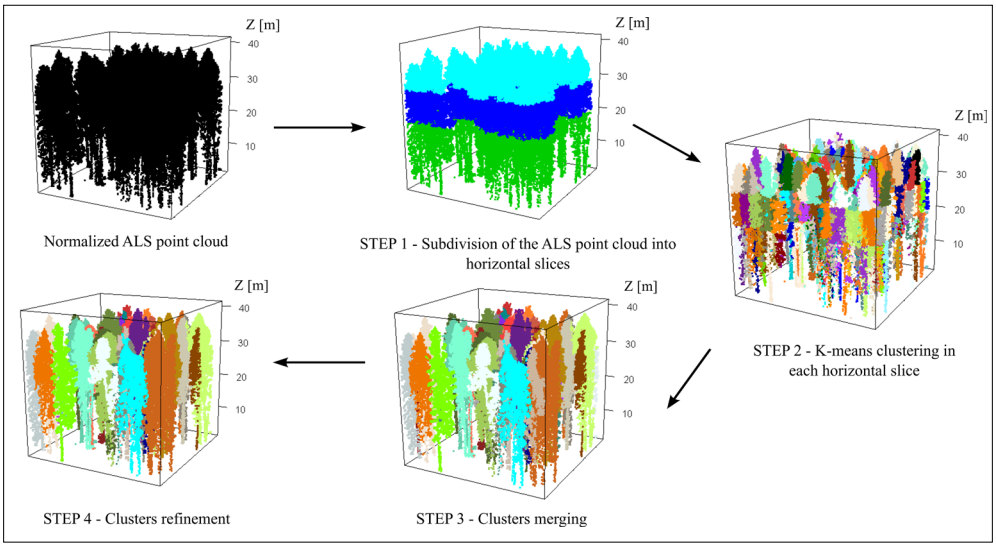

Figure 3 - Overview of the 3D individual tree crown delineation method. *Z* represents normalized heights of an ALS point cloud.

Step 1 - Subdivision of the ALS point cloud into horizontal slices

The initial point cloud is subdivided into three horizontal slices by Otsu thresholding [Otsu, 1979]. Otsu determines global thresholds which minimize the within-class variance. It is a popular method used by some ITC delineation studies for selecting threshold values [Ene et al., 2012; Dalponte et al., 2015].

Step 2 - K-means clustering in each horizontal slice

In each horizontal slice a CHM with 0.5 m resolution is created and a local maxima (LM) filtering is applied using a moving window with different sizes. The size of the moving window is user-defined and can vary for different horizontal slices. Using the position of the LM in each slice as centers, a K-means clustering algorithm is applied to generate clusters in each slice. We used the implementation of the R-package *stats* version 2.15.3. For each resulting clusters the *X* and *Y* cluster center coordinates are defined as arithmetic mean of *X* and *Y* coordinates of the points in each cluster.

As moving window is set empirically, a sensitivity analysis is carried out on three moving windows (ws) with the same sizes at each horizontal slice (Tab. 2). Based on the results of

the previous sensitivity analysis, we further inspected windows (*w*) (with different sizes among the three horizontal slices (Tab. 3).

Step 3 - Clusters merging

The K-means clusters are merged across all slices. The merging starts with the highest clusters (defined by the highest point of each cluster) as the tallest trees are well visible in the uppermost canopy layer. The lower clusters are assigned to the highest cluster if the 2D Euclidean distances between the lower cluster centers and the highest cluster center are within a predefined radius calculated as *w**CHM. This radius value is defined differently depending on to which horizontal slice the highest cluster belongs to. Each iteration will start with a new highest cluster, which has not been already assigned to the previous highest clusters. At the end of all iterations, all initial K-means clusters with the same assignment are merged into the same cluster.

Table 2 - Combinations of four cubic moving window sizes.

	ws1	*ws2*	*ws3*	*ws4*
Top slice	11	9	7	5
Middle slice	11	9	7	5
Bottom slice	11	9	7	5

Table 3 - Combinations of four moving window sizes, altering the window size in different slices.

	w1	*w2*	*w3*	*w4*
Top slice	9	9	9	7
Middle slice	9	9	7	7
Bottom slice	9	7	7	7

Step 4 - Clusters refinement

Clusters resulted from Step 3 are sorted by height in the same way as in the previous step. Starting with the highest clusters, neighboring clusters are merged based on an overlapping area criterion. The overlapping area is defined as the percentage of the overlapping points with respect to the total number of points within the cluster. Overlapping percentage for both considered clusters are calculated and if any of the two overlapping percentages is higher than the threshold *OA*[%], they are merged. Otherwise, the next neighboring cluster with an overlapping is considered. The described procedure is repeated for all lower clusters and then the same process is replicated for the next highest cluster. All merging is completed at the end of this step. The resulting clusters are projected onto the horizontal plane. For each plot, an expected minimum crown area (*MinA*) is defined (e.g. 2 m²). If the projected crown area is smaller than *MinA*, the cluster is removed.

To better define the overlapping criterion for merging, we have carried out another sensitivity analysis to test *OA* thresholds from 40% up to 70%. The *MinA* used in this study is obtained from the field measurements (Tab. 1). The constraint was used to avoid clusters that are too small, which could be a result of noise. In the situation where the field reference data

are missing *MinA* can be approximated using a semivariogram analysis [Woodcock et al., 1988], a preliminary watershed segmentation, or by measurements recorded in a previous forest inventory.

Step 5 - Delineation of Individual Tree Crowns

The tree clusters represent ITCs, which are delineated as convex hulls. Tree attributes including tree position, tree height and crown area are generated. The ITC position *(X, Y)* and the tree height *(Z)* are extracted using the highest ALS point within a tree cluster. The crown area is computed as the convex hull of the *X* and *Y* coordinates of the tree cluster.

Reference delineation method

To generate a reference individual tree crown data set, we used a delineation method that exploits both CHM and ALS point cloud with normalized *Z* coordinates, implemented in the R-package *itcSegment*. First, a CHM is generated with a spatial resolution of 0.5 m using a nearest neighbor interpolation and then smoothed by a Gaussian low-pass filter (LPF) with a 3x3 moving window. A set of seed points $S=\{s_1,\ldots,s_N\}$ is defined using a filter based on local maxima. For pixels higher than 2.5 m, a LPF with a 5x5 moving window was used. A region map L is defined as $L_{i,j} = k$ if (I, j) is a seed point with index k, otherwise $L_{i,j} = 0$. Starting from L, regions grow according to the following procedure: considering a region map point $L_{i,j} \neq 0$ and taking its neighbor pixels in the CHM. A neighbor pixel is added to the region n if all three conditions are fulfilled: i) the distance between the neighbor pixel and the seed point s_n is smaller than 10 m; ii) the height of the considered neighbor pixel is greater than the height of the seed point s_n multiplied by a user-defined parameter called $Perc_{Tresh}$ varying between 0 and 1. The value was set to 0.7. This procedure is repeated until no more pixels are added to any regions. From each region the first returns are extracted and Otsu thresholding [Otsu, 1979] is applied to the normalized heights. Using first returns that are higher than the Otsu threshold, 2D convex hulls are generated from the *X* and *Y* coordinates to create the final ITCs.

Design of experiment

Accuracy assessment

For accuracy assessment, we followed the tree matching process introduced by Eysn et al. [2015]. If several field-measured trees matched with the same ITC derived from ALS data, only the one with shortest 2D distance and shortest height difference was compared. The performances of the delineation methods were evaluated using three delineation accuracy measures: omission error (*OE*), commission error (*CE*), and accuracy index (*AI*). The ratio between the number of field trees that were not delineated (C_F) and the actual number of field-measured trees (N_F) defined the *OE* [Eq.1]). The ratio between the number of ITCs that were not matched (C_{ITC}) with a field measurement and the number of field-measured trees (N_F) defined the *CE* [Eq. 2]:

$$OE = \frac{C_F}{N_F} 100\% \quad [1]$$

$$CE = \frac{C_{ITC}}{N_F} 100\% \quad [2]$$

The *AI* [Pouliot et al., 2005] incorporates both error types into a single metric:

$$AI = 100\% - (OE + CE) \quad [3]$$

The same accuracy measures were used in the sensitivity analysis. The setting of *w* and *OA*, which achieved the highest *AI* were selected for the remaining experiments.
The accuracy of tree attributes was assessed for the *n* correctly detected trees by mean differences (*MD*) and Root-mean-square errors (*RMSE*) as:

$$MD = \frac{\sum_{i=1}^{n} e_i}{n} \quad [4]$$

$$RMSE = \sqrt{\frac{\sum_{i=1}^{n} e_i^2}{n}} \quad [5]$$

where e_i for the tree height and crown area was calculated as the difference between the field-derived and the ALS-derived estimates. For the tree position, e_i was computed by Euclidean distance between the field measurement and the ALS estimated position. The relationship between ITC attributes estimated from the ALS data and the field measurements was assessed by coefficient of determination (r^2) (or square of the Pearson correlation coefficient). We also qualitatively evaluated our results against the Reference delineation method that was proved to work successfully in a comparative study in Alpine forests as Method 2 described in Eysn et al. [2015].

Forest structure

Forest structure refers to attributes that quantify the forest such as spatial arrangement and size of trees. We selected four measures to characterize forest structure: mean *DBH*, number of stems per hectare, mean nearest neighbor distance and Gini coefficient of basal area. *DBH* is a measure of tree size and the number of stems per hectare is a measure of density. Furthermore, mean nearest neighbor distance is used to describe the variation of tree spacing. Structural diversity which is related to dimeter distribution can be assessed with different indices (e.g. Shannon index, Simpson index, Gini coefficient). On the basis of previous studies the Gini coefficient was found to be the most suitable [Lexerød and Eid, 2006; O'Hara et al., 2007]. We used the Gini coefficient [Gini, 1912] to describe the level of homogeneity or heterogeneity of the forest [Bollandsås et al., 2008]. The Gini coefficient values are bound between zero (indicating homogeneous) and one (indicating heterogeneous). Hence, uneven aged stands would have higher Gini coefficient values than even aged stands.

Data thinning

In order to test the robustness of the 3D delineation method with low point densities, the original ALS data (with mean pulse density of 60 pulses m^{-2}) were thinned. In particular, the following mean point densities were considered: 50, 30, 20, 10, 6 and 4 pulses m^{-2} (Fig. 4). The data thinning of ALS data was executed on pulse level using the module *lasthin* of the LAStools software, a popular tool to test effects of point density on forest attributes [Jakubowski et al., 2013]. To maintain the fairly regular spatial distribution of the ALS pulses, the thinning was performed on randomly selected points from different grid sizes to obtain lower point densities. A similar approach was used by Hansen et al. [2015]. The thinning of each point density was repeated ten times and our delineation method was applied to each of the ten thinnings. At the end, the average delineation accuracy of ten thinnings in terms of *AI* was calculated. To test if the differences among accuracies obtained with thinned and original data were significant, we carried out a two-sided Mann-Whitney-Wilcoxon test.

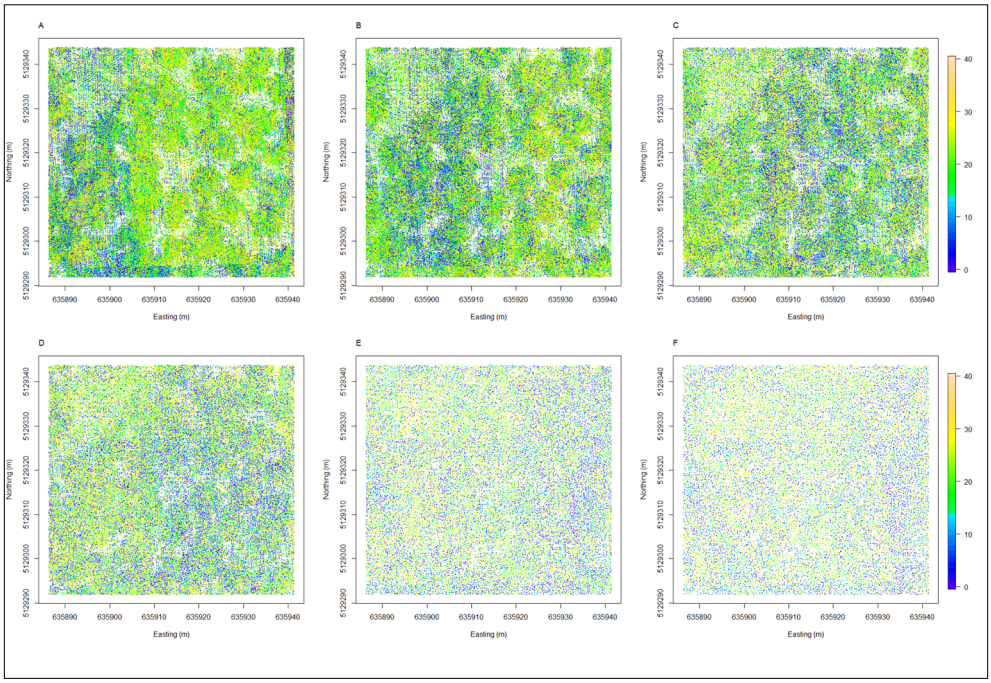

Figure 4 - The area of a plot with different pulse densities: a) 60 pulses m^{-2}; b) 30 pulses m^{-2}; c) 20 pulses m^{-2}; d) 10 pulses m^{-2}; e) 6 pulses m^{-2}; f) 4 pulses m^{-2}.

Results

Sensitivity analysis

To understand the relationship between accuracy and window size for initial clustering, we started with cubic windows or a box where window size was the same in all three slices (Tab. 2). According to Popescu et al. [2002] if the window size is too large, the

delineation method tends to have higher *OE*. On the opposite if the window size is too small, the delineation method tends to have higher *CE*. Our results in Table 4 confirmed the findings of abovementioned report and showed that the best compromise between *OE* and *CE* was obtained by moving windows *ws*2 (9, 9, 9) and *ws*3 (7, 7, 7), which reached substantially higher *AI* (around 34%) than *ws*1 (11, 11, 11) and *ws*4 (5, 5, 5). Assuming that the uppermost canopy layer has a high pulse density and larger crowns, the clusters of pulses on the top slice should be larger. The pulse density drops below the canopy and so the crown size, thus the clusters of pulses should be smaller in the lower slices. Thus, we decided to investigate several configurations of *w* where window size format for lower slices are smaller resembling a vertical pulse density distribution scenario that could be more appropriate and corresponding to the geometry of a tree. Table 3 lists the experimented configurations *w* (*bottom, middle, top*): *w*1 (9, 9, 9), *w*2 (7 ,9, 9), *w*3 (7, 7, 9) and *w*4 (7, 7, 7). Table 5 presents the sensitivity analysis results for the original point density at 60 pulses per m^{-2} for window sizes from *w*1 to *w*4 and for overlapping area from 40% to 70%. From Table 5 it is evident that an increase of the overlapping area from 40% to 70% increases the *CE* and decreases the *OE*. In terms of overlapping, both 50% and 60% provided the best results. If we would exclude *w*4 where the range of accuracy for different overlappings are significantly higher, the *AI* differences for other window sizes for different overlappings are only marginal at around 1% or less. The *CE* and *OE* of different window configurations showed expected tendency as above-mentioned. However, altering window size at lower slices did not lead to higher delineation accuracy and there were no other patterns observed. As the combination of window size *w*1(9, 9, 9) and overlapping area at 50% had the highest accuracy, it was chosen as the setting for the remaining analysis.

The sensitivity analysis for the thinned data was also performed. The highest accuracies are highlighted in Tables 6 to 11. For each of the thinned point densities we produced ten random thinnings. For each parameter combination, the mean *AI* is showed. It emerged that window sizes *w*1, *w*2, and *w*3 reached quite similar results with overlapping areas at 40% and 50%, and their differences were within the range of around 1%.

Table 4 - Omission error (*OE* [%]), commission error (*CE* [%]), accuracy index (*AI* [%]) and number of detected ITCs (N) on the original point cloud carried out with different window sizes (*w*($slice_{low}$, $slice_{middle}$, $slice_{top}$)) and overlapping areas (*OA*).

	***ws*1 (11, 11, 11)**				***ws*2 (9, 9, 9)**				***ws*3 (7, 7, 7)**				***ws*4 (5, 5, 5)**			
OA	***OE***	***CE***	***AI***	***N***	***OE***	***CE***	***AI***	***N***	***OE***	***CE***	***AI***	***N***	***OE***	***CE***	***AI***	***N***
40%	74.3	1.8	23.9	156	64.0	3.2	32.9	222	53.5	14.5	32.3	353	37.6	59.5	2.9	720
50%	70.5	2.4	27.2	179	60.3	5.5	34.3	256	51.4	18.3	30.4	392	34.6	71.8	-6.3	812
60%	69.2	2.8	27.9	189	58.5	7.5	34.0	275	50.1	23.8	26.1	428	33.2	78.5	-11.7	862
70%	68.9	3.7	27.4	195	57.8	9.3	32.9	290	48.5	27.3	24.2	458	32.3	85.5	-17.8	907

Table 5 - Omission error (*OE* [%]), commission error (*CE* [%]) and accuracy index (*AI* [%]) on the original point cloud carried out with different window sizes ($w(slice_{low}, slice_{middle}, slice_{top})$) and overlapping areas (*OA*).

	w1 (9, 9, 9)			*w2* (7, 9, 9)			*w3* (7, 7, 9)			*w4* (7, 7, 7)		
OA	***OE***	***CE***	***AI***	***OE***	***CE***	***AI***	***OE***	***CE***	***AI***	***OE***	***CE***	***AI***
40%	64.0	3.2	32.9	63.2	3.7	33.1	61.9	5.6	32.4	53.5	14.5	32.3
50%	60.3	5.5	34.3	60.7	5.8	33.5	58.4	8.3	33.3	51.4	18.3	30.4
60%	58.5	7.5	34.0	59.6	7.1	33.3	56.4	9.8	33.8	50.1	23.8	26.1
70%	57.8	9.3	32.9	58.7	8.8	32.6	55.3	12.2	32.6	48.5	27.3	24.2

Table 6 - Accuracy index (*AI* [%]) obtained by sensitivity analysis for point density of 4 pulses m^{-2} carried out with different parameter settings ($w(slice_{low}, slice_{middle}, slice_{top})$ = window size, *OA* = overlapping area).

OA	***w1* (9, 9, 9)**	***w2* (7, 9, 9)**	***w3* (7, 7, 9)**	***w4* (7, 7, 7)**
40%	**28.2**	28.0	27.6	24.8
50%	27.5	27.5	27.7	23.1
60%	27.4	27.0	27.0	22.1
70%	27.0	26.7	26.6	21.4

ITC delineation

The results of *OE*, *CE* and *AI* of the proposed and the Reference delineation method were presented as the average over all plots. The delineation accuracy in terms of *OE*, *CE* and *AI* for the proposed method were 60.3%, 5.5%, 34.3%, respectively; for the Reference delineation method, they were 57.4%, 8.6%, 34.0%, respectively. In summary, there was only a marginal difference in terms of *AI* between the proposed 3D method and the Reference delineation method, with the 3D method achieving lower *CE* with slightly higher *OE*.

Table 7 - Accuracy index obtained by sensitivity analysis for point density of 6 pulses m^{-2} carried out with different parameter settings ($w(slice_{low}, slice_{middle}, slice_{top})$ = window size, *OA* = overlapping area).

OA	***w1* (9, 9, 9)**	***w2* (7, 9, 9)**	***w3* (7, 7, 9)**	***w4* (7, 7, 7)**
40%	28.8	28.9	28.8	25.7
50%	**29.0**	28.5	28.8	23.2
60%	28.7	28.2	27.9	21.9
70%	27.8	27.8	27.4	21.4

Table 8 - Accuracy index obtained by sensitivity analysis for point density of 10 pulses m^{-2} carried out with different parameter settings ($w(slice_{low}, slice_{middle}, slice_{top})$ = window size, *OA* = overlapping area).

OA	*w1* (9, 9, 9)	*w2* (7, 9, 9)	*w3* (7, 7, 9)	*w4* (7, 7, 7)
40%	28.9	28.8	**30.0**	26.4
50%	29.2	28. 9	29.2	23.8
60%	28.6	27.9	28.4	21.9
70%	28.2	27.5	27.6	20.0

Table 9 - Accuracy index obtained by sensitivity analysis for point density of 20 pulses m^{-2} carried out with different parameter settings ($w(slice_{low}, slice_{middle}, slice_{top})$ = window size, *OA* = overlapping area).

OA	*w1* (9, 9, 9)	*w2* (7, 9, 9)	*w3* (7, 7, 9)	*w4* (7, 7, 7)
40%	29.3	**30.2**	29.7	25.9
50%	29.4	29.7	29.6	23.3
60%	28.7	28.2	28.4	21.5
70%	27.1	26.8	27.3	19.7

Table 10 - Accuracy index obtained by sensitivity analysis for point density of 30 pulses m^{-2} carried out with different parameter settings ($w(slice_{low}, slice_{middle}, slice_{top})$ = window size, *OA* = overlapping area).

OA	*w1* (9, 9, 9)	*w2* (7, 9, 9)	*w3* (7, 7, 9)	*w4* (7, 7, 7)
40%	30.1	29.9	29.5	27.5
50%	**30.6**	30.1	29.6	25.2
60%	29.9	29.1	29.2	23.0
70%	28.8	28.3	28.2	21.0

Table 11 - Accuracy index obtained by sensitivity analysis for point density of 50 pulses m^{-2} carried out with different parameter settings ($w(slice_{low}, slice_{middle}, slice_{top})$ = window size, *OA* = overlapping area).

OA	*w1* (9, 9, 9)	*w2* (7, 9, 9)	*w3* (7, 7, 9)	*w4* (7, 7, 7)
40%	29. 9	30.8	30.7	29.4
50%	30.2	30.8	**31.0**	27.8
60%	29.5	30.0	30.3	25.4
70%	29.0	29.3	29.4	22.5

ITC attributes estimation

For the correctly delineated ITCs the accuracies of tree position, crown area and tree height are showed in Table 12. The accuracies of the tree positions estimated by the proposed 3D delineation method and the Reference delineation method were 2.13 m and 2.33 m, respectively. Regarding the crown area the 3D method overestimated its value (*MD* = 9.77 m^2) while the Reference delineation method achieved better results (MD = 5.86 m^2) with a small underestimation. The correlation between the two ALS-derived crown areas and field measurements were low, with r^2 at 0.17 for the 3D methods and 0.20 for the Reference method. For the estimation of tree heights, both methods reached the same r^2 at 0.96. The proposed 3D method overestimated the tree heights by 0.79 m and the Reference delineation method underestimated them by 0.48 m.

Table 12 - Accuracy of tree position, crown area and tree height for the 3D and Reference delineation method. Only ITCs matching a field measured tree are considered. *MD* = Mean Difference, *RMSE* = Root Mean Square Error, r^2 = coefficient of determination.* Mean distance of the field tree position and the ITC position.

Method	3D delineation method			Reference delineation method		
	MD	*RMSE*	r^2	*MD*	*RMSE*	r^2
Tree position* [m]	1.54	2.13	-	1.89	2.33	-
Crown area [m^2]	-9.77	47.77	0.17	5.86	15.69	0.20
Tree height [m]	-0.79	1.54	0.96	0.48	1.43	0.96

Effect of forest structure

The forest structure was described by four measures: Gini coefficient of *BA*, mean *DBH*, number of stems per hectare, and mean nearest neighbour distance. Figure 5 displays their effects on the delineation accuracy in terms of *OE* and *CE*. For the Gini coefficient of *BA* and mean *DBH*, it is evident that two major groups of plots are formed. The first group represented by the symbols ● and ■ has the heterogeneous Gini coefficient of *BA* above 0.5 and greater mean *DBH* above 42 cm. It represents mixed tree species within a plot containing uneven aged coniferous (Norway spruce, Larch and Silver fir) and broadleaves (Common alder, Sycamore maple, Silver Birch, European Birch, Rowan and Aspen). A second group represented by ○ and □ belongs to homogeneous tree species plots with even aged coniferous trees. The *OE* was higher for the mixed trees species plots than for the homogeneous tree species plots, wherein the *CE* was similar for both. From the number of stems per hectare and their mean nearest neighbour distance, we can see how the horizontal distribution of trees and the tree spacing affect the delineation accuracy. For the heterogeneous group of plots, a high number of stems per hectare and a low mean nearest neighbor distance resulted in higher *OE*. The second group of plots with less trees per hectare and a larger tree spacing resulted in lower *OE*. Unlike the *OE*, *CE* is very similar for most plots in both groups. Lastly, for each forest structure measure we fitted a linear regression model to *OE*s and *CE*s (Fig. 5). All forest structure measures have a significant relationship at significance level of 0.05 with *OE* but their relationship is not significant with *CE*. Thus, the forest structure measures affected the accuracy of ITC delineation and had more influence on *OE* than *CE*.

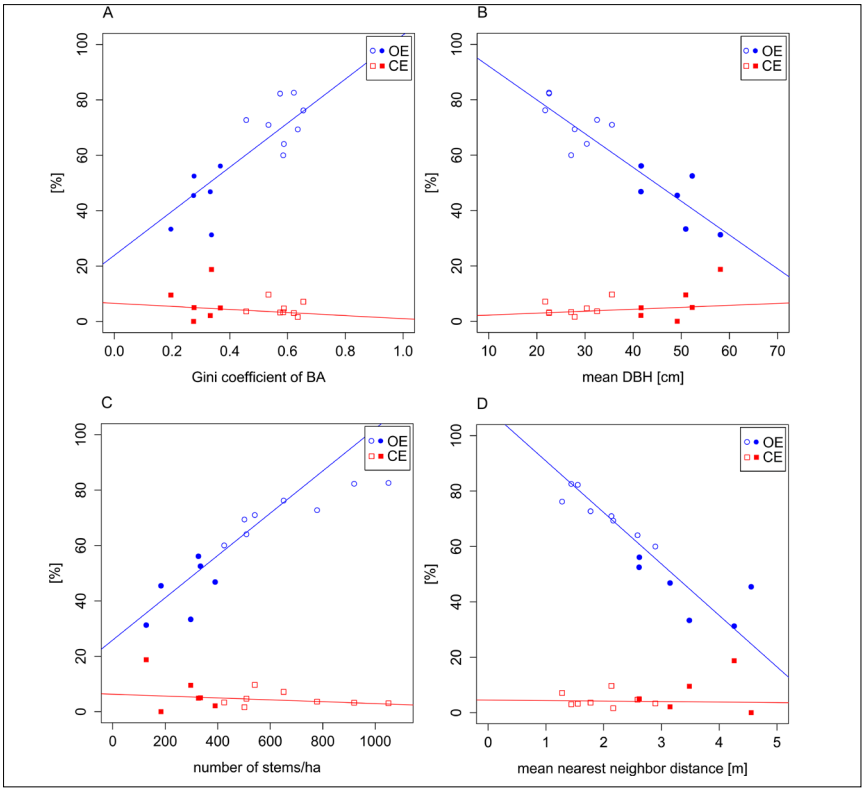

Figure 5 - Effect of forest structure in terms of (A) Gini coefficient of basal area (*BA*), (B) mean *DBH*, (C) number of stems per hectare and (D) mean nearest neighbor distance, on the omission errors (*OE*) and commission errors (*CE*). The blue circles and red squares represent the results of *OE* and *CE*, respectively. Each symbol represents the value of each plot and the solid lines are fitted with ordinary linear regression. The filled signs represent homogeneous plots in contrast to the empty signs representing heterogeneous plots.

Effect of point density

Figure 6 shows the performance of the proposed 3D delineation method in terms of *AI*, *OE* and *CE* at seven different point densities. For each point density, the best performing parameters were chosen based on sensitivity analysis. The mean values and standard deviation bars for each of the thinnings were calculated over ten random repetitions. Overall, from a point density of 4 pulses m^{-2} until a point density of 60 pulses m^{-2} the *AI* increased by 6.1% (Fig. 6). The results suggest that with a higher point density a higher delineation accuracy is reached. To test if the differences of delineation accuracies (*AI*) between different point density data sets were statistically significant, we performed a Mann-Whitney-Wilcoxon test at $\alpha = 0.05$ level (Fig. 7). The outcome showed the differences between the accuracies of the original point density (60 points m^{-2}) and the thinned data sets are all significant. The difference in accuracy is also significant in most cases between 4 points m^{-2} and the other thinned data sets (except for 6 points m^{-2}). Moreover, it is also significant between thinned data set at 6 points m^{-2} and data sets at 30 and 50 points m^{-2}.

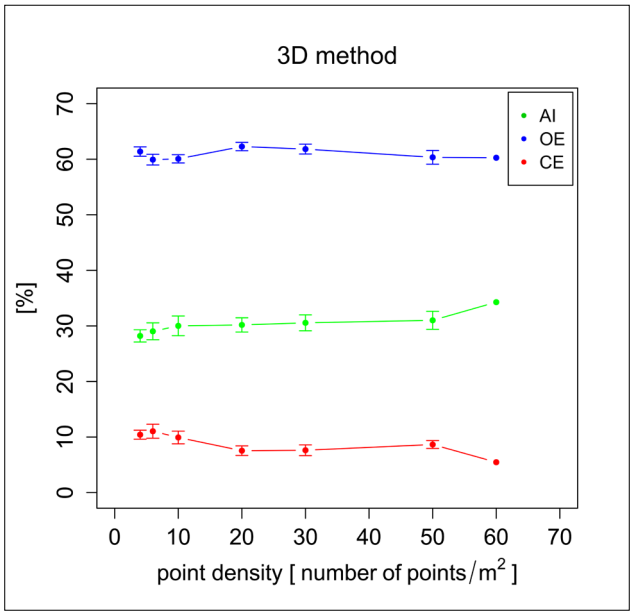

Figure 6 - Performance of the 3D delineation method at different point densities. The blue, red and green circles represent the results of the omission error (*OE*), commission error (*CE*) and accuracy index (*AI*), respectively. For each point density ten repetitions of thinning were carried out and their mean values and the standard deviation bars are presented.

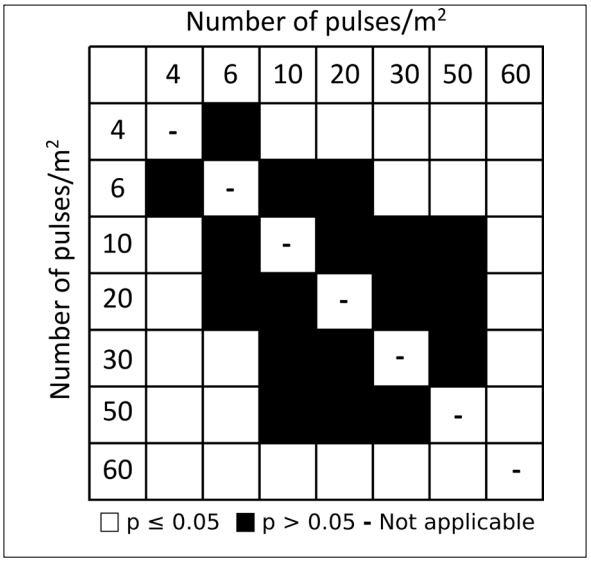

Figure 7 - Mann-Whitney-Wilcoxon test for the pairwise accuracy indexes at different point densities with □ represents significant and ■ represents not significant.

Discussion

The presented 3D delineation method has two important parameters: the size of moving window and the overlapping area (*OA*). The moving window can be adapted in each horizontal slice and the a priori knowledge of the expected crown size of a plot can be used as constraint. Local knowledge of the crown size can be obtained from field measurements or by prediction based on tree height if an allometric equation exists [Popescu et al., 2002]. The sensitivity analysis for the window sizes was done on two stages. Firstly, we tested cubic windows (*ws*) where window size was kept constant for each slice and then we refined the analysis only using the sizes that were providing the best results. The output of the first stage was that windows *ws*1 (11, 11, 11) and *ws*4 (5, 5, 5) were not suitable, as they provided quite low accuracies. Thus, in the second stage we considered only 9 and 7 as possible window dimensions and we defined a new configuration (*w*) with smaller window sizes for the slices at the lower heights: *w*1 (9, 9, 9), *w*2 (7, 9, 9), *w*3 (7, 7, 9), *w*4 (7, 7, 7). The new configuration of window size was based on the assumption that less points are gathered at lower level and that crowns are usually smaller under the canopy cover. From the results of the sensitivity analysis on the original point density, we concluded that the window size (*w*) had greater impact on the 3D delineation accuracy than the overlapping area (*OA*). Moreover, the range of *AI*s obtained at different window sizes is quite large, while the variations of *AI*s obtained at different overlapping areas (%) are actually quite small. In general, the best results were obtained by *w*1 (9, 9, 9) and *OA* 50%, though the accuracy of *w*1, *w*2, *w*3, at *OA* 50% and 60% were very similar. For thinned data the sensitivity analysis revealed that the window sizes *w*1, *w*2 and *w*3, with overlapping at 40% and 50% reached similar and the highest accuracies. It is worth noting that, the best window sizes for point densities 10, 20 and 50 pulses per m^{-2} were not *w*1 (9, 9, 9), even if the differences in accuracy were very marginal (from Tab. 6 to Tab. 11).

For the original point density data the proposed 3D delineation method and the Reference delineation method provided very similar results. The accuracies of both delineation methods are in line to those reported in other studies in coniferous and broadleaved forests [Vauhkonen et al., 2011], Alpine spruce and mixed forests [Reitberger et al., 2009], and different Alpine forests [Eysn et al., 2015].

Regarding the ITC attributes estimation, the 3D delineation and the Reference delineation methods achieved similar accuracies. Even with high point density data, the obtained tree position accuracy was not high. The relatively high tree position error can be explained either by the complex structure of our study area which is challenging (e.g. tilted trees, crown shape, high stem density) (Fig. 2), or by errors occurred in the field measurements of the plot position with GNSS, or by the complex topography (e.g. steep slope) [Monnet and Mermin, 2014]. Particularly on a steep slope higher than 20°, where the treetops are likely to be tilted to the valley side, a horizontal positional difference between the treetop and its stem could be possible. Steep slopes can also lead to an overestimation of ALS derived tree height, because the tree height is calculated as the distance between the tree top (highest normalized point inside the cluster) and the ground surface below the tree top point [Hollaus et al., 2006; Kaartinen et al., 2012]. Thus, the ALS data and the error inherited in the generation of DTM from the ALS point clouds are less precise in steep terrain [Hollaus et al., 2006]. Another error in height estimation can be related to the field-derived measurements, either caused by the error of allometric equation used, or

by subjectivity in the field measurements with Vertex hypsometer [Kitahara et al., 2010; Vasilescu, 2013]. Kitahara et al. [2010] found that the mean percentage difference of tree height measurements repeated three times by different surveyors are 3.6% for coniferous trees and 8.7% for broadleaves.

Tree heights obtained by the 3D delineation method were overestimated by 0.79 m and those obtained by the Reference delineation method were underestimated by 0.48 m. Such difference is caused by different ways of extraction of tree crown pulses. The 3D method extracted tree height as the highest pulse within an ITC cluster. The Reference method extracted tree height at 95th percentile of all heights within an ITC segment. The crown area was overestimated by the 3D delineation method and underestimated by the Reference method. The Reference delineation method defined a height threshold above which all first return pulses were accounted for crown area computation. While the proposed method simply took all pulses in a cluster for crown area calculation. In summary, the accuracy of tree attributes estimated by both methods are at good level as compared to previous studies [e.g. Kaartinen et al., 2012; Eysn et al., 2015].

Analyzing the effect of four forest structure measures on delineation accuracy, we find that pure tree species and even aged plots achieved lower *OE* as compared to mixed tree species and uneven aged plots. Comparing with pure tree species and even aged plots, the plots with mixed tree species and uneven ages in general had a higher Gini coefficient of *BA*, a higher number of stems per hectare, a smaller mean *DBH* and a smaller mean nearest neighbour distance between trees, which clearly led to higher *OE*. The *CE*, however, did not vary so much among different forest structures. In a related study, Eysn et al. [2014] reported that delineation accuracies with the Pellizzano test site were also comparatively low possibly caused by the high forest structure diversity.

The point density analysis revealed that the delineation accuracy of the 3D delineation method is higher with the original density at 60 pulses m^{-2} (Fig. 6). Previous studies concluded that point densities higher than 20 pulses m^{-2} did not have an important effect on the delineation results [Reitberger et al., 2009; Kaartinen et al., 2012; Yao et al., 2014]. Kaartinen et al. [2012] reported that increasing point density from 2 and 4 pulses m^{-2} to 8 pulses m^{-2} had only marginal improvement on delineation accuracy. The studies of Reitberger et al. [2009] and Yao et al. [2014] concluded that a point density higher than 10 pulses m^{-2} did not improve the performances of ITC delineation. However, Kaartinen et al.'s [2012] study focused mainly on 2D methods based on CHM, where the vertical structure was not explored. In our tests, the delineation accuracy increased with higher point density and it achieved marginal improvements when we increased the point density from 10 to 50 pulses m^{-2}. The Mann-Whitney-Wilcoxon test showed that differences in accuracy among the thinned datasets are not statistically significant at $\alpha = 0.05$ between point densities 6, 10, 20, 30 and 50 pulses m^{-2}, except between point densities 6 m^{-2} and 30 pulses m^{-2}, and 6 m^{-2} and 50 pulses m^{-2}. This indicates the increase of point density from 6 to 50 pulses m^{-2} does not lead to interesting improvement in accuracy. The highest accuracy is achieved with the original point density (60 points m^{-2}) and the improvement in accuracy is tested significantly different when compared to all other thinned data sets. Simulation of thinned data by reducing a high-density ALS datasets are frequently used to give insight into the effect of point density [Magnussen et al., 2010; Jakubowski et al., 2013; Hansen et al., 2015]. However, we have to acknowledge thinning is only a simulation of the expected real

ALS flight at lower densities. An ideal option would be to obtain different point densities with the same scanner.

Conclusions

In this paper, a 3D ITC delineation method based on ALS data was presented and evaluated. The results were compared with a well-established Reference delineation method. Both methods reached similar delineation accuracies and both were effective in tree attributes estimation. We found that forest structure attributes such as stem density, distribution of trees, number of stems per hectare, and the evenness expressed by Gini coefficient of basal area, had significant influence on the delineation accuracy. We also observed that the omission error was lower in stands with a homogeneous forest structure and that the forest structure only had a slight effect on the commission error. In addition, due to the complex forest structure of our study site, the results have demonstrated that the proposed 3D delineation method was flexible and suitable to be applied in different forest conditions. Our method was robust and effective even with low point densities. Our thinning experiments have shown that the delineation accuracy was similar for point densities varying from 10 to 50 points m^{-2}. Overall, the delineation accuracy improved when the point density was increased and the top accuracy was achieved with the highest density at 60 points m^{-2}.

Acknowledgements

This work represents the outcome of Kaja Kandare's PhD project FORESTFUSION funded by the Edmund Mach Foundation, Trento, Italy. The authors would like to thank Dr. Lorenzo Frizzera for his help in the field data collection supported by Edmund Mach Foundation. Project Alpine Space 2-3-2-FR NEWFOR funded by the European Commission within the European Territorial Cooperation program "Alpine Space" supported the ALS data acquisition used in this study.

References

Bollandsås O.M., Buongiorno J., Gobakken T. (2008) - *Predicting the growth of stands of trees of mixed species and size: A matrix model for Norway.* Scandinavian Journal of Forest Research, 23: 167-178. doi: http://dx.doi.org/10.1080/02827580801995315.

Brandtberg T., Warner T.A., Landenberger R.E., McGraw J.B. (2003) - *Detection and analysis of individual leaf-off tree crowns in small footprint, high sampling density lidar data from the eastern deciduous forest in North America*. Remote Sensing of Environment, 85: 290-303. doi: http://dx.doi.org/10.1016/S0034-4257(03)00008-7.

Dalponte M., Coomes D.A. (2016) - *Tree-centric mapping of forest carbon density from airborne laser scanning and hyperspectral data*. Methods in Ecology and Evolution. doi: http://dx.doi.org/10.1111/2041-210X.12575.

Dalponte M., Reyes F., Kandare K., Gianelle D. (2015) - *Delineation of individual tree crowns from ALS and hyperspectral data: a comparison among four methods*. European Journal of Remote Sensing, 48: 365-382. doi: http://dx.doi.org/10.5721/EuJRS20154821.

Duncanson L.I., Cook B.D., Hurtt G.C., Dubayah R.O. (2014) - *An efficient, multi-layered crown delineation algorithm for mapping individual tree structure across*

multiple ecosystems. Remote Sensing of Environment, 154: 378-386. doi: http://dx.doi.org/10.1016/j.rse.2013.07.044.

Ene L., Næsset E., Gobakken T. (2012) - *Single tree detection in heterogeneous boreal forests using airborne laser scanning and area-based stem number estimates*. International Journal of Remote Sensing, 33: 5171-5193. doi: http://dx.doi.org/10.1080/01431161.2012.657363.

Eysn L., Hollaus M., Lindberg E., Berger F., Monnet J.-M., Dalponte M., Kobal M., Pellegrini M., Lingua E., Mongus D., Pfeifer N. (2015) - *A benchmark of lidar based single tree detection methods using heterogeneous forest data from the Alpine space*. Forests, 6: 1721-1747. doi: http://dx.doi.org/10.3390/f6051721.

Eysn L., Hollaus M., Monnet J.M., Dalponte M., Kobal M., Pellegrini M., Lindberg E., Mongus D., Berger F. (2014) - *NEWFOR Single Tree Detection Benchmark - report*. Wien, Austria.

Ferraz A., Bretar F., Jacquemoud S., Gonçalves G., Pereira L., Tomé M., Soares P. (2012) - *3-D mapping of a multi-layered Mediterranean forest using ALS data*. Remote Sensing of Environment, 121: 210-223. doi: http://dx.doi.org/10.1016/j.rse.2012.01.020.

Gini C. (1912) - *Variabilità e mutabilità contributo llo studio delle distribuzioni e delle relazioni statistich*e. Cuppini P. (Ed.), Bologna, 156 pp.

Gupta S., Weinacker H., Koch B. (2010) - *Comparative analysis of clustering-based approaches for 3-D single tree detection using airborne fullwave lidar data*. Remote Sensing, 2: 968-989. doi: http://dx.doi.org/10.3390/rs2040968.

Hansen E.H., Gobakken T., Næsset E. (2015) - *Effects of pulse density on digital terrain models and canopy metrics using airborne laser scanning in a tropical rainforest*. Remote Sensing, 7: 8453-8468. doi: http://dx.doi.org/10.3390/rs70708453.

Hollaus M., Wagner W., Eberhöfer C., Karel W. (2006) - *Accuracy of large-scale canopy heights derived from LiDAR data under operational constraints in a complex alpine environment. ISPRS* Journal of Photogrammetry and Remote Sensing, 60: 323-338. doi: http://dx.doi.org/10.1016/j.isprsjprs.2006.05.002.

Holopainen M., Kankare V., Vastaranta M., Liang X., Lin Y., Vaaja M., Yu X., Hyyppä J., Hyyppä H., Kaartinen H., Kukko A., Tanhuanpää T., Alho P. (2013) - *Tree mapping using airborne, terrestrial and mobile laser scanning - A case study in a heterogeneous urban forest*. Urban Forestry and Urban Greening, 12: 546-553. doi: http://dx.doi.org/10.1016/j.ufug.2013.06.002.

Hyyppä J., Inkinen M. (1999) - *Detecting and estimating attributes for single trees using laser scanner*. The Photogrammetric Journal of Finland, 16: 27-42.

Hyyppä J., Kelle O., Lehikoinen M., Inkinen M. (2001) - *A segmentation-based method to retrieve stem volume estimates from 3-D tree height models produced by laser scanners*. IEEE Transactions on Geoscience and Remote Sensing, 39: 969-975. doi: http://dx.doi.org/10.1109/36.921414.

Hyyppä J., Yu X., Hyyppä H., Vastaranta M., Holopainen M., Kukko A., Kaartinen H., Jaakkola A., Vaaja M., Koskinen J., Alho P. (2012) - *Advances in forest inventory using airborne laser scanning.* Remote Sensing, 4: 1190-1207. doi: http://dx.doi.org/10.3390/rs4051190.

Jakubowski M.K., Guo Q., Kelly M. (2013) - *Tradeoffs between lidar pulse density and forest measurement accuracy*. Remote Sensing of Environment, 130: 245-253. doi:

http://dx.doi.org/10.1016/j.rse.2012.11.024.

Kaartinen H., Hyyppä J., Yu X., Vastaranta M., Hyyppä H., Kukko A., Holopainen M., Heipke C., Hirschmugl M., Morsdorf F., Næsset E., Pitkänen J., Popescu S., Solberg S., Wolf B.M., Wu J.-C. (2012) - *An international comparison of individual tree detection and extraction using airborne laser scanning*. Remote Sensing, 4: 950-974. doi: http://dx.doi.org/10.3390/rs4040950.

Kitahara F., Mizoue N., Yoshida S. (2010) - *Effects of training for inexperienced surveyors on data quality of tree diameter and height measurements*. Silva Fennica, 44: 657-667. doi: http://dx.doi.org/10.14214/sf.133.

Lähivaara T., Seppänen A., Kaipio J.P., Vauhkonen J., Korhonen L., Tokola T., Maltamo M. (2014) - *Bayesian approach to tree detection based on airborne laser scanning data*. IEEE Transactions on Geoscience and Remote Sensing, 52: 2690-2699. doi: http://dx.doi.org/10.1109/TGRS.2013.2264548.

Lee H., Slatton K.C., Roth B.E., Cropper W.P. (2010) - *Adaptive clustering of airborne LiDAR data to segment individual tree crowns in managed pine forests*. International Journal of Remote Sensing, 31: 117-139. doi: http://dx.doi.org/10.1080/01431160902882561.

Lexerød N.L., Eid T. (2006) - *An evaluation of different diameter diversity indices based on criteria related to forest management planning*. Forest Ecology and Management, 222: 17-28. doi: http://dx.doi.org/10.1016/j.foreco.2005.10.046.

Li W., Guo Q., Jakubowski M.K., Kelly M. (2012) - *A new method for segmenting individual trees from the lidar point cloud*. Photogrammetric Engineering & Remote Sensing, 78: 75-84. doi: http://dx.doi.org/10.14358/PERS.78.1.75.

Lindberg E., Eysn L., Hollaus M., Holmgren J., Pfeifer N. (2014) - *Delineation of tree crowns and tree species classification from full-waveform airborne laser scanning data using 3-D ellipsoidal clustering*. IEEE Journal of Selected Topics in Applied Earth Observations and Remote Sensing, 7: 3174-3181. doi: http://dx.doi.org/10.1109/JSTARS.2014.2331276.

Lu X., Guo Q., Li W., Flanagan J. (2014) - *A bottom-up approach to segment individual deciduous trees using leaf-off lidar point cloud data*. ISPRS Journal of Photogrammetry and Remote Sensing, 94: 1-12. doi: http://dx.doi.org/10.1016/j.isprsjprs.2014.03.014.

Magnussen S., Næsset E., Gobakken T. (2010) - *Reliability of LiDAR derived predictors of forest inventory attributes: A case study with Norway spruce*. Remote Sensing of Environment, 114: 700-712. doi: http://dx.doi.org/10.1016/j.rse.2009.11.007.

McElhinny C., Gibbons P., Brack C., Bauhus J. (2005) - *Forest and woodland stand structural complexity: Its definition and measurement*. Forest Ecology and Management, 218: 1-24. doi: http://dx.doi.org/10.1016/j.foreco.2005.08.034.

Monnet J.M., Mermin È. (2014) - *Cross-correlation of diameter measures for the co-registration of forest inventory plots with airborne laser scanning data*. Forests, 5: 2307-2326. doi: http://dx.doi.org/10.3390/f5092307.

Morsdorf F., Meier E., Kötz B., Itten K.I., Dobbertin M., Allgöwer B. (2004) - *LIDAR-based geometric reconstruction of boreal type forest stands at single tree level for forest and wildland fire management.* Remote Sensing of Environment, 92: 353-362. doi: http://dx.doi.org/10.1016/j.rse.2004.05.013.

Næsset E. (2002) - *Predicting forest stand characteristics with airborne scanning laser using a practical two-stage procedure and field data*. Remote Sensing of Environment,

80: 88-99. doi: http://dx.doi.org/10.1016/S0034-4257(01)00290-5.

Neumann M., Starlinger F. (2001) - *The significance of different indices for stand structure and diversity in forests*. Forest Ecology and Management, 145: 91-106. doi: http://dx.doi.org/10.1016/S0378-1127(00)00577-6.

O'Hara K.L., Hasenauer H., Kindermann G. (2007) - *Sustainability in multi-aged stands: An analysis of long-term plenter systems*. Forestry, 80: 163-181. doi: http://dx.doi.org/10.1093/forestry/cpl051.

Ørka H.O., Dalponte M., Gobakken T., Næsset E., Ene L.T. (2013) - *Characterizing forest species composition using multiple remote sensing data sources and inventory approaches*. Scandinavian Journal of Forest Research, 28: 677-688. doi: http://dx.doi.org/10.1080/02827581.2013.793386.

Otsu N. (1979) - *A threshold selection method from gray-level histograms*. IEEE Transaction on Systems, Man and Cybernetics, 9: 62-66. doi: http://dx.doi.org/10.1109/TSMC.1979.4310076.

Packalen P., Strunk J.L., Pitkänen J.A., Temesgen H., Maltamo M. (2015) - *Edge-tree correction for predicting forest inventory attributes using area-based approach with airborne laser scanning*. IEEE Journal of Selected Topics in Applied Earth Observations and Remote Sensing, 8: 1274-1280. doi: http://dx.doi.org/10.1109/JSTARS.2015.2402693.

Pedersen R.Ø., Bollandsås O.M., Gobakken T., Næsset E. (2012) - *Deriving individual tree competition indices from airborne laser scanning*. Forest Ecology and Management, 280: 150-165. doi: http://dx.doi.org/10.1016/j.foreco.2012.05.043.

Persson Å., Holmgren J., Soderman U. (2002) - *Detecting and measuring individual trees using an airborne laser scanner*. Photogrametric Engineering & Remote Sensing, 68: 925-932.

Popescu S.C., Wynne R.H., Nelson R.F. (2002) - *Estimating plot-level tree heights with lidar: local filtering with a canopy-height based variable window size*. Computers and Electronics in Agriculture, 37: 71-95. doi: http://dx.doi.org/10.1016/S0168-1699(02)00121-7.

Pouliot D.A., King D.J., Pitt D.G. (2005) - *Development and evaluation of an automated tree detection - delineation algorithm for monitoring regenerating coniferous forests*. Canadian Journal of Forest Research, 35: 2332-2345. doi: http://dx.doi.org/10.1139/X05-145.

Reitberger J., Schnörr C., Krzystek P., Stilla U. (2009) - *3D segmentation of single trees exploiting full waveform LIDAR data*. ISPRS Journal of Photogrammetry and Remote Sensing, 64: 561-574. doi: http://dx.doi.org/10.1016/j.isprsjprs.2009.04.002.

Scrinzi G., Galvagni D., Marzullo L. (2010) - *I nuovi modelli dendrometrici per la stima delle masse assestamentali in Provincia di Trento*. Provincia Autonoma di Trento - Servizio Foreste e Fauna, Trento.

Shi J., Malik J. (2000) - *Normalized cuts and image segmentation*. IEEE Transactions on Pattern Analysis and Machine Intelligence, 22: 888-905. doi: http://dx.doi.org/10.1109/34.868688.

Solberg S., Næsset E., Bollandsås O.M. (2006) - *Single tree segmentation using airborne laser scanner data in a structurally heterogeneous spruce forest*. Photogrammetric Engineering & Remote Sensing, 72: 1369-1378. doi: http://dx.doi.org/0099-

1112/06/7212-1369.

Takahashi T., Yamamoto K., Senda Y., Tsuzuku M. (2005) - *Estimating individual tree heights of sugi (Cryptomeria japonica D. Don) plantations in mountainous areas using small-footprint airborne LiDAR*. Journal of Forest Research, 10: 135-142. doi: http://dx.doi.org/10.1007/s10310-004-0125-8.

Tang F.F., Zhang X.H., Liu J.N. (2007) - *Segmentation of tree crown model with complex structure from airborne LiDAR data*. Geoinformatics 2007: Remotely Sensed Data and Information, 67520A. doi: http://dx.doi.org/10.1117/12.760476.

Tang S., Dong P., Buckles B.P. (2013) - *Three-dimensional surface reconstruction of tree canopy from lidar point clouds using a region-based level set method*. International Journal of Remote Sensing, 34: 1373-1385. doi: http://dx.doi.org/10.1080/01431161.2012.720046.

Vasilescu M.M. (2013) - *Standard error of tree height using vertex III*. Bulletin of the Transilvania University of Braşov, Series II: Forestry, Wood Industry, Agricultural Food Engineering 6, 6.

Vauhkonen J., Ene L., Gupta S., Heinzel J., Holmgren J., Pitkanen J., Solberg S., Wang, Y., Weinacker H., Hauglin K.M., Lien V., Packalen P., Gobakken T., Koch B., Næsset E., Tokola T., Maltamo M. (2011) - *Comparative testing of single-tree detection algorithms under different types of forest*. Forestry, 85: 27-40. doi: http://dx.doi.org/10.1093/forestry/cpr051.

Wang Y., Weinacker H., Koch B. (2008) - *A lidar point cloud based procedure for vertical canopy structure analysis and 3D single tree modelling in forest*. Sensors, 8: 3938-3951. doi: http://dx.doi.org/10.3390/s8063938.

Woodcock C.E., Strahler A.H., Jupp D.L.B. (1988) - *The use of variograms in remote sensing: II. Real digital images*. Remote Sensing of Environment, 25: 349-379. doi: http://dx.doi.org/10.1016/0034-4257(88)90109-5.

Yao W., Krull J., Krzystek P., Heurich M. (2014) - *Sensitivity analysis of 3D individual tree detection from LiDAR point clouds of temperate forests*. Forests, 5: 1122-1142. doi: http://dx.doi.org/10.3390/f5061122.

Paper II

Int J Appl Earth Obs Geoinformation 60 (2017) 72–82

Contents lists available at ScienceDirect

Int J Appl Earth Obs Geoinformation

journal homepage: www.elsevier.com/locate/jag

Individual tree crown approach for predicting site index in boreal forests using airborne laser scanning and hyperspectral data

Kaja Kandare[a,b,*], Hans Ole Ørka[b], Michele Dalponte[c], Erik Næsset[b], Terje Gobakken[b]

[a] FoxLab, Joint CNR-FEM Initiative, Fondazione E. Mach, Via E. Mach 1, 38010, San Michele all'Adige, TN, Italy
[b] Department of Ecology and Natural Resource Management, Norwegian University of Life Sciences, P.O. Box 5003, N-1432 Ås, Norway
[c] Department of Sustainable Agro-Ecosystems and Bioresources, Research and Innovation Centre, Fondazione E. Mach, Via E. Mach 1, 38010 San Michele all'Adige, TN, Italy

ARTICLE INFO

Keywords:
ALS
Hyperspectral data
Individual tree crowns
Biophysical attribute prediction
Site index
Forestry
Fusion
Remote sensing

ABSTRACT

Site productivity is essential information for sustainable forest management and site index (SI) is the most common quantitative measure of it. The SI is usually determined for individual tree species based on tree height and the age of the 100 largest trees per hectare according to stem diameter. The present study aimed to demonstrate and validate a methodology for the determination of SI using remotely sensed data, in particular fused airborne laser scanning (ALS) and airborne hyperspectral data in a forest site in Norway. The applied approach was based on individual tree crown (ITC) delineation: tree species, tree height, diameter at breast height (DBH), and age were modelled and predicted at ITC level using 10-fold cross validation. Four dominant ITCs per 400 m^2 plot were selected as input to predict SI at plot level for Norway spruce (*Picea abies* (L.) Karst.) and Scots pine (*Pinus sylvestris* L.). We applied an experimental setup with different subsets of dominant ITCs with different combinations of attributes (predicted or field-derived) for SI predictions. The results revealed that the selection of the dominant ITCs based on the largest DBH independent of tree species, predicted the SI with similar accuracy as ITCs matched with field-derived dominant trees (RMSE: 27.6% vs 23.3%). The SI accuracies were at the same level when dominant species were determined from the remotely sensed or field data (RMSE: 27.6% vs 27.8%). However, when the predicted tree age was used the SI accuracy decreased compared to field-derived age (RMSE: 27.6% vs 7.6%). In general, SI was overpredicted for both tree species in the mature forest, while there was an underprediction in the young forest. In conclusion, the proposed approach for SI determination based on ITC delineation and a combination of ALS and hyperspectral data is an efficient and stable procedure, which has the potential to predict SI in forest areas at various spatial scales and additionally to improve existing SI maps in Norway.

1. Introduction

Forest site productivity is the potential of a particular forest stand to produce aboveground wood volume (Skovsgaard and Vanclay, 2008). Information on forest site productivity is an important prerequisite for a wide range of forestry applications. Reliable site productivity measures are essential for sustainable forest management in order to estimate yields and carbon stock of forest stands to ensure a sustainable supply of timber products, and to formulate silvicultural strategies (Coops, 2015; Eid and Økseter, 1999; Splechtna, 2001). The most common quantitative measure and widely accepted method of forest site productivity characterization is site index (SI) (Skovsgaard and Vanclay, 2008). The SI of a forest stand is defined as expected height of the trees at a given base age (e.g. 40 years) for certain tree species (Skovsgaard and Vanclay, 2008). Commonly, the dendrocentric approaches for the SI determination are based on the measurements, in each forest stand, of the height and age of the largest dominant trees, in terms of diameter or height, which refer to upper social classes (Skovsgaard and Vanclay, 2008). These measurements are then averaged, usually for the 100 largest trees per hectare and referred as dominant height and age, which subsequently are used as input to calculate the SI. The dominant height of a stand reflects the productivity of a fully stocked even-aged stand as it is independent from the stem density, and it is least affected by thinning (Skovsgaard and Vanclay, 2008). However, the site productivity can also be determined with geocentric approaches based on site properties, such as edaphic (soil properties), topography

* Corresponding author at: FoxLab, Joint CNR-FEM Initiative, Fondazione E. Mach, Via E. Mach 1, San Michele all'Adige, TN 38010, Italy.
E-mail addresses: kaja.kandare@fmach.it, kandare.kaja@gmail.com (K. Kandare), hans.ole.orka@nmbu.no (H.O. Ørka), michele.dalponte@fmach.it (M. Dalponte), erik.naesset@nmbu.no (E. Næsset), terje.gobakken@nmbu.no (T. Gobakken).

http://dx.doi.org/10.1016/j.jag.2017.04.008
Received 23 September 2016; Received in revised form 6 April 2017; Accepted 13 April 2017

(altitude, slope, aspect, and landform) and climate parameters (precipitation and temperature) (Clutter et al., 1983; Nothdurft et al., 2012; Paulo et al., 2014; Sharma et al., 2012), which were not considered in the current study.

Biophysical attributes such as tree species, tree height, stem diameter, and tree age are crucial for assessing the SI. In practice, the SI calculations are often based on field surveys or photo interpretations using aerial imagery. Such collection of data is expensive, time consuming, and logistically difficult (Eid et al., 2004). Furthermore, the SI changes over time due to various factors, such as atmospheric deposition of nitrogen and other nutrients, climatic changes, etc. (Boisvenue and Running, 2006; Messaoud and Chen, 2011; Sharma et al., 2011). Thus, affordable methods to retrieve the SI of a specific site and at a specific time is required.

Remote sensing technologies, such as aerial photography, airborne laser scanning (ALS), spaceborne or airborne multispectral and hyperspectral images enable observation of forest areas at different temporal and geographical scales (Coops et al., 2004; Yu et al., 2015; Zhao et al., 2011). Many studies have reported that ALS-predicted biophysical attributes may increase the accuracy of SI determination (Chen and Zhu, 2012; Holopainen et al., 2010; Tompalski et al., 2015a). In general, there are two prominent remotely sensed-based approaches to assess biophysical attributes for management purposes: area-based approach (ABA) (Næsset, 2002) and individual tree crown (ITC) approach (Hyyppä et al., 2001). In ABA, biophysical attributes are predicted for each plot or element (e.g. grid cell) of a population with the size of each element being equal to the area of the plots from which the predictive relationships are derived, while in ITC approaches biophysical attributes are determined for each detected tree, i.e. ITC level determination. In both ABA and ITC approaches, attributes can be predicted using parametric or non-parametric methods.

Previous studies on an automated determination of SI assisted by remotely sensed data are few in numbers. Véga et al. (2009) generated SI and age maps based on ABA using historical aerial photographs, and ALS data. In this study, spaceborne multispectral imagery data were used to classify Jack pine trees and to extract stand boundaries. Subsequently, average dominant height was predicted from photogrammetric point clouds, and age-height models were fitted to time series of predicted dominant height values. Packalén et al. (2011) estimated SI for homogeneous Eucalyptus plantations combining ALS data and age taken from a stand register. The dominant height was expressed as a linear model using ABA with ALS explanatory variables such as height quantiles and mean height per plot. Then, the dominant height was modeled assuming a nonlinear relationship described with the Chapman-Richards equation to predict SI directly in one stage. Vehmas et al. (2011) assessed the site quality of mature boreal forests using ALS data. Five different fertility classes were correctly classified in 58% of the forest stands. Tompalski et al. (2015b) determined SI for coastal temperate rainforests using ALS data and satellite multispectral imagery, i.e. Landsat. Annual time series of Landsat were utilized to delineate stand boundaries and to determine the time since last disturbance, which was used as proxy for calculating stand age. From the ALS data, stand dominant height was predicted. Chen and Zhu (2012) used SI models to predict site quality for *Pinus radiata* plantations based on ALS data. The stand dominant height was calculated from ITCs and the age was known from the dates the plantation was established.

In the above-mentioned studies, SI is mainly determined starting from an area-based prediction of the required biophysical attributes. This is the most common approach, however recently many algorithms and methods have been developed to predict biophysical attributes at ITC level. Such ITC approaches allow for a higher spatial detail and scalable determination of biophysical attributes than the ABA. To the best of our knowledge, only few studies (Chen and Zhu, 2012; Gatziolis, 2007) partially exploited the ITC information for SI determination. However, since the SI is defined by biophysical attributes of the dominant trees which are the ones that usually are identified with the greatest accuracy applying ITC approach (Holmgren and Persson, 2004; Maltamo et al., 2004; Solberg et al., 2006), we hypothesize that using ITC framework for SI determination could be an appropriate approach for SI determination. Due to some potential advantages of ITC-based methods over the ABA (e.g. higher spatial scalability), it is highly relevant to gain more experience and evidence of the potentials and performance of SI determination based on biophysical attributes derived from remotely sensed data at ITC level. Furthermore, the dominant trees measured in the field do not always correspond to dominant ITCs, as there are different ways to select the dominant ITCs (e.g. by species and diameter at breast height, DBH). Thus, the effect of selected dominant ITCs on SI accuracy is not known. In addition, the changes in SI accuracy when ITC-based biophysical attributes are substituted with the field observations have never been analyzed and the SI determination adapted to the ITC framework should be explored more deeply.

The biophysical attributes needed for SI determination at ITC level are tree species, height, DBH, and age. The tree species information is typically obtained from aerial photographs, ALS, multispectral or hyperspectral imagery (Dalponte et al., 2015, 2014; Kim et al., 2009; Ørka et al., 2009; Yao et al., 2012). However, hyperspectral imagery seems to be the most promising data source for species classification (Dalponte et al., 2012; Ørka et al., 2013). The tree height and DBH can be predicted from ALS and aerial photographs (Hyyppä and Inkinen, 1999; Næsset and Økland, 2002). Regarding tree age, it is uncommon to determine this attribute from remotely sensed data, with the exception that this attribute traditionally has been assessed by manual photo interpretation in operational forest management inventories (e.g. Eid, 1996). However, very few studies have explored this topic based on automated methods, and in particular at the ITC level (Buddenbaum et al., 2005; Racine et al., 2014; Skoupý et al., 2012). As it is clear from these examples, each of these biophysical attributes can be predicted using more than one source of remotely sensed data – either individually or in combination. The combination of complementary remotely sensed data has shown to improve the accuracy of the prediction of the above-mentioned attributes (Dalponte et al., 2008; Tonolli et al., 2011). In particular, ALS and optical data are complementary by their nature: ALS data provide detailed information on the three-dimensional (3D) forest structure (e.g. tree heights), while optical data (in particular hyperspectral images) can provide detailed information on spectral properties of the canopy, which can be useful for prediction of qualitative attributes (e.g. tree species).

Therefore, the main goal of this study is to demonstrate and validate the potential of an ITC approach for determination of the SI from remotely sensed data. Based on predicted ITC level attributes we determined biophysical attributes at plot level in order to predict the SI. We defined an experimental setup with two subsets of dominant ITCs, inside which several experiments using different combinations of biophysical attributes for SI determination were considered. The specific objectives of this study are:

1) to make prediction models using combined ALS and airborne hyperspectral data to predict ITC level biophysical attributes (species, height, DBH, and age) and evaluate the models applying 10-fold cross validation;
2) to investigate and evaluate effects of dominant ITCs selection on the SI accuracy at plot level;
3) to evaluate differences in the SI accuracy when predicting the SI using different combinations of biophysical attributes (predicted vs field-derived) at plot level.

The uniqueness of this study is that it represents a first attempt to fully exploit the ITC information for SI determination using a combination of ALS and airborne hyperspectral data. As these data are becoming the most commonly used in the scientific, as well as the practical

forestry communities (Dalponte et al., 2014, 2012; Ørka et al., 2013; Vaglio Laurin et al., 2014), extending the opportunities for forest resource characterization using such data may benefit science as well as forest management.

2. Materials

2.1. Study site

The 853 ha study area is located in the boreal forest region in the Våler municipality (59°30′N 10°55′E, 70–120 m above sea level) in southeastern Norway. The dominant species are Norway spruce (*Picea abies* (L.) Karst.) and Scots pine (*Pinus sylvestris* L.). Younger stands have large proportions of deciduous species dominating by birch trees (*Betula spp.*). The active forest management in the forest area is directed towards the timber production with clear-cuts.

2.2. Field data

In 2010, 153 circular systematically distributed forest inventory plots were measured. The size of each plot was 400 m^2. For all trees inside the plots with DBH > 4 cm the tree position, species, and DBH were recorded. Tree height was measured only on selected sample trees (approximately 10 trees per plot). The polar tree coordinates were established by using measurements of distance and angle from the plot center. These measurements were carried out with a tape measure and compass with a sight. The plot center was measured using differential GPS and GLONASS receiver. Out of 9414 recorded trees, 52% were spruce, 25% were pine, and 23% were broadleaves. These trees will be denoted "forest inventory trees". Summary statistics of these trees appear in Table 1.

In July 2013, 96 of the forest inventory plots dominated by either spruce or pine were revisited to measure data for site index determination. In each plot the four largest trees according to DBH of the dominant species were selected as sample trees, which corresponds as closely as possible to the definition of the dominant trees, i.e., the 100 largest trees per ha (Rennolls, 1978), given the limited plot size of 400 m^2. For each sample tree the position, height, and DBH were recorded. For further age analyses, core samples of two trees per plot were taken at 1.3 m height. Out of 384 recorded trees, 58% were spruce and 42% were pine trees. The trees from this inventory are referred to as "site trees" and summary statistics appear in Table 2.

In the laboratory, the age was obtained by counting growth rings on the core samples. The ring widths were measured manually with the LINTAB™ 6 tree-ring measurement station and the TSAP-Win™ software for tree-ring measurement.

The average height and age of the site trees reflected dominant height and age of a plot. The dominant height, dominant species and age per plot were used to calculate field-derived SI. SI model was derived from inverse models of the dominant height growth models for Norway spruce (Tveite, 1977), and Scots pine (Braastad, 1980; Tveite, 1976) at a base age of 40 years. Summary statistics of dominant height, age, and SI appear in Table 3. Out of the 96 plots, 56 were dominated by spruce and 40 were dominated by pine.

Table 1
Range, mean, and standard deviation (SD) of the forest inventory tree's characteristics: diameter at breast height (dbh) and height (h).

Characteristic	Range	Mean	SD
dbh [cm]	4.0–55.0	13.2	8.9
h [m]	2.10–31.00	15.94	5.48

Table 2
Range, mean, and standard deviation (SD) of the site tree characteristics: diameter at breast height (dbh), height (h), and age.

Characteristic	Range	Mean	SD
dbh [cm]	13.2–55.0	28.8	7.5
h [m]	11.25–32.00	20.80	4.13
age [yrs]	23 –231	80.9	48.8

Table 3
Range, mean, and standard deviation (SD) of the average plot characteristics: dominant height (H), age (AGE), and site index (SI).

Characteristic	Range	Mean	SD
H [m]	4.68–26.60	16.11	3.78
AGE [yrs]	23.5–208.5	80.8	47.1
SI [m]	5.21–25.70	15.59	5.17

2.3. ALS and hyperspectral data

ALS and airborne hyperspectral data were simultaneously acquired over the study area on 9th of September 2011. The flying altitude was 1500 m above ground level. Twenty-one flight lines were flown between 10:48 AM and 2:22 PM, having sun zenith angle between 59° and 61°. ALS data were acquired using the Leica ALS70 system with a pulse repetition frequency of 180 kHz. The system recorded up to five returns per pulse and the average pulse density was 2.4 pts/m^2.

Hyperspectral data were acquired using the HySpex VNIR-1600 sensor with spatial resolution of 0.5 m. The images consisted of 80 bands between 410 nm and 990 nm with 7.2 nm spectral resolution. All the hyperspectral images were acquired in non-nadir conditions regarding the field plots. Hyperspectral data were orthorectified using a DTM derived from ALS data by the data vendor. To minimize co-registration problems the vendor also applied a transformation based on tree top detection in the two datasets. In the pre-processing, the hyperspectral images were atmospherically corrected using the QUAC algorithm (Bernstein et al., 2005). Afterwards, the value of each pixel was normalized with respect to the sum of the values of the same pixel in all the bands to reduce a minor difference in reflectance occurring between the different images (Yu et al., 1999).

3. Methods

3.1. Overview

The ITCs were delineated based on the ALS data using a 3D delineation method (Kandare et al., 2016). Further, the hyperspectral and ALS data were extracted for each ITC, and independent ALS and hyperspectral variables such as height quantiles and band means were computed. Using such variables, tree species, tree height, stem diameter, and age were modeled and predicted at ITC level. From the ITC level predictions, dominant height, species and age were obtained at plot level. The dominant species were calculated as the species with the highest sum of basal area per plot. The dominant height and age predictions for a given tree species were used to determine SI based on the previously mentioned SI model also applied for determining field-derived SI (Braastad, 1980; Tveite, 1977, 1976). Details on the outlined methodological sequence are provided in the following sections.

3.2. Delineation of individual tree crowns

The ITC delineation method was based on the normalized ALS point cloud and cluster analysis. The full details of the method can be found in Kandare et al. (2016). In the rest of this paragraph, the steps of the delineation method are described at a general level.

Initially, ALS returns below 1.5 m were removed from the point cloud, and the ALS point cloud was horizontally sliced into three slices using thresholds calculated by Otsu thresholding (Otsu, 1979). Within each horizontal slice, a canopy height model (CHM) with a 0.50 m resolution was created. To each slice the local maxima (LM) filtering was applied using a circular moving window. The size (w) of the window was set to 5 − 5 − 5 from the bottom slice to the top slice. Using the position of the LM in each slice as centers, ALS returns were spatially clustered according to X–Z coordinates applying a K-means algorithm.

Further, the K-means clusters were iteratively merged across all the slices after ranking clusters in descending order by height. The lower clusters were merged to the highest cluster if the two-dimensional Euclidean distances between the lower cluster centers and the highest cluster center were within a predefined radius calculated as w_x * CHMresolution, where x = bottom, middle, or top slice of the highest cluster.

In the next step, the newly formed clusters were iteratively merged based on the overlapping area criterion after ranking clusters in descending order by height. The overlapping percentages for the highest and lower cluster were calculated as the percentage of the overlapping points with respect to total number of points within the cluster. If any of the two overlapping percentages was higher than or equal to 60%, which was set empirically, clusters were merged. Otherwise, the next neighboring cluster was considered. The described procedure was repeated for the remaining neighboring clusters. At the end, all clusters with projected area on the horizontal plane smaller than 2 m^2 were eliminated. ITCs were delineated as convex hulls from the 3D clusters of the ALS returns. The ITC position was extracted from the cluster's highest ALS return.

3.3. ITC level ALS and hyperspectral variables

ALS variables were calculated from each ITC's ALS returns, thus in total 27 ALS variables were defined, see Table 4. The crown area was computed as a convex hull from all pulses above an Otsu height threshold, which divided each cluster into crown and trunk pulses.

Hyperspectral variables were computed from the image pixels located within each ITC. However, before the variables were calculated the pixels, whose reflectance value in the blue portion of the spectrum (442.13 nm) was higher than a threshold defined with the Otsu algorithm (Otsu, 1979), were removed (Dalponte et al., 2014) to reduce noise and effects from shadowing. The average value of pixels was calculated within each ITC for all 80 bands, and they are referred to as band means (from B1 to B80). From the band means, 16 vegetation indices were computed (Table 5).

3.4. ITC level attribute prediction

Only ITCs for which positions were inside the field plot boundaries were selected and considered in the subsequent analysis. ITCs were matched to the closest field-observed trees according to their horizontal distance if the vertical distance was smaller than 5 m.

Table 4
Variables calculated from ALS point cloud belonging to each individual tree crown.

Variable	Description
h_{max}	Maximum height
h_{sd}	Standard deviation of height
h_{var}	Variance of height
h_{CV}	Coefficient of variation of height
h_{qx}	x% quantile of height (x = 10, 20, 30, 40, 50, 60, 70, 80, 90)
d_{qx}	Cumulative proportional canopy densities calculated for the respective quantiles h_{qx}
h_{ku}	Kurtosis of height
h_{sk}	Skewness of height
CA	Crown area

A schematic view of the procedure for predicting ITC attributes using ALS and hyperspectral data appears in Fig. 1. Tree species and stem diameter models were calibrated with all ITCs matched with forest inventory trees (N = 2462), whilst the tree height model was calibrated with the ITCs matched to the forest inventory trees with the field-derived heights (N = 653). Tree age was calibrated only with the ITCs that matched with the site trees containing age measurements (N = 147). Species-specific models were used for predicting tree height, stem diameter, and tree age because different trees species will have different crown structure and spectral responses given the same age and dimension. Moreover, such models have been examined and demonstrated to be accurate models for forest inventories (Ørka et al., 2010; Packalén and Maltamo, 2006).

Tree species classification was carried out with a support vector machine (SVM) classifier using all hyperspectral variables and $h_{\max}$, h_{qx}, and d_{qx} ALS variables. The SVM implementation in the "kernlab"-package (Karatzoglou et al., 2015) in the R software (R Development Core Team, 2008) was used. The selection of the proper penalty factor, i.e. parameter C, was done using a grid search strategy, and the value of 10 turned out to the best out of tested values 1, 10, 100, and 1000. This parameter setting is important because it defines the degree of penalized loss when a training error occurs. The weights for different species classes were set as ratio between the number of trees of the most frequent species and the number of trees of each species.

Tree height was modelled as a linear regression of the maximum height frequently used in ITC inventories (Hyyppä et al., 2001). A species-specific linear model was fitted:

$$h_{ij} = b_0 + b_1 * h_{max\,ij} + \varepsilon_{ij} \quad (1)$$

where h_{ij} is height (m) of tree i and species j measured in field, h_{maxij} is the maximum ALS height (m) of the corresponding tree, b_0 and b_1 are fixed parameters, and ε_{ij} is the error for tree i of species j ($\varepsilon_{ij} \sim N(0, \sigma_\varepsilon^2)$).

Stem diameter was modelled as a linear regression of the ALS maximum height, and crown area. Both ALS variables endorsed to be important in stem diameter modeling (Persson et al., 2002; Popescu et al., 2004) and to be robust in boreal forest conditions (Hyyppä et al., 2001; Kalliovirta and Tokola, 2005; Persson et al., 2002). A fitted species-specific linear model was:

$$dbh_{ij} = b_0 + b_1 * h_{max\,ij} + b_2 * CA_{ij} + b_3 * h_{max\,ij} * CA_{ij} + \varepsilon_{ij} \quad (2)$$

where dbh_{ij} is field-derived DBH (cm) of tree i and species j, h_{maxij} is the maximum ALS height (m), and CA_{ij} is crown area (m^2) of the corresponding tree, b_0–b_3 are fixed parameters, and ε_{ij} is the error for tree i of species j ($\varepsilon_{ij} \sim N(0, \sigma_\varepsilon^2)$).

Tree age was modelled with species-specific Poisson regression since age can be regarded as count data. Independent variables for age regression were selected from the ALS and hyperspectral variables in a two-step procedure. Variable selection was conducted for each tree species separately. First, pre-screening of variables was carried out with the random forest (RF) regression (Breiman, 1999) implemented in "randomForest"-package in the R software (Liaw and Wiener, 2015). The 25 most important variables were selected. Then the Poisson model was fitted using an exhaustive search in terms of Akiake information criterion (AIC) (Calcagno and Mazancourt, 2010) with up to four independent variables.

Tree age data were collected only for spruce and pine trees. However, the ITCs might be classified as broadleaves, too. Thus, a general model was built for broadleaves, where the variable selection was conducted on both tree species, spruce and pine. The final fitted species-specific age model was:

$$P(Age_{ij} = age \mid \mu_{ij}) = \frac{e^{-\mu_{ij}} (\mu_{ij})^{age}}{age!}, \quad age = 0, 1, 2\ldots \quad (3)$$

Table 5
Computation of the vegetation indices.

Normalized difference vegetation index	$NDVI = \left[\frac{949.80\text{nm} - 645.20\text{nm}}{949.80\text{nm} + 645.20\text{nm}}\right]$
Green normalized difference vegetation index	$GNDVI = \left[\frac{949.80\text{nm} - 543.67\text{nm}}{949.80\text{nm} + 543.67\text{nm}}\right]$
Difference vegetation index	$DVI = (949.80\text{nm} - 645.20\text{nm})$
Atmospherically resistant vegetation index	$\text{ARVI} = 949.80\,\text{nm} - \left[\frac{2 \cdot 652.45\,\text{nm} - 478.40\,\text{nm}}{949.80\,\text{nm}}\right] + (2{\cdot}652.45\,\text{n} - 478.40\,\text{nm})$
Enhanced vegetation index	$EVI = 2.5\left[\frac{949.80\,\text{nm} - 710.47\,\text{nm}}{710.47\,\text{nm} + 6 \cdot 652.45\,\text{nm} - 7.5 \cdot 478.40\,\text{nm} + 1}\right]$
Simple ratio index	$SR = \left(\frac{949.80\text{nm}}{710.47\text{nm}}\right)$
Modified red edge simple ratio index	$mSR = \left(\frac{753.99\text{nm} - 442.13\text{nm}}{703.22\text{nm} - 442.13\text{nm}}\right)$
Infrared percentage vegetation index	$IPVI = \left(\frac{949.80\text{nm}}{949.80\text{nm} + 688.71\text{nm}}\right)$
Plant senescence reflectance index	$PSRI = \left(\frac{681.46\text{nm} - 500.15\text{nm}}{753.99\text{nm}}\right)$
Structure insensitive pigment index	$SIPI = \left(\frac{797.5\text{nm} - 442\text{nm}}{797.5\text{nm} - 681\text{nm}}\right)$
Vogelmann red edge index 1	$VOG1 = \left(\frac{739.48\text{nm}}{717.72\text{nm}}\right)$
Water band index	$WBI = \left(\frac{899.03\text{nm}}{971.55\text{nm}}\right)$
Carotenoid reflectance index 1	$CRI1 = \left(\frac{1}{507.41\text{nm}} - \frac{1}{550.92\text{nm}}\right)$
Carotenoid reflectance index 2	$CRI2 = \left(\frac{1}{507.41\text{nm}} - \frac{1}{703.22\text{nm}}\right)$
Anthocyanin reflectance index 1	$ARI1 = \left(\frac{1}{550.92\text{nm}} - \frac{1}{703.22\text{nm}}\right)$
Anthocyanin reflectance index 2	$ARI2 = 800\text{nm}\left(\frac{1}{550.92\text{nm}} - \frac{1}{703.22\text{nm}}\right)$

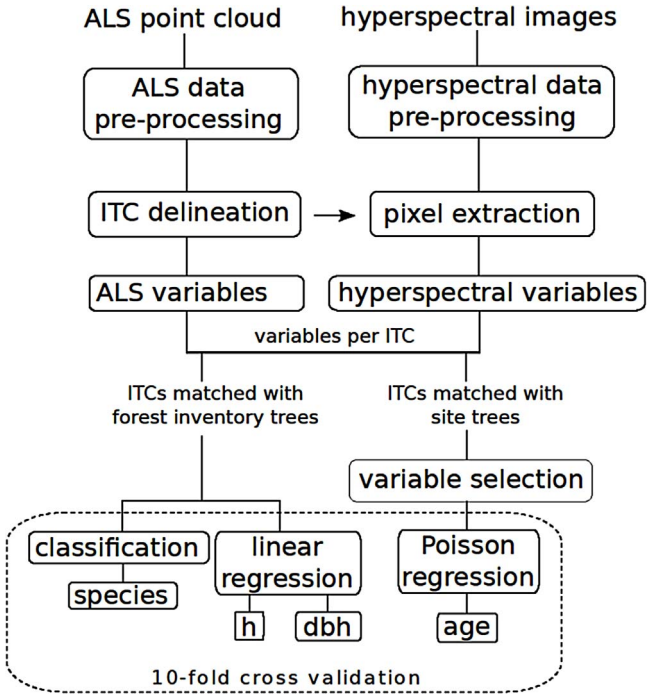

Fig. 1. Flowchart explaining the procedure of the ITC level biophysical attributes determination.

where μ_{ij} is the mean of the predicted Poisson distribution for the tree i and species j, such as spruce, pine, and general, model:

$$\mu_{ispruce} = e^{b_0+b_1*B23+b_2*B80+b_3*h_{q50}+b_4*CA} \quad (4)$$

$$\mu_{ipine} = e^{b_0+b_1*B57+b_2*B60+b_3*B79+b_4*VOG1} \quad (5)$$

$$\mu_{igeneral} = e^{b_0+b_1*B18+b_2*B80+b_3*h_{max}+b_4*CA} \quad (6)$$

3.5. Accuracy assessment and statistical analysis at ITC level

The accuracy of the ITC delineation method was assessed by analyzing omission and commission errors. The omission error was calculated as a rate of field-observed trees that could not be matched. The commission error was calculated as a rate of ITCs that could not be matched.

The models for the ITC level attributes were validated using a 10-fold cross validation approach, dividing the 153 field plots into 10 subsets. In each subset, the model was fitted using nine calibration sets (training set) and validated using the subset left out (validation set).

The species classification accuracy was evaluated in terms of overall accuracy, kappa accuracy, and producer's accuracy of the three classes (spruce, pine, and broadleaves). The model accuracy for height, DBH, and age was evaluated with the root mean square error (RMSE), mean difference (MD), and the coefficient of determination (r^2) computed as the square value of Pearson correlation coefficient.

3.6. Plot level attribute prediction and accuracy assessment

The biophysical attributes predicted for each tree were used to calculate plot level dominant species, dominant height, and age. The experimental setup consisted of two different cases, i.e. where the plot level dominant biophysical attributes were selected A) in three experiments (A1–A3) from all ITCs and B) in two experiments (B1 and B2) only from ITCs that matched with the field-derived site trees, i.e. dominant trees. In particular, we determined the SI from different combinations of input data (Table 6):

Table 6
The combination of input data in different experiments for determining site index. RS means remotely sensed-derived and FI indicates field inventory-derived biophysical attributes.

	Experiments				
	A1	A2	A3	B1	B2
Dominant species	RS	RS	FI	RS	RS
Dominant height	RS	RS	RS	RS	RS
Age	RS	FI	RS	RS	FI

A) all ITCs:

From the four dominant ITCs per plot, the average plot level dominant height and age were computed. The dominant ITCs were selected by the largest predicted DBH independently from the predicted species. The dominant species were calculated from all ITCs as the species with the highest sum of basal area per plot.

A1) dominant species, height and age were calculated from the predicted ITC attributes based on remotely sensed data;

A2) dominant species and height were calculated from the predicted ITC attributes based on remotely sensed data. The plot age was calculated from the field-derived site trees.

A3) dominant height and age were calculated from the predicted ITC attributes based on remotely sensed data. The dominant species were determined from the field observations;

B) ITCs matched with the site trees:

From the matched ITCs with the site trees, the average plot level dominant height and age were computed. The dominant species were calculated from the dominant ITCs as the species with the highest sum of basal area per plot. For some plots, not all the four site trees were matched with ITCs. In such cases, only the matched ITCs were used. When no ITCs were matched with the site trees, plot level attributes in experiments B1 and B2 were not available.

B1) dominant species, height and age were calculated from the predicted ITC attributes based on remotely sensed data.

B2) dominant species and height were calculated from the predicted ITC attributes based on remotely sensed data. The plot age was calculated from the field-derived site trees.

The accuracy of the calculated dominant height, age, and the SI was evaluated with the root mean square error (RMSE), mean difference (MD), standard deviation of the differences (SDD), and the squared Pearson correlation coefficient (r^2). The accuracy of dominant species per plot was assessed with overall accuracy and kappa accuracy.

4. Results

4.1. Accuracy assessment of predicted attributes at ITC level

The omission and commission errors of the ITC delineation method were of 67% and 9%, respectively. The tree species classification reached an overall accuracy of 80%, a kappa accuracy of 0.67, and producer's accuracies for spruce, pine, and broadleaves trees of 83%, 82%, and 64%, respectively. The prediction accuracies of tree height, stem diameter, and age are summarized in Table 7. The tree height was predicted with an RMSE of 1.16 m (6.5% of the mean), and the species-specific height models explained 93% of the variation of forest inventory tree heights. The species-specific stem diameter models explained 60% of the variation of forest inventory trees with RMSE of 4.77 cm (25.9%). The species-specific model of age reached an r^2 of 46%, and an RMSE of 35.57 years for the site trees.

Table 7
The tree level statistics for predicted height (h), stem diameter (dbh), and age with species-specific regression models for ITCs: root mean square error (RMSE), mean difference (MD), coefficient of determination (r^2) and number of observations (N). The respective statistics in percent of the field-derived mean value are in brackets.

	RMSE	MD	r^2	N
h	1.16 m (6.5%)	−0.18 m (−1.0%)	0.93	653
dbh	4.77 cm (25.9%)	−0.55 cm (−3.0%)	0.60	2462
age	35.57 yrs (43.5%)	−0.31 yrs (0.4%)	0.46	147

Table 8
The statistics for dominant species (SP), dominant height (H), age (AGE), and site index (SI) where assessments are presented for both species (spruce and pine) combined. The plot level attributes are evaluated in terms of: overall accuracy (OA), kappa accuracy (KA), root-mean-square error (RMSE), mean difference (MD), standard deviation of the differences (SDD), and coefficient of determination (r^2). Statistics in percentage of mean field-derived values are in brackets. − indicates that attributes were derived from field.

		Experiments				
		A1 (96 plots)	A2 (96 plots)	A3 (96 plots)	B1 (89 plots)	B2 (89 plots)
SP	OA [%]	93%		–	94%	
	KA	0.85			0.89	
H	RMSE [m]	1.12 (5.5%)			1.18 (5.8%)	
	MD [m]	0.43 (1.7%)			0.22 (1.1%)	
	SDD [m]	1.04 (5.1%)			1.17 (5.7%)	
	r^2	0.93			0.92	
AGE	RMSE [yrs]	34.01 (42.1%)	–	34.01 (42.1%)	32.81 (39.8%)	–
	MD [yrs]	−0.76 (−0.9%)		−0.76 (−0.9%)	−0.14 (−0.2%)	
	SDD [yrs]	34.18 (42.2%)		34.18 (42.2%)	33.00 (40.0%)	
	r^2	0.49		0.49	0.52	
SI	RMSE [m]	4.30 (27.6%)	1.18 (7.6%)	4.33 (27.8%)	3.62 (23.3%)	1.15 (7.4%)
	MD [m]	1.91 (12.2%)	0.40 (2.5%)	1.97 (12.7%)	1.17 (7.5%)	0.34 (2.2%)
	SDD [m]	3.87 (24.8%)	1.13 (7.2%)	3.88 (24.9%)	3.44 (22.2%)	1.11 (7.1%)
	r^2	0.44	0.96	0.44	0.58	0.96

4.2. Accuracy assessment of predicted attributes and site index at plot level

The calculated accuracies of dominant species, height, age, and site index are presented in Table 8. In general, the dominant heights were predicted with high accuracy in all experiments, and the accuracies were of the same magnitude for spruce and pine plots (Fig. 2). The same was found for predicted dominant species in experiments A1, A2, B1, and B2. The predicted age in experiments A1, A3 and B1, resulted in quite similar accuracies. For spruce plots the age was overpredicted with 4 years, while for pine plots the age was underpredicted with 4 years.

The field-derived and predicted SI values for the five experiments appear in Fig. 3. The highest SI accuracy was retrieved when the age was derived from the field data (experiments A2 and B2 in Table 8). The lowest SI accuracy was obtained when all plot level attributes were predicted (experiments A1 and B1 in Table 8). From the SI results of experiments A1 vs A3, we can infer that predicted dominant species did not affect the SI because the accuracy was relatively constant regardless of the applied strategy for tree species determination (calculated from ITCs predictions or taken from the field recordings). The results of five experiments also revealed that the selection of the four dominant ITCs (experiments A1, A2, and A3 vs B1, and B2) from which the plot attributes were calculated did not change the accuracy of the SI.

The SI residuals (field-derived SI − predicted SI) calculated in experiment A1 were compared with field-derived age and dominant height. It is evident that SI was underpredicted for young plots (< 60 years) and overpredicted for mature plots (> 100 years) (Fig. 4). Among the young plots, pine plots were more prone to underprediction

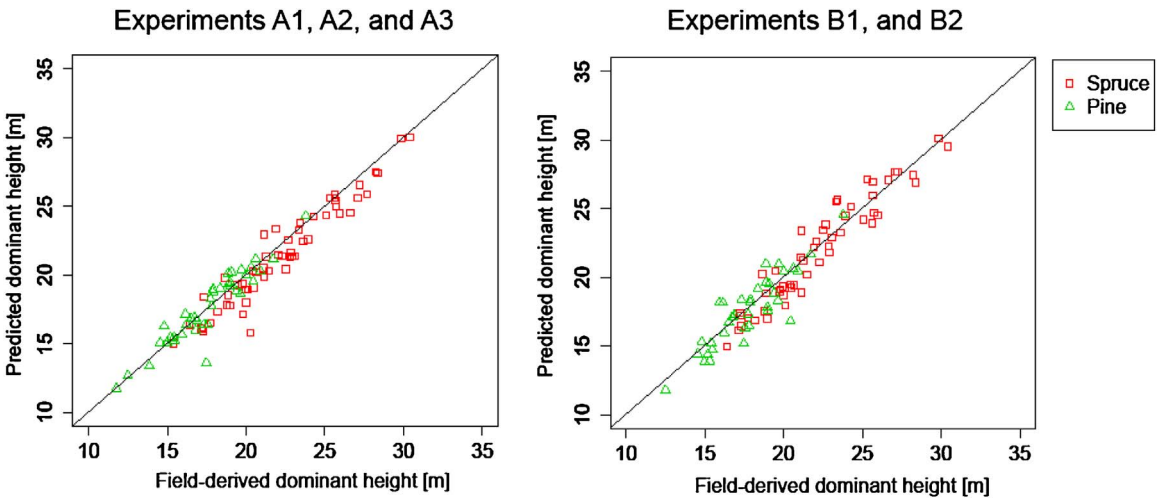

Fig. 2. Field-derived versus predicted dominant height for experiments A1–A3 (left) and experiments B1, B2 (right).

compared to spruce plots. The opposite was observed for mature plots for which spruce plots were more prone to overprediction of the SI. In addition, the SI residuals for spruce plots were more scattered compared to the pine plots. No particular trend was found comparing the SI residuals versus field-derived dominant heights at plot level. In experiment A2 (Fig. 5) the SI was predicted using field-derived age, therefore the SI residuals were smaller compared with experiment A1.

5. Discussion

5.1. ITC level attribute assessment

ITC level attributes were predicted with models that related field-derived tree attributes to ALS and hyperspectral variables. The classification accuracy of tree species was high for spruce and pine trees, but moderate for deciduous trees. Nevertheless, the main commercial species in Norway are spruce and pine, and they account for about 75% of the total forest volume ("The national forest inventory, 2011–2015," 2016). In the same study area, Dalponte et al. (2015) classified ITCs at pixel level using SVM and found similar classification accuracies as we did. Our classification results are in the same range as other studiers from boreal forest (Maltamo et al., 2014; Ørka et al., 2013). The tree height was predicted with high accuracy, while the stem diameter accuracy was lower. Even so, the stem diameter prediction accuracy is still comparable to results obtained in other studies (Dalponte et al., 2011; Ørka et al., 2010; Popescu, 2007). The

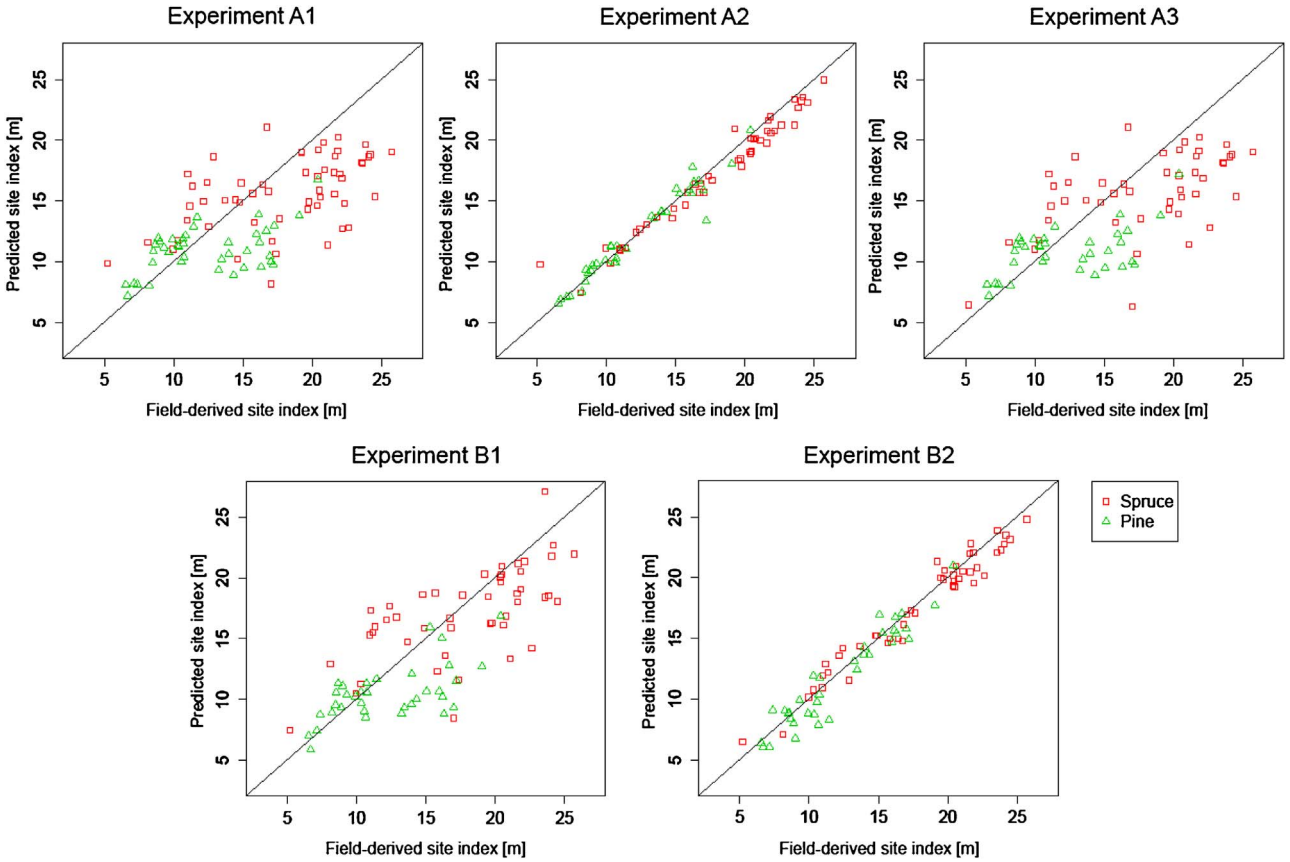

Fig. 3. Field-derived versus predicted site index for experiments A1, A2, A3, B1 and B2 at plot level. The solid line indicates a perfect fit.

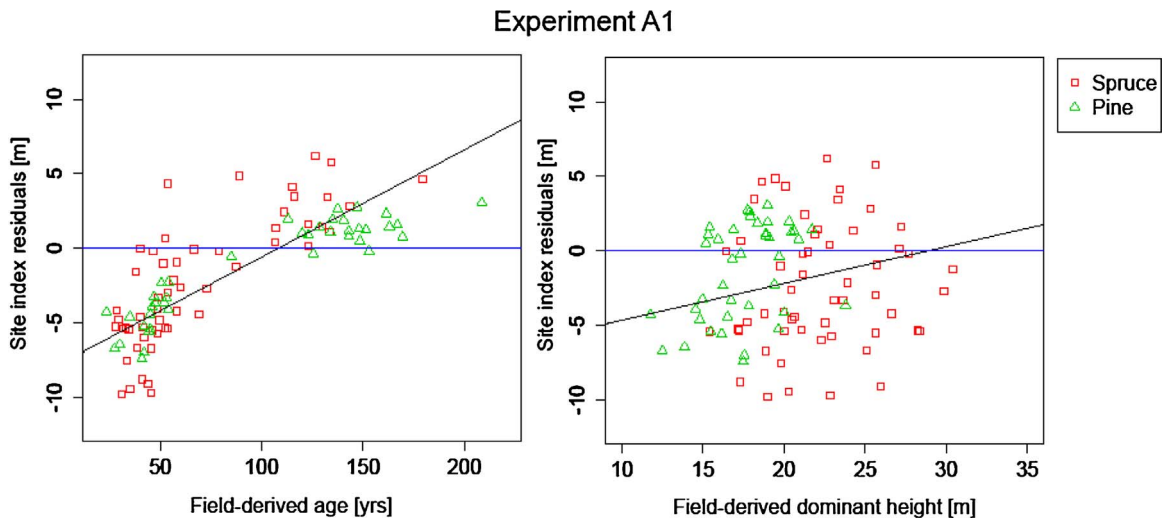

Fig. 4. Field-derived age versus predicted site index (SI) residuals (left) and field-derived dominant heights versus predicted site index (SI) residuals (right) obtained in experiment 1. The blue line represents zero and black line represents an ordinary least square fitted line to SI residuals. (For interpretation of the references to colour in this figure legend, the reader is referred to the web version of this article.)

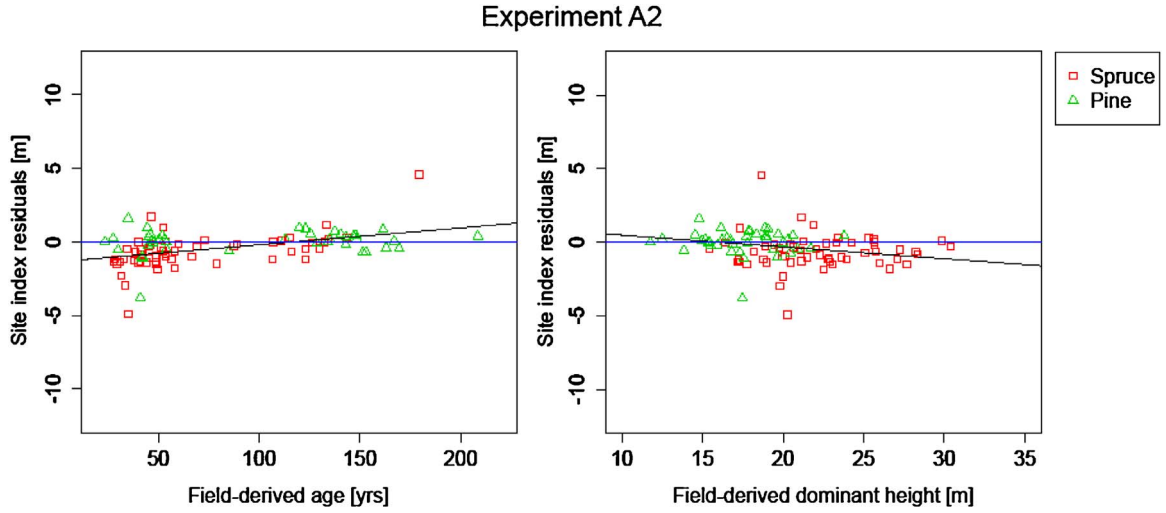

Fig. 5. Field-derived age versus predicted site index residuals (left) and field-derived dominant heights versus predicted site index residuals (right) obtained in experiment 3. The blue line represents zero and black line represents an ordinary least square fitted line to SI residuals. (For interpretation of the references to colour in this figure legend, the reader is referred to the web version of this article.)

tree age modeling was a challenging task and only moderate accuracies were obtained.

Age is strongly related to stand structure, species composition, and site history (Niemann, 1995; Pretzsch, 2009). Although these factors will influence the forest structure-related variables derived from ALS and hyperspectral data, we obtained low accuracies for age prediction. For ALS variables, we found the median and maximum ALS height together with the crown area as important variables. As the SI models used in our study are derived from growth models based on age and height, we cannot use only the ALS height derived variables to predict age. Such a relationship can be deceptive, because trees at the age of 40 from different site condition or type can grow to different heights. Thus, including hyperspectral variables can be important to obtain a stable age model. In our study, most of the variables used in the age models were selected from the hyperspectral data, which illustrates the importance of the hyperspectral variables. In general, the green spectral bands are related to the changes in physiological characteristics such as chlorophyll content, and pigments and the near-infrared bands are related to the changes in forest structure. In fact, with the tree age the leaf pigments (Linder, 1972) and canopy structure (Ishii and McDowell, 2002) are changing. Moreover, in a study by Bortolot (2000) it was found that the spectral signature in the near-infrared bands is varying with respect to the forest age. In the present study, the hyperspectral variables used for spruce and pine models were extracted from the green (B18 = 536.4 nm, B23 = 572.7 nm) and the near-infrared (B57 = 819.3 nm, B60 = 841.0 nm, B79 = 978.8 nm, B80 = 986.1 nm) parts of the spectrum. Surprisingly, only one vegetation index, VOG1, which is sensitive to the combined effects of foliage chlorophyll concentration, canopy leaf area, and water content, appeared to be important for the pine model (Eq. (5)).

5.2. Plot level attribute and site index assessment

The prediction of the dominant height, age, and SI depend on a correct detection of the dominant trees. In this regard, the usual phenomenon in ITC delineation of large omission errors for small or suppressed trees will not influence the results. Indeed, the dominant trees can be easily detected (Solberg et al., 2006). In the current study, we did not have information on social classes to confirm if the four selected ITCs per plot were dominant but we assumed the selection of the dominant ITCs according to largest DBH of the same species did not influence the SI determination. In forest inventory, dominant trees are

usually the trees with the largest DBH or basal area, therefore, we followed this definition.

Using the dominant ITCs, as identified by stem diameter predictions, to calculate the dominant tree heights from ITCs at plot level turned out to be reliable in terms of accuracy. In fact, similar studies reported the benefit of ALS variables for accurately predicting heights, specially for the tallest trees in a stand (Holopainen et al., 2010; Packalén et al., 2011; Tompalski et al., 2015a). Furthermore, the high accuracy of dominant height prediction obtained with ALS has shown to improve the accuracy of predicted SI (Ham et al., 2013; Tompalski et al., 2015a).

A correct determination of the dominant species is important for selecting a corresponding SI model. From the results on SI, it should be noticed that whether the dominant species were determined from the field observations (experiment A3) or from the predictions (experiment A1) the differences in SI accuracy predictions were negligible. This is also related to the fact that the species classification accuracy for the dominant species was high (kappa accuracy above 0.85). Although, the selection of the four largest ITCs in our study was independent of the tree species, we assumed that the largest ITCs belonged to the dominant trees. In particular, dominant ITC height, age, and SI accuracies did not substantially change whether the largest ITCs were selected based on largest DBH (experiment A1) or based on ITCs matched with site trees i.e. dominant trees (experiment B1).

A strong relationship between stand age and dominant tree height has been found in a forest with age ranging from 11 to 94 years, where the variability of tree age was small (Racine et al., 2014). However, the strength of such relationship is quite variable due to variations in forest management practices, site fertility, and other growing conditions (Kalliovirta and Tokola, 2005; Racine et al., 2014; Véga and St-Onge, 2009). The dominant height is highly correlated with stand age in even-aged stands. Moreover, the age-structure relationship in mixed-age stands is more ambiguous (Ung et al., 2001) since the strength of the relationship become asymptotic with aging (Sharma et al., 2011). In our study, the mean plot age ranged from 23.5 to 208.5 years (SD of 47.1 years), which certainly influenced the height-age relationship. Since the height growth will decrease with increasing age, it will result in an asymptotic relationship and less accurate predictions. According to some previous studies (Kimes et al., 1996; Niemann, 1995), stand age could be predicted reasonably well only in young forest stands where the height growth is large. Furthermore, the reflectance in the visible part of the spectrum decreases with tree age (Buddenbaum et al., 2005; Gates et al., 1965), while the reflectance in the near-infrared increases in the young forests compared to the old forests (Bortolot, 2000). In mature stands, usually more forest gaps and uneven-age trees appear causing lower age accuracy. Thus, it is suggested to apply different models for mature and young forest stands if such a delineation of a stands is available.

So far, previous studies have shown that the benefit of remotely sensed data, particularly for the tree heights (Lee and Lucas, 2007; Næsset and Økland, 2002), and species determination (Dalponte et al., 2012; Ørka et al., 2013). The accuracy of age predictions vary considerably between different studies and it seems to be strongly effected by forest management strategies and type of forest. Moreover, the existing stand age predictions are often considered to be uncertain in forest management (Maltamo et al., 2009; Racine et al., 2014). The use of remotely sensed data for SI determination is quite promising due to the spatial resolution of the data and timeliness of the data acquisition. Although SI maps are commonly used in practise, their accuracies are low. Eid and Moum (1999) assessed the accuracy of three different SI maps used in practise. They found quite large errors (MD varying from −27.6% to 7.5% and SDD varying from 19.3% to 37.6%) compared to the field-derived SI. Thus, our approach for predicting SI has a great potential to improve existing SI maps in an objective, and automatic way. Moreover, it provides results in a similar range of accuracy (MD = 12.2% and SDD 24.8%).

5.3. ITC approach for SI determination

The advantages of using an ITC approach is its spatial scalability and that the individual tree variations are taken into account (Dalponte and Coomes, 2016). In this regard, the ITCs used to determine SI can be aggregated to any area − e.g. network of grid cells − independently of a stand size. Thus, the scale of the output SI map could be of any resolution. Moreover, Eid and Moum (1999) showed that the SI accuracy depends on a size and definition of area of interest. They produced SI maps based on stand polygons and independent polygons (respresenting more similar and larger forest areas). The forest stand had large variation in SI compared to the independent SI maps. This is likely because other criteria than SI are important for stand deliniation, e.g. stand history, size, even-aged, and forest operations. Thus, the ITC approach for SI prediction proposed in the current study can provide a means to summarize SI in more homogenous areas within a stand (e.g. grid cells) and even at a sub-plot level. Similar can be done with the ABA but we have to bear in mind that the ITC approach is more similar to the field inventory protocol and has greater scalability compared to the ABA.

All variables needed to predict SI using the proposed approach can be predicted with a certain accuracy. The predicted dominant tree species and height achieved high accuracies when using remotely-sensed data no matter with which strategy the dominant ITCs were selected in experimets A and B. The weakest predictions were obtained for the age in both experimets, A and B. Thus, one can observe that the accuracy of the input attributes, such as dominant height and species classification, of the SI models contributed the most to the high SI accuracy. On the contrary, the age reached lowest accuracies and effected the most the SI accuracy. Still, the major challenge is to get a reliable age prediction. Therefore, future research should focus on means to improve the age determination of ITCs of the dominant trees. Use of multi-temporal data from repeated ALS surveys is one such option (Hollaus et al., 2015).

6. Conclusion

Plot level-derived biophysical attributes via ITC approach using ALS and hyperspectral data provided a reliable input for the determination of site productivity. The results of this study suggest that the selection of the dominant ITCs do not affect the accuracy of the predicted site index. The accuracies of dominant height and species were high in contrast to errors related to age predictions. Age prediction based on remotely sensed data is still a challenging task, especially in a mixed-age stands. However, when an even-aged stands are observed, the ABA can be complementary to the ITC approach. However, further investigations are needed to assess age at higher accuracy. To conclude, the proposed ITC approach demonstrated to be capable of providing a stable and consistent solution for determining site index of the forest areas and potentially at any grid cell resolution. In the future, it would be interesting to investigate and compare different remotely sensed data in predicting site index.

Acknowledgements

This work represents the outcome of Kaja Kandare's PhD project FORESTFUSION funded by the Edmund Mach Foundation, Trento, Italy. This research was partially supported by the hyper Bio project (project 244599) financed by the BIONÆR program of the Research Council of Norway and TerraTec AS. We would also like to thank TerraTec AS for collection and processing of ALS and hyperspectral data.

References

Bernstein, L.S., Adler-Golden, S.M., Sundberg, R.L., Levine, R.Y., Perkins, T.C., Berk, A.,

Ratkowski, A.J., Felde, G., Hoke, M.L., 2005. A new method for atmospheric correction and aerosol optical property retrieval for VIS-SWIR multi- and hyperspectral imaging sensors: QUAC (QUick Atmospheric Correction). International Geoscience and Remote Sensing Symposium (IGARSS) 3549–3552. http://dx.doi.org/10.1109/IGARSS.2005.1526613.

Boisvenue, C., Running, S.W., 2006. Impacts of climate change on natural forest productivity – evidence since the middle of the 20th century. Global Change Biol. 12, 862–882. http://dx.doi.org/10.1111/j.1365-2486.2006.01134.x.

Bortolot, Z.J., 2000. Determining Stand Ages in a Hyperspectral Image Using Artificial Neural Networks. University of British Columbia.

Braastad, H., 1980. Tilvekstmodellprogram for furu (growth model computer programs for Pinus sylvestris). Rep. Nor. For. Rese. Inst. 35, 265–359.

Breiman, L. (University of C., 1999. Random forest. *Mach. Learn.* **45**, 1–35. doi:10.1023/A:1010933404324.

Buddenbaum, H., Schlerf, M., Hill, J., 2005. Classification of coniferous tree species and age classes using hyperspectral data and geostatistical methods. Int. J. Remote Sens. 26, 5453–5465. http://dx.doi.org/10.1080/01431160500285076.

Chen, Y., Zhu, X., 2012. Site quality assessment of a Pinus radiata plantation in Victoria Australia, using LiDAR technology. South. For. 74, 217–227. http://dx.doi.org/10.2989/20702620.2012.741767.

Clutter, J.L., Fortson, J.C., Piennar, L.V., Brister, G.H., Bailey, R.L., 1983. Timber Management: a Quantitative Approach. John Wiley and Sons, New York.

Coops, N.C., Wulder, M.A., Culvenor, D.S., St-onge, B., 2004. Comparison of forest attributes extracted from fine spatial resolution multispectral and lidar data. Can. J. For. Res. 30, 855–866. http://dx.doi.org/10.5589/m04-045.

Coops, N.C., 2015. Characterizing forest growth and productivity using remotely sensed data. Curr. For. Rep. 195–205. http://dx.doi.org/10.1007/s40725-015-0020-x.

Dalponte, M., Coomes, D.A., 2016. Tree-centric mapping of forest carbon density from airborne laser scanning and hyperspectral data. Methods Ecol. Evol. 7, 1236–1245. http://dx.doi.org/10.1111/2041-210X.12575.

Dalponte, M., Bruzzone, L., Gianelle, D., 2008. Fusion of hyperspectral and LIDAR remote sensing data for classification of complex forest areas. IEEE Trans. Geosci. Remote Sens. 46, 1416–1427. http://dx.doi.org/10.1109/TGRS.2008.916480.

Dalponte, M., Bruzzone, L., Gianelle, D., 2011. A system for the estimation of single-tree stem diameter and volume using multireturn LIDAR Data. IEEE Trans. Geosci. Remote Sens. 49, 2479–2490. http://dx.doi.org/10.1109/TGRS.2011.2107744.

Dalponte, M., Bruzzone, L., Gianelle, D., 2012. Tree species classification in the southern Alps based on the fusion of very high geometrical resolution multispectral/hyperspectral images and LiDAR data. Remote Sens. Environ. 123, 258–270. http://dx.doi.org/10.1016/j.rse.2012.03.013.

Dalponte, M., Ørka, H.O., Ene, L.T., Gobakken, T., Næsset, E., 2014. Tree crown delineation and tree species classification in boreal forests using hyperspectral and ALS data. Remote Sens. Environ. 140, 306–317. http://dx.doi.org/10.1016/j.rse.2013.09.006.

Dalponte, M., Ene, L.T., Marconcini, M., Gobakken, T., Næsset, E., 2015. Semi-supervised SVM for individual tree crown species classification. ISPRS J. Photogramm. Remote Sens. 110, 77–87. http://dx.doi.org/10.1016/j.isprsjprs.2015.10.010.

Eid, T., Økseter, P., 1999. Bestandsuavhengig bonitering og konsekvenser. Rapport fra skogforskningen 8/99.

Eid, T., Moum, S.O., 1999. Bestandsuavhengig bonitering og nøyaktighet, Rapport Fra Skogforskningen. Norsk Institutt for Skogforskning, Ås.

Eid, T., Gobakken, T., Næsset, E., 2004. Comparing stand inventories for large areas based on photo-interpretation and laser scanning by means of cost-plus-loss analyses. Scand. J. For. Res. 19, 512–523. http://dx.doi.org/10.1080/02827580410019463.

Eid, T., 1996. Kontroll av skogbruksplandata fra «Understøttet fototakst» (Control of forest management planning data from Supported photo inventory). Aktuelt fra Skogforsk 8, 21.

Gatziolis, D., 2007. LiDAR-derived site index in the U.S. Pacihic northwest-challenges and opportunities. In: ISPRS workshop on laser scanning 2007 and SilviLaser 2007. Espoo, Finland. pp. 136–143.

Ham, S., Mikhailova, E., Gering, L., Post, C., Bridges, W., Cox, S., 2013. Temporal analysis of field SSURGO, and LiDAR-derived site indices in the southeastern United States. Soil Sci. 178, 325–334. http://dx.doi.org/10.1097/SS.0b013e3182a743e5.

Hollaus, M., Eysn, L., Maier, B., Pfeifer, N., 2015. Site index assessment based on multi-temporal ALS data. In: SilviLaser 2015 La Grande Motte. France. pp. 159–161.

Holmgren, J., Persson, Å., 2004. Identifying species of individual trees using airborne laser scanner. Remote Sens. Environ. 90, 415–423. http://dx.doi.org/10.1016/S0034-4257(03)00140-8.

Holopainen, M., Vastaranta, M., Haapanen, R., Yu, X., Hyyppä, J., Kaartinen, H., Viitala, R., Hyyppä, H., 2010. Site-type estimation using airborne laser scanning and stand register data. Photogramm. J. Finland 22, 16–32.

Hyyppä, J., Inkinen, M., 1999. Detecting and estimating attributes for single trees using laser scanner. Photogramm. J. Finland 16, 27–42.

Hyyppä, J., Kelle, O., Lehikoinen, M., Inkinen, M., 2001. A segmentation-based method to retrieve stem volume estimates from 3-D tree height models produced by laser scanners. IEEE Trans. Geosci. Remote Sens. 39, 969–975. http://dx.doi.org/10.1109/36.921414.

Ishii, H., McDowell, N., 2002. Age-related development of crown structure in coastal Douglas-fir trees. For. Ecol. Manage. 169, 257–270. http://dx.doi.org/10.1016/S0378-1127(01)00751-4.

Kalliovirta, J., Tokola, T., 2005. Functions for estimating stem diameter and tree age using tree height, crown width and existing stand database information. Silva Fennica 39, 227–248.

Kandare, K., Ørka, H.O., Chan, J.C., Dalponte, M., 2016. Effects of forest structure and airborne laser scanning point cloud density on 3D delineation of individual tree crowns. Eur. J. Remote Sens. 49, 337–359. http://dx.doi.org/10.5721/EuJRS20164919.

Karatzoglou, A., Smola, A., Hornik, K., 2015. The Kernlab Package. Tutorial.

Kim, S., McGaughey, R.J., Andersen, H.-E., Schreuder, G., 2009. Tree species differentiation using intensity data derived from leaf-on and leaf-off airborne laser scanner data. Remote Sens. Environ. 113, 1575–1586. http://dx.doi.org/10.1016/j.rse.2009.03.017.

Kimes, D.S., Holben, B.N., Nickeson, J.E., McKee, W.A., 1996. Extracting forest age in a Pacific Northwest forest from thematic mapper and topographic data. Remote Sens. Environ. 56, 133–140. http://dx.doi.org/10.1016/0034-4257(95)00230-8.

Lee, A.C., Lucas, R.M., 2007. A LiDAR-derived canopy density model for tree stem and crown mapping in Australian forests. Remote Sens. Environ. 111, 493–518. http://dx.doi.org/10.1016/j.rse.2007.04.018.

Liaw, A., Wiener, M., 2015. Package "randomForest". Breiman and Cutler's random forests for classification and regression. Tutorial.

Linder, S., 1972. Seasonal variation of pigments in needles: a study of Scots pine and Norway spruce seedlings grown under different nursery conditions. Studia Forestalia Suecica 100, 1–37.

Maltamo, M., Mustonen, K., Hyyppä, J., Pitkänen, J., Yu, X., 2004. The accuracy of estimating individual tree variables with airborne laser scanning in a boreal nature reserve. Can. J. For. Res. 1801, 1791–1801. http://dx.doi.org/10.1139/X04-055.

Maltamo, M., Packalén, P., Suvanto, A., Korhonen, K.T., Mehtätalo, L., Hyvönen, P., 2009. Combining ALS and NFI training data for forest management planning: a case study in Kuortane, Western Finland. Eur. J. For. Res. 128, 305–317. http://dx.doi.org/10.1007/s10342-009-0266-6.

Maltamo, M., Ørka, H.O., Bollandsås, O.M., Gobakken, T., Næsset, E., 2014. Using pre-classification to improve the accuracy of species-specific forest attribute estimates from airborne laser scanner data and aerial images. Scand. J. For. Res. 7581, 1–10. http://dx.doi.org/10.1080/02827581.2014.986520.

Messaoud, Y., Chen, H.Y.H., 2011. The influence of recent climate change on tree height growth differs with species and spatial environment. PLoS One 6. http://dx.doi.org/10.1371/journal.pone.0014691.

Næsset, E., Økland, T., 2002. Estimating tree height and tree crown properties using airborne scanning laser in a boreal nature reserve. Remote Sens. Environ. 79, 105–115. http://dx.doi.org/10.1016/S0034-4257(01)00243-7.

Næsset, E., 2002. Predicting forest stand characteristics with airborne scanning laser using a practical two-stage procedure and field data. Remote Sens. Environ. 80, 88–99. http://dx.doi.org/10.1016/S0034-4257(01)00290-5.

Niemann, K.O., 1995. Remote-sensing of forest stand age using airborne spectrometer data. Photogramm. Eng. Remote Sens. 61, 1119–1127.

Nothdurft, A., Wolf, T., Ringeler, A., Böhner, J., Saborowski, J., 2012. Spatio-temporal prediction of site index based on forest inventories and climate change scenarios. For. Ecol. Manage. 279, 97–111. http://dx.doi.org/10.1016/j.foreco.2012.05.018.

Ørka, H.O., Næsset, E., Bollandsås, O.M., 2010. Effects of different sensors and leaf-on and leaf-off canopy conditions on echo distributions and individual tree properties derived from airborne laser scanning. Remote Sens. Environ. 114, 1445–1461. http://dx.doi.org/10.1016/j.rse.2010.01.024.

Ørka, H.O., Næsset, E., Bollandsås, O.M., 2009. Classifying species of individual trees by intensity and structure features derived from airborne laser scanner data. Remote Sens. Environ. 113, 1163–1174. http://dx.doi.org/10.1016/j.rse.2009.02.002.

Ørka, H.O., Dalponte, M., Gobakken, T., Næsset, E., Ene, L.T., 2013. Characterizing forest species composition using multiple remote sensing data sources and inventory approaches. Scand. J. For. Res. 28, 677–688. http://dx.doi.org/10.1080/02827581.2013.793386.

Otsu, N., 1979. A threshold selection method from gray-level histograms. IEEE Trans. Syst. Man Cybernet. 9, 62–66. http://dx.doi.org/10.1109/TSMC.1979.4310076.

Packalén, P., Maltamo, M., 2006. Predicting the plot volume by tree species using airborne laser scanning and aerial photographs. For. Sci. 52, 611–622.

Packalén, P., Mehtätalo, L., Maltamo, M., 2011. ALS-based estimation of plot volume and site index in a eucalyptus plantation with a nonlinear mixed-effect model that accounts for the clone effect. Ann. For. Sci. 68, 1085–1092. http://dx.doi.org/10.1007/s13595-011-0124-9.

Paulo, J.A., Palma, J.H.N., Gomes, A.A., Faias, S.P., Tomé, J., Tomé, M., 2014. Predicting site index from climate and soil variables for cork oak (Quercus suber L.) stands in Portugal. New For. 46, 293–307. http://dx.doi.org/10.1007/s11056-014-9462-4.

Persson, Å., Holmgren, J., Soderman, U., 2002. Detecting and measuring individual trees using an airborne laser scanner. Photogram. Eng. Remote Sens. 68, 925–932.

Popescu, S.C., Wynne, R.H., Scrivani, J.A., 2004. Fusion of small-footprint lidar and multispectral data to estimate plot-level volume and biomass in deciduous and pine forests in Virginia, USA. For. Sci. 50, 551–565.

Popescu, S.C., 2007. Estimating biomass of individual pine trees using airborne lidar. Biomass Bioenergy 31, 646–655. http://dx.doi.org/10.1016/j.biombioe.2007.06.022.

Pretzsch, H., 2009. Forest Dynamics, Growth and Yield: From Measurement to Model. Springer-Verlag Berlin Heidelberg, Berlin, pp. 664. http://dx.doi.org/10.1007/978-3-540-88307-4.

Development Core Team, R., 2008. R: A Language and Environment for Statistical Computing [WWW Document]. R Foundation for Statistical Computing, Vienna, Austria. URL http://www.r-project.org (Accessed 22 September 2016).

Racine, E.B., Coops, N.C., St-Onge, B., Begin, J., 2014. Estimating forest stand age from LiDAR-derived predictors and nearest neighbor imputation. For. Sci. 60, 128–136. http://dx.doi.org/10.5849/forsci.12-088.

Rennolls, K., 1978. Top Height; its definition and estimation. Commonwealth For. Rev. 57, 215–219.

Sharma, R.P., Brunner, A., Eid, T., Øyen, B.H., 2011. Modelling dominant height growth from national forest inventory individual tree data with short time series and large age errors. For. Ecol. Manage. 262, 2162–2175. http://dx.doi.org/10.1016/j.foreco.

2011.07.037.
Sharma, R.P., Brunner, A., Eid, T., 2012. Site index prediction from site and climate variables for Norway spruce and Scots pine in Norway. Scand. J. For. Res. 27, 619–636. http://dx.doi.org/10.1080/02827581.2012.685749.
Skoupý, O., Zejdová, L., Hanuš, J., 2012. The use of hyperspectral remote sensing for mapping the age composition of forest stands. J. For. Sci. 58, 287–297.
Skovsgaard, J.P., Vanclay, J.K., 2008. Forest site productivity: a review of the evolution of dendrometric concepts for even-aged stands. Forestry 81, 13–31. http://dx.doi.org/10.1093/forestry/cpm041.
Solberg, S., Næsset, E., Bollandsås, O.M., 2006. Single tree segmentation using airborne laser scanner data in a structurally heterogeneous spruce forest. Photogramm. Eng. Remote Sens. 72, 1369–1378 (0099-1112/06/7212-1369).
Splechtna, B.E., 2001. Height growth and site index models for Pacific silver fir in southwestern British Columbia. B.C. J. Ecosyst. Manage. 1, 1–14.
The national forest inventory, 2011–2015 [WWW Document], 2016. URL https://ssb.no/en/jord-skog-jakt-og-fiskeri/statistikker/lst (Accessed 22 September 2016).
Tompalski, P., Coops, N.C., White, J.C., Wulder, M.A., 2015a. Augmenting site index estimation with airborne laser scanning data. For. Sci. 61, 861–873. http://dx.doi.org/10.5849/forsci.14-175.
Tompalski, P., Coops, N.C., White, J.C., Wulder, M.A., Pickell, P.D., 2015b. Estimating forest site productivity using airborne laser scanning data and landsat time series. Can. J. Remote Sens. 41, 232–245. http://dx.doi.org/10.1080/07038992.2015.1068686.
Tonolli, S., Dalponte, M., Neteler, M., Rodeghiero, M., Vescovo, L., Gianelle, D., 2011. Fusion of airborne LiDAR and satellite multispectral data for the estimation of timber volume in the Southern Alps. Remote Sens. Environ. 115, 2486–2498. http://dx.doi.org/10.1016/j.rse.2011.05.009.
Tveite, B., 1976. Bonitetskurver for Furu (Site-index Curves for Scots Pine (Pinus Sylvestris (L.))). Norsk institutt for skogforskning, Manus. (Upubl.).
Tveite, B., 1977. Bonitetskurver for gran (Site-index curves for Norway spruce (Picea abies (L.) karst)). Rep. Nor. For. Res. Inst. 33, 1–84.
Ung, C.H., Bernier, P.Y., Raulier, F., Fournier, R.A., Lambert, M.C., Régnière, J., 2001. Biophysical site indices for shade tolerant and intolerant boreal species. For. Sci. 47, 83–95.
Véga, C., St-Onge, B., 2009. Mapping site index and age by linking a time series of canopy height models with growth curves. For. Ecol. Manage. 257, 951–959. http://dx.doi.org/10.1016/j.foreco.2008.10.029.
Vaglio Laurin, G., Chen, Q., Lindsell, J.A., Coomes, D.A., Frate, F.D., Guerriero, L., Pirotti, F., Valentini, R., 2014. Above ground biomass estimation in an African tropical forest with lidar and hyperspectral data. ISPRS J. Photogramm. Remote Sens. 89, 49–58. http://dx.doi.org/10.1016/j.isprsjprs.2014.01.001.
Vehmas, M., Eerikäinen, K., Peuhkurinen, J., Packalén, P., Maltamo, M., 2011. Airborne laser scanning for the site type identification of mature boreal forest stands. Remote Sens. 3, 100–116. http://dx.doi.org/10.3390/rs3010100.
Yao, W., Krzystek, P., Heurich, M., 2012. Tree species classification and estimation of stem volume and DBH based on single tree extraction by exploiting airborne full-waveform LiDAR data. Remote Sens. Environ. 123, 368–380. http://dx.doi.org/10.1016/j.rse.2012.03.027.
Yu, B., Ostland, I.M., Gong, P., Pu, R.L., 1999. Penalized discriminant analysis of in situ hyperspectral data for conifer species recognition. IEEE Trans. Geosci. Remote Sens. 37, 2569–2577.
Yu, X., Hyyppä, J., Karjalainen, M., Nurminen, K., Karila, K., Vastaranta, M., Kankare, V., Kaartinen, H., Holopainen, M., Honkavaara, E., Kukko, A., Jaakkola, A., Liang, X., Wang, Y., Hyyppä, H., Katoh, M., 2015. Comparison of laser and stereo optical, SAR and InSAR point clouds from air- and space-borne sources in the retrieval of forest inventory attributes. Remote Sens. 7, 15933–15954. http://dx.doi.org/10.3390/rs71215809.
Zhao, K., Popescu, S., Meng, X., Pang, Y., Agca, M., 2011. Characterizing forest canopy structure with lidar composite metrics and machine learning. Remote Sens. Environ. 115, 1978–1996. http://dx.doi.org/10.1016/j.rse.2011.04.001.

Paper III

remote sensing

MDPI

Article

Prediction of Species-Specific Volume Using Different Inventory Approaches by Fusing Airborne Laser Scanning and Hyperspectral Data

Kaja Kandare [1,2,*], Michele Dalponte [3], Hans Ole Ørka [2], Lorenzo Frizzera [3] and Erik Næsset [2]

1 FoxLab, Joint CNR-FEM Initiative, Fondazione E. Mach, Via E. Mach 1, 38010 San Michele all'Adige (TN), Italy

2 Faculty of Environmental Sciences and Natural Resource Management, Norwegian University of Life Sciences, P.O. Box 5003, N-1432 Ås, Norway; hans-ole.orka@nmbu.no (H.O.Ø.); erik.naesset@nmbu.no (E.N.)

3 Department of Sustainable Agro-Ecosystems and Bioresources, Research and Innovation Centre, Fondazione E. Mach, Via E. Mach 1, 38010 San Michele all'Adige (TN), Italy; michele.dalponte@fmach.it (M.D.); lorenzo.frizzera@fmach.it (L.F.)

* Correspondence: kaja.kandare@fmach.it; Tel.: +386-41-292-200

Academic Editors: Jixian Zhang, Jixian Zhang, Lars T. Waser and Prasad S. Thenkabail
Received: 16 February 2017; Accepted: 21 April 2017; Published: 26 April 2017

Abstract: Fusion of ALS and hyperspectral data can offer a powerful basis for the discrimination of tree species and enables an accurate prediction of species-specific attributes. In this study, the fused airborne laser scanning (ALS) data and hyperspectral images were used to model and predict the total and species-specific volumes based on three forest inventory approaches, namely the individual tree crown (ITC) approach, the semi-ITC approach, and the area-based approach (ABA). The performances of these inventory approaches were analyzed and compared at the plot level in a complex Alpine forest in Italy. For the ITC and semi-ITC approaches, an ITC delineation algorithm was applied. With the ITC approach, the species-specific volumes were predicted with allometric models for each crown segment and aggregated to the total volume. For the semi-ITC and ABA, a multivariate *k*-most similar neighbor method was applied to simultaneously predict the total and species-specific volumes using leave-one-out cross-validation at the plot level. In both methods, the ALS and hyperspectral variables were important for volume modeling. The total volume of the ITC, semi-ITC, and ABA resulted in relative root mean square errors (RMSEs) of 25.31%, 17.41%, 30.95% of the mean and systematic errors (mean differences) of 21.59%, −0.27%, and −2.69% of the mean, respectively. The ITC approach achieved high accuracies but large systematic errors for minority species. For majority species, the semi-ITC performed slightly better compared to the ABA, resulting in higher accuracies and smaller systematic errors. The results indicated that the semi-ITC outperformed the two other inventory approaches. To conclude, we suggest that the semi-ITC method is further tested and assessed with attention to its potential in operational forestry applications, especially in cases for which accurate species-specific forest biophysical attributes are needed.

Keywords: species-specific volume; semi-individual tree crown; individual tree crown; area-based approach; *k*-MSN; airborne laser scanning; hyperspectral data; data fusion; forestry

1. Introduction

Stem volume is one of the most relevant resource attributes of forest inventories. In most European countries, volume is usually estimated or modeled based on field measurements [1]. In the Nordic countries, conventional forest inventories at various geographical scales have over the past few decades been enhanced by using remotely sensed data such as airborne laser scanning (ALS) and stereo aerial photography [2,3]. It has been shown that for local management planning, data from ALS may reduce

the overall costs by reducing the economic losses caused by incorrect decisions due to erroneous data [4]. One of the biggest challenges in remote sensing-assisted inventories is the discrimination among tree species [5]. Moreover, combining ALS data with hyperspectral images may improve the accuracy of species identification [6]. The tree species information is needed for many forest applications, especially to retrieve species-specific forest biophysical properties, such as volume and diameter at breast height (DBH), to derive biodiversity indicators and to plan silvicultural activities and cutting regimes.

Due to accurate three-dimensional measurements obtained by ALS [7,8], the ALS technology has become one of the most valuable remote sensing methods for providing forest information. By using ALS data, biophysical attributes such as volume, height, DBH, crown area, and stem density can be derived or modeled with high accuracies [2,9–12]. However, the estimation of biophysical attributes can be challenging in dense, multispecies, heterogeneous forest stands [13,14]. In the past, ALS data were examined to classify the tree species at the individual tree crown (ITC) level using shape, structure, and intensity features of the tree crowns [5,15]. In addition, when species-specific biophysical attributes are required, ALS data are often fused with optical images, i.e., color-infrared [16–18], multispectral [19,20], or hyperspectral [21,22] images, in order to improve the tree species classification [6,23,24]. Recently, multi- or hyper-spectral ALS sensors were developed with a high potential to be used as a future single-sensor solution for forest mapping [25–27]. Currently, remotely sensed hyperspectral data are the most promising data source for classifying tree species due to their ability to detect subtle variations in the chemical and structural properties of the tree canopy. Likewise, other studies demonstrated the success of identifying tree species in other ecosystems [28,29]. Thus, the remote sensing technologies that currently are considered to have the greatest potential to improve forest attribute characterization are ALS, describing the 3D forest structure, and hyperspectral imagery, outperforming other techniques for the identification of tree species [30]. The fusion of both has the potential to improve the forest attribute prediction accuracy [31].

Most local forest management inventories assisted by ALS data follow the area-based approach (ABA). For field sample plots distributed across the area of interest, several variables are extracted from the ALS echoes describing structural properties, for which the statistical relationships with field-measured biophysical attributes are constructed. The relationships, typically in the form of regression models, are then used to predict biophysical attributes for larger areas [9,32]. As an alternative, individual trees can be identified and the forest resource variables can be estimated as an aggregate of individual tree properties. To obtain tree attributes, the ITC approach was introduced [33]. With the ITC approach, crown segments are detected and delineated by applying segmentation algorithms [34,35]. The crown segments, often referred to as ITCs, can contain none, one, or several trees. In particular, this approach presumes that one crown segment contains exclusively one tree. For each crown segment, various ALS-derived structural variables are extracted, such as height and crown area. Based on these variables, the biophysical attributes, such as volume and DBH, are predicted for each segment and can be aggregated to other scales, e.g., a forest stand. Detection errors, i.e., omission error (failure to detect a tree or segmenting multiple trees into a single crown segment) and commission error (detecting an object that is not a tree or splitting a single tree into multiple crown segments), usually lead to underprediction of the forest biophysical attributes [36]. To overcome this problem, the semi-ITC approach has been proposed [37], which, in contrast to the ITC approach, allows a crown segment to contain multiple trees.

Several studies in Finland aimed to estimate species-specific forest volume using the combination of ALS data and aerial imagery based on ABA for three species groups: Norway spruce, Scots pine, and deciduous [16–18,38]. All these studies used a non-parametric *k*-most similar neighbor (*k*MSN) approach [39] based on Packalén and Maltamo [16]. Packalén and Maltamo [16] compared two approaches for determining species-specific volumes at the plot level. The first approach predicted the total volume using ALS data, upon which the species-specific volume was obtained by multiplying the total volume by the proportion of each tree species obtained from aerial photographs and fuzzy

classification. The second approach used the *k*MSN method for simultaneous prediction of volumes by tree species. The *k*MSN method resulted in more accurate species-specific volume estimates, except for the total volume where the fuzzy classification performed slightly better. Packalén and Maltamo [17] extended the *k*MSN approach from the previous study [16] to a stand level and tested the simultaneous prediction of volume, stem number, basal area, basal area median diameter, and tree height for the same tree species groups. The attributes of coniferous tree species were predicted accurately and those of deciduous trees less accurately, since they were minority species. Vauhkonen et al. [38] tested the performance of alpha shape metrics calculated from ALS data combined with image variables for species-specific volume predictions at the plot level. They demonstrated that using only ALS variables resulted in less accurate estimates compared to using combined ALS and images variables. Niska et al. [18] compared the *k*MSN method with three artificial neural network modeling methods: the multilayer perceptron (MLP), support vector regression (SVR), and self-organizing map (SOM) at the plot and stand level. The results revealed that the SVR and MLP models reached the greatest prediction accuracy, the *k*MSN a lower accuracy, and the SOM the smallest prediction accuracy. It should be noted that the SVR and MLP yielded negative estimates to some extent, whereas the *k*MSN and SOM estimates were always within the range of the modeling data.

In Norway, Breidenbach et al. [37] determined species-specific volumes for four dominant tree species (spruce, pine, birch, and aspen) using the ABA and semi-ITC approaches, combining the ALS and multispectral data. They applied the *k*NN approach using MSN and random forest (RF) methods for calculating statistical distances between the neighbors. The volumes predicted with the semi-ITC approach resulted in smaller RMSE compared with the ABA results. Ørka et al. [23] evaluated tree species composition in a Norwegian forest using (1) ALS data, (2) multispectral imagery, (3) hyperspectral imagery, (4) fused ALS and multispectral data, and (5) fused ALS and hyperspectral data. Subsequently, they predicted the basal area for spruce, pine, and deciduous trees for three inventory approaches: ABA, semi-ITC, and ITC. For the ABA and semi-ITC approach, the *k*NN algorithm with an Euclidean distance matrix was applied. The results suggested that the greatest species accuracy was achieved by fusing the ALS and hyperspectral data. The ITC approach resulted in the highest accuracy for deciduous species, while the ABA performed the best for the other tree species.

As mentioned above, different remote sensing-assisted forest inventory approaches have been suggested to assess species-specific forest attributes. Each of them has their own pros and cons. The advantage of the ABA is that it provides predictions with small systematic errors, i.e., mean differences, but at the same time only the attributes of the main tree species can be predicted with high accuracy, while for the minority species the errors were large and consequently resulted in inaccurate species-specific attributes [23]. The ITC-based approaches are suitable for developing species-specific models which could lead to more accurate stand-level estimations, particularly for mixed stands. The main drawback of the ITC procedure are the under-predictions due to problems in detecting suppressed and understory trees, especially in stands with a complex forest structure. We expect that a solution for alleviating systematic errors lies in the semi-ITC approach, which has not been sufficiently explored and tested in various forest conditions and ecosystems. In fact, only a few studies have evaluated and compared the results of species-specific volumes and basal areas obtained from different remote sensing-assisted forest inventory approaches [23,37]. In particular, most of these studies were carried out in boreal forest conditions, accounting for spruce, pine, and deciduous tree species groups. Moreover, most of the remote sensing-assisted inventory methods combine ALS data with aerial photogrammetry or multispectral imagery to obtain species-specific volumes. The fusion of complementary data sources, in particular ALS and hyperspectral data, typically result in greater accuracies in contrast to using the respective data separately [6,23,40]. Therefore, the fusion of ALS and hyperspectral data can offer a powerful basis for discriminating tree species and enables an accurate prediction of species-specific attributes. The *k*NN approach has grown in popularity due to its ability to successfully and simultaneously relate multiple forest attributes derived from field observations to remotely sensed data [41]. However, to the very best of our knowledge, there are no studies to date

that have tested the ITC, semi-ITC, and ABA approaches on a comparative basis with emphasis on species-specific volumes.

Thus, the main goal of the present study was to predict and evaluate the species-specific volume in a complex Alpine forest based on fused ALS and airborne hyperspectral data using three remote sensing-assisted forest inventory approaches, i.e., the ITC, semi-ITC, and ABA. The performances of all three inventory approaches were analyzed and compared for the total volume and volume of five species classes.

2. Materials and Methods

2.1. Data Set Description

2.1.1. Study Area

The 32 km^2 study area is located in an Italian Alpine forest in Pellizzano (46°17′22″N, 10°46′05″E), situated in the province of Trento. The altitude of the forest area ranges from 900 to 2200 m above sea level. The forest is dominated by Norway spruce (*Picea abies* (L.) Karst.), with the presence of other coniferous species (e.g., larch (*Larix decidua* Mill.), silver fir (*Abies alba* Mill.)) and broadleaves species (e.g., rowan (*Sorbus aucuparia* L.), aspen (*Populus tremula* L.), silver birch (*Betula pendula* Roth), and sycamore maple (*Acer pseudoplatanus* L.)). At higher altitudes, the forest is sparse, whereas at lower altitudes, the forest structure is more complex, varying from a one- to multi-layer forest with patches of mixed and homogeneous tree species composition. The forest is managed by selective logging focusing on the productive forest area, especially Norway spruce, and trees are harvested according to their stem diameter.

2.1.2. Field Data

Between the summers of 2013 and 2015, 47 circular sample plots were surveyed. The size of the sample plots was 700 m^2. The center location of each plot was determined with global navigation satellite system (GLONASS) measurements, resulting in a positional error of less than 1 m. At each sample plot, the tree locations were recorded as polar coordinates by measuring the azimuth and range to the center of the plot. For all trees within the sample plot, stem diameter at breast height and tree species were recorded. Tree height for randomly selected trees was measured using a Vertex III hypsometer. Tree heights of the remaining trees were predicted with allometric equations [1]. In each sample plot, only trees with a DBH greater than 7.5 cm were considered in the analysis. Dead or damaged trees were also excluded. In total, 1283 field trees were available for the analysis. The tree level and plot level statistics are summarized in Table 1. The tree species observed for the 1283 trees were: 76.5% Norway spruce, 9.0% larch, 6.2% rowan, 1.7% silver fir, 1.5% silver birch, 1.4% sycamore maple, and 3.7% other minority broadleaves. For the following analysis, we grouped tree species into five classes to predict species-specific volumes using the ITC and semi-ITC approaches: Norway spruce, larch, rowan, silver fir, and other broadleaves (silver birch, sycamore maple, and other minority broadleaves). The field statistics for the total and species-specific volumes are represented in Table 2.

2.1.3. ALS and Hyperspectral Data and Pre-Processing

ALS data were acquired with a Riegl LMS-Q680i sensor between the 7th and 9th of September 2012. The flying speed was approximately 51 m s^{-1} at the altitude of 660 m above ground level with the pulse repetition frequency of 400 kHz. For each emitted pulse, up to seven returns were recorded and the mean point density was 48 points m^{-2}. A digital terrain model (DTM) was extracted from the ALS points with a grid of 0.5 m by the vendor. In the preprocessing, underlying DTM elevations were subtracted from the ALS point elevations to convert ALS point elevations to heights above ground. From these ALS points, a raster canopy height model (CHM) of the area was created with the resolution of 0.5 m.

Table 1. Statistics of the field-observed biophysical attributes at the tree and plot level (SD = standard deviation, DBH = diameter at breast height, H = height, BA = basal area, V = volume).

	Biophysical Attributes	Range (Min-Max)	Mean	SD
Tree level	DBH (cm)	8.0–89.0	33.7	19.7
	H (m)	3.50–42.60	22.37	9.90
	BA (m^2)	0.01–0.62	0.08	0.12
	V (m^3)	0.01–9.21	1.54	1.72
Plot level	Mean DBH (cm)	13.5–71.8	38.0	12.8
	Mean H (m)	7.93–37.90	23.92	7.12
	Stem number (ha)	14–1132	386	228
	BA (m^2 ha^{-1})	0.63–85.73	46.26	21.22
	V (m^3 ha^{-1})	2.47–1363.35	590.28	321.76

Table 2. Statistics of the field-observed total and species-specific volumes for five species classes at the plot level.

Field Volume	Mean (m^3 ha^{-1})	SD (m^3 ha^{-1})	Relative SD (m^3 ha^{-1})
Total	590.28	321.76	54.51
Silver fir	34.88	24.85	71.25
Larch	102.37	114.16	111.51
Other broadleaves	9.64	14.47	150.21
Norway spruce	513.40	318.50	62.04
Rowan	3.36	6.98	207.34

Twenty-one hyperspectral images were acquired on the 13th of June 2013 by an AISA Eagle II sensor with a spatial resolution of 1 m. The minimum overlap among the images was 20%. The images consisted of 65 spectral bands between 403.09 nm and 995.31 nm. The hyperspectral strips were mosaicked into one image. For each pixel, the normalized difference vegetation index (NDVI) was computed based on the red and infrared wavelengths of 646.72 nm and 815.27 nm, respectively, and pixels with NDVI below 0.5 were removed in order to reduce noise and shadowing effects. Afterwards, the value of each pixel was normalized with respect to the sum of the values of the same pixel in all the bands to reduce the minor differences in radiance occurring between the different images [42]. The hyperspectral images were orthorectified using ALS data by the data vendor.

2.2. Methodology

2.2.1. Overview

The flowchart for the species-specific volume prediction for the three remote sensing inventory approaches using ALS and hyperspectral data is presented in Figure 1. For the ITC approach, the predicted volumes were summed per plot and scaled to m^3 per hectare, and for the semi-ITC and ABA approaches, the volumes were scaled to per-hectare values before modelling. In the case of the ITC and semi-ITC approaches, ALS and hyperspectral variables were calculated for each crown segment, whereas for the ABA variables, they were calculated for each subsample plot (sample plot halves). In the ITC approach, the tree species and DBH were predicted per segment. Subsequently, the allometric models were applied to predict species-specific volumes, which were summed up to have the total volume. For the semi-ITC approach and the ABA, the total and species-specific volumes were predicted simultaneously by a non-parametric multivariate *k*NN method using leave-one-out (LOO) cross-validation at the plot level.

The basic idea of the *k*NN method is that biophysical attributes within the target data are predicted by imputing them from the *k* nearest neighbors within the reference data. The nearness of neighbors is measured with the distance matrix between predictors (e.g., ALS and hyperspectral variables), which

are known in the reference and target data sets [43]. For the distance matrix, the most similar neighbor (MSN) method was applied, where the nearness of the k-nearest neighbors was defined in terms of weighted Euclidean distance in a conical search space. We chose this distance as from some preliminary analysis it appeared to be the most suitable among the random forest proximity, Euclidean distance, Euclidean distance without normalization, and Mahalanobis distance for this specific problem. Thus, we applied the *k*MSN, which is a particular type of the *k*NN methods. One property of the *k*MSN method is that the predictions are always within the range of the observed distribution. The main advantages of the *k*MSN approach are that the multivariate responses include the simultaneous predictions of the volumes and preserve their complex variance-covariance structure [39], along with their robustness to handle the outliers or extreme values in the data. The main disadvantage is that the *k*MSN approaches normally require a larger number of observations, although some studies have shown that reasonable results can be obtained also with a limited number of sample plots [37,44,45].

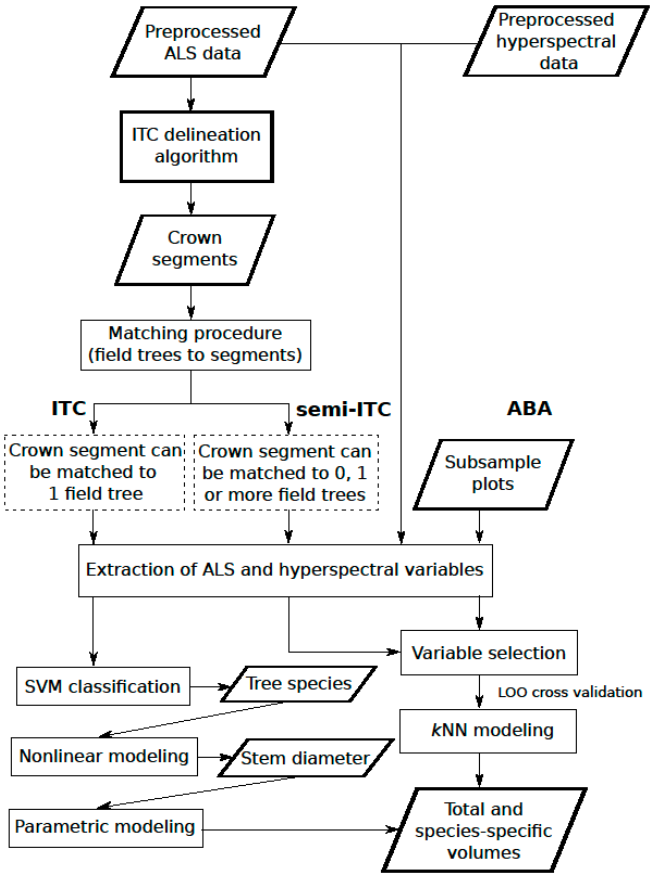

Figure 1. Flowchart of the procedure for predicting total and species-specific volumes.

2.2.2. ITC Delineation Method

To avoid ground hits and effects of rocks and small vegetation, all echoes with the height below 2 m were removed from the point cloud in the preprocessing step. The ITC delineation for the ITC and semi-ITC approaches was conducted with the algorithm implemented in the "itcSegment"-package in the R software [46] based on ALS data. For each crown segment, position, height (h_{max}), and crown area (CA) were calculated. The position and height were determined from the highest ALS point within a crown segment. The crown area (CA) was extracted with the convex hull. The height and crown area were used as ALS variables. The hyperspectral variables were computed for each crown segment as the average value of pixels for all 65 bands, and they are referred to as band means (from $B1$ to $B65$). This step was the same for both the ITC and the semi-ITC approach.

2.2.3. ITC Approach

The ITC approach assumes that each delineated crown segment contains one field tree. The matching procedure of the crown segments and field trees was different from the classical methods [34,47]. An empirical threshold for the permitted distance (horizontal or vertical) between the "matched" crown segment and field tree was avoided. In particular, each segment was matched to the closest field tree according to a 3D distance. To confirm a good match, we fitted a simple linear regression with the field tree height as response (h) and crown segment maximum height as predictor (h_{max}):

$$h_i = b_0 + b_1 \times h_{max_i} + \varepsilon_i, \quad (1)$$

where i corresponds to a crown segment, b_0 and b_1 are fixed parameters, ε_i is the error of tree i ($\varepsilon_i \sim N(0, \sigma^2)$), and σ^2 is the model variance. The prediction interval was defined as:

$$h_i \pm t_{n-p}^{\frac{0.95}{2}} \hat{\sigma} \sqrt{1 + h_{max_i} (X'X)^{-1} h'_{max_i}}, \quad (2)$$

where t stands for the t-distribution, n means a number of segments, p represents a number of model parameters, and X is a design matrix. Out of 629 segments, 25 segments' fitted heights were not within the prediction interval (Figure 2). These 25 segments were excluded from the tree species and stem diameter modeling but not from the accuracy analysis. Breidenbach et al. [37] applied the same procedure to exclude segments with incorrect field trees from modeling. After matching, the ALS and hyperspectral variables were merged for each crown segment.

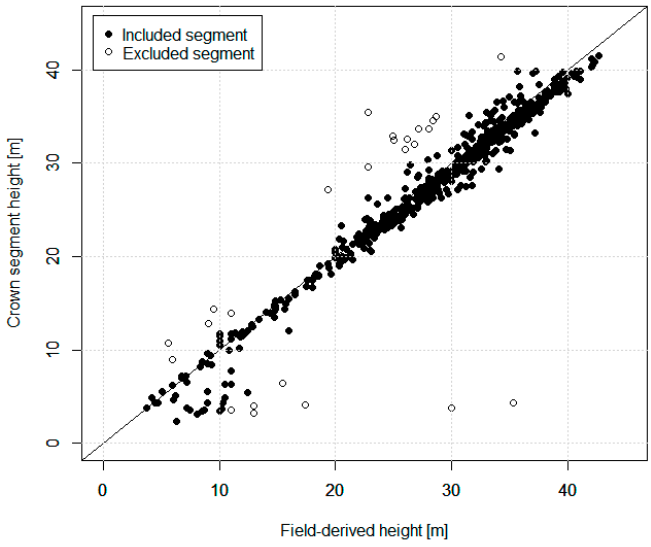

Figure 2. The field-derived tree height of the matched field trees and the respective maximum airborne laser scanning (ALS) height of crown segments.

The tree species were classified at the pixel level with a support vector machine (SVM) classifier using hyperspectral variables. We used the SVM implementation in the R package "kernlab" [48]. The penalty factor (C) was selected with a grid search strategy, testing values of 1, 10, 100, and 1000. The value of 10 turned out to reach the highest classification accuracy. The weights for different species classes were set as a ratio between the number of trees of the most frequent species and the number of trees of each species. The predicted species for each pixel were aggregated within each crown segment according to a majority rule.

The stem diameter at breast height (cm) was predicted for each crown segment using a nonlinear regression model, taken from the study of Dalponte and Coomes [49] conducted on the same dataset. The fitted species-specific nonlinear model was:

$$DBH_{ij} = \varepsilon_j \times {h_{max_{ij}}}^{\rho_j} \times \left(1 + \vartheta_j CA_{ij}\right) \quad (3)$$

where $h_{max_{ij}}$ is the maximum crown segment height (m), CA_{ij} is the crown area (m), and ε_j, ρ_j and ϑ_j are parameters determined in [49]. Indices i and j correspond to segment and species, respectively. Knowing the predicted species and stem diameter, the species-specific volumes were predicted based on allometric models for temperate species of Scrinzi et al. [1]:

$$\hat{V}_{ij} = a_j \times \left(D\hat{B}H_{ij} - d_j\right)^{b_j} \times \left(h_{max_{ij}}\right)^{c_j}, \quad (4)$$

where a_j, b_j, c_j, and d_j are parameters taken from species-specific tables derived from trees in the Trentino province [1]. Finally, the volume was summarized for each species at the plot level.

2.2.4. Semi-ITC Approach

The semi-ITC approach presumes that a crown segment can contain none, one, or more field trees. Thus, each field tree was matched to the closest segment according to a 3D distance. The field derived values of the total and species-specific volumes were assigned to each segment. For the segments that were matched with more than one field tree, the tree volumes were summed up over the total and species-specific volumes. The segments with no match had zero values for all volumes. In the following analysis, all the segments were used for the modelling and accuracy analysis.

The *k*MSN prediction method, implemented in the R package "yaimpute" [50], was applied using the total and species-specific volumes per segment derived from the field observations as response variables and the selected predictor variables per segment derived from the ALS and hyperspectral variables as covariates. The predictor variables were selected with the variable selection method *varSelection* implemented in the R package "yaimpute" [50]. For the selection, the remotely sensed variables were added to the *k*MSN model based on the computed generalized root mean square distance (grmsd) between the predicted and observed response variables among the field observations. The grmsd computes the root mean square distance between the observed and predicted volumes over several variables simultaneously. The variable that was related to the largest grmsd was removed. Finally, the selected predictor variables were: CA, h_{max}, $B4$ (428.96 nm), $B13$ (509.16 nm), $B14$ (518.10 nm), $B29$ (655.98 nm), $B31$ (674.49 nm), $B33$ (693.00 nm), and $B43$ (786.82 nm). The number of the nearest neighbors was selected empirically and the distance to the nearest neighbors, i.e., crown segments, was defined by the MSN distance matrix based on the predictor variables.

2.2.5. ABA

In order to increase the number of plots, i.e., neighbors, important for the *k*MSN method, we subdivided the 47 sample plots into halves, resulting in 94 subsample plots with a size of 350 m^2. The same procedure was applied by Breidenbach et al. [37]. The ALS canopy height- and density-related variables calculated for each subsample plot were the ones also used in other studies [9,23], using the lower limit of the canopy defined by a threshold value of 2 m [9,51,52]. The ALS variables were computed for the first, intermediates, and last returned laser pulses, denoted x, from 1 to 3, respectively: maximum ($h_{\max\_x}$), mean (h_{mean_x}), skewness (h_{sk_x}), kurtosis (h_{ku_x}), and coefficient of variation (h_{cv_x}) of the ALS heights (m) and quantiles corresponding to the 0, 10, 20,...,90 percentiles of the ALS heights ($h_{q10\_x} - h_{q90\_x}$). Furthermore, 10 vertical slices of equal height were defined as a range between the lowest laser canopy height (2 m) and the 90th percentile of the canopy height. Then, the canopy density variables ($d_{1\_x} - d_{10\_x}$) were calculated as the proportions of laser pulses above each vertical slice to the total number of pulses. Additionally, the canopy volume (C_{Vol}) was calculated as the cell-wise difference between rasterized height values (m) of the first (F_{ij}) and last (L_{ij}) returned pulses of the i-th pixel in the j-th sample plot as $C_{Vol} = \sum_j^J (F_{ij} - L_{ij}) \times length(F_{ij})$. The hyperspectral variables were the same as for the semi-ITC. Additionally, the NDVI and the difference vegetation

index (DVI) were computed for each plot as both indices can be potentially good explanatory variables for the volume prediction [53,54].

The variable selection and prediction method employed were the same as for the semi-ITC approach. For the simultaneous volumes prediction, 18 variables were selected: h_{CV_2}, h_{max_1}, h_{q20_1}, h_{q50_1}, h_{q10_2}, h_{q40_2}, h_{q20_3}, h_{q30_3}, d_{10_2}, d_{4_3}, $B3$ (420.34 nm), $B14$ (518.10 nm), $B16$ (535.98 nm), $B20$ (572.65 nm), $B27$ (637.47 nm), $B35$ (711.62 nm), $B38$ (739.59 nm), and $B54$ (891.00 nm). To avoid overfitting, the number of variables should be smaller than the number of samples. In addition, adding more predictor variables in the training data does not always improve the *k*NN model accuracy [55]. Then, we applied the *k*MSN distance metric to find the reference plots for the target plots based on the selected variables above. The number of the nearest neighbors used was based on preliminary tests according to the balance between the highest accuracy and the smallest systematic error.

2.2.6. Accuracy Assessment

For the ITC approach, the tree species classification accuracy was validated at the ITC-level with a 3-fold cross-validation using the overall accuracy (OA), kappa coefficient (KA), the producer's and user's accuracies derived from the confusion matrix. The accuracy of the predicted stem diameter at the ITC-level was assessed with the root mean square error (RMSE), and the mean differences (MD) as an indicator of the systematic error were calculated as

$$RMSE = \sqrt{\frac{\sum_{i=1}^{n}\left(observed_{ij} - predicted_{ij}\right)^2}{n}}, \quad (5)$$

$$MD = \frac{\sum_{i=1}^{n}\left(observed_{ij} - predicted_{ij}\right)}{n} \quad (6)$$

where n is the sample size (number of segments) and i denotes a segment for which the observed and predicted attributes for the j-th species class were calculated. The relative RMSE and MD were calculated by dividing with the mean of the observed values. Additionally, the squared correlation (r^2) was computed as the Pearson's correlation coefficient of observed and predicted values. The accuracy and the systematic error of the total and species-specific volume models at the plot level were calculated with the same statistics as above, where the sample size represented the number of sample plots and i denoted the plot.

The reliability of the predicted volumes by the semi-ITC and ABA was tested by means of LOO cross-validation. For the semi-ITC and ABA approaches, the crown segments and subsample plots, respectively, belonging to the same sample plot, were subsequently left out in the cross-validation process. The accuracies of the predicted total and species-specific volumes at the plot level by both approaches were evaluated with the same measures as for the ITC approach. We performed the Wilcoxon signed rank test to test if the differences between the observed and predicted volumes for all inventory approaches were significantly different at a significance level of 0.05. The Friedman test at the same significance level was applied to check the significance of the differences in the distribution of the differences between the observed and predicted species-specific volumes among sample plots for the three inventory approaches. In addition, we conducted Conover post-hoc analysis in order to decide which pairs of the three inventory approaches were significantly different from each other for each species class volume.

3. Results

3.1. ITC Approach

The ITC segmentation method delineated 629 segments within the 47 plots. The omission and commission errors were 51% and 4%, respectively. When calculating hyperspectral variables per crown, one crown was removed due to the effects from shadowing. Thus, the following analysis comprised

628 crown segments. The tree species overall and kappa accuracies were 85.2% and 0.57, respectively, where the producer's and user's accuracies are shown in Table 3. The predicted stem diameter per each crown segment resulted in an RMSE of 11.0 cm (relative RMSE = 23.40%) and MD of 0.43 cm (relative MD = 0.92%) with the explained proportion of the variance of 0.61. Knowing the predicted species, the species-specific volumes were predicted and aggregated at the plot level (Table 4 and Figure 3). We also checked if the RMSE of the predicted volumes were within the standard deviation of the field volumes (Table 2). In this regard, the RMSEs of the volumes for larch, Norway spruce, and rowan classes were within the standard deviation of the observed volumes while the volumes of the species classes other broadleaves and silver fir were not. Moreover, the Wilcoxon signed rank test showed that the volume differences between the observations and predictions were statistically different for all species classes ($p \leq 0.05$), except for the larch and rowan classes.

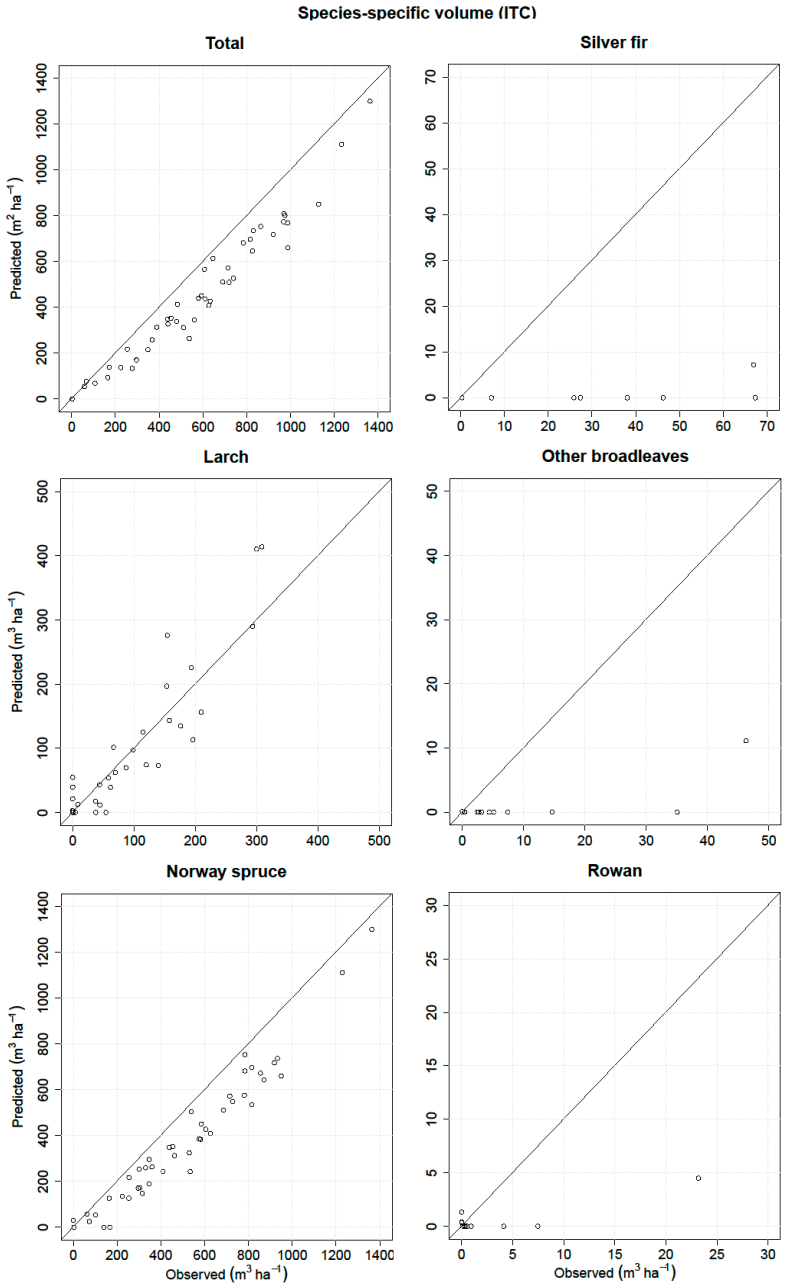

Figure 3. Observed versus predicted total and species-specific volumes at the plot level derived from the individual tree crown (ITC) method.

Table 3. Producer's and user's accuracies of tree species classification at the ITC level.

	Silver Fir	Larch	Other Broad Leaves	Norway Spruce	Rowan
Producer's accuracy (%)	16.7	71.6	14.3	90.1	75.0
User's accuracy (%)	100	58.1	50.0	92.2	81.8

Table 4. Results of the predicted volumes derived from the ITC approach, aggregated to the plot level (* = differences between the predicted and observed volumes are significantly different from zero ($p \leq 0.05$), RMSE = root mean square error, and MD = mean differences).

Volume	RMSE (m^3 ha^{-1})	Relative RMSE (%)	MD (m^3 ha^{-1})	Relative MD (%)	r^2
Total	152.18	25.78	132.37	22.43 *	0.95
Silver fir	40.53	116.2	33.98	97.41 *	0.27
Larch	48.7	47.57	−5.29	−5.17	0.90
Other broadleaves	14.71	152.67	8.77	91.02 *	0.58
Norway spruce	151.26	29.46	130.34	25.39 *	0.95
Rowan	6.21	184.71	2.77	82.25	0.76

3.2. Semi-ITC Approach

For the semi-ITC approach, the same segmentation method was employed as for the ITC approach, but with different matching procedures where every field tree was matched to the closest segments. Fifty-four segments out of 628 remained without any field match. The number of nearest neighbors was selected empirically, according to the smallest RMSE and MD values. We choose three neighbors, even if two or four revealed similar results. The predicted volumes were aggregated at the plot level (Table 5) and displayed in Figure 4. The highest accuracies were reached for total, Norway spruce, and larch volumes, while the lowest accuracies were obtained for silver fir, other broadleaves, and rowan volumes. The relative RMSE of the predicted silver fir, other broadleaves, and rowan volumes were also greater than the relative standard deviations of the corresponding observed volumes (Table 2). The predicted volumes for total, larch, and Norway spruce resulted in minor systematic errors with relatively high r square correlations, except for larch. All the predicted volumes were underpredicted except for the total and Norway spruce volumes. Regarding the Wilcoxon signed rank statistic, the differences between the observed and predicted volumes were not statistically significant ($p > 0.05$) for all species classes.

Table 5. Results of the predicted volumes derived from the semi-ITC approach extended to the plot level.

Volume	RMSE (m^3 ha^{-1})	Relative RMSE (%)	MD (m^3 ha^{-1})	Relative MD (%)	r^2
Total	102.78	17.41	–1.59	–0.27	0.90
Silver fir	15.35	258.48	1.04	17.5	0.16
Larch	76.02	96.95	5.91	7.54	0.51
Other broadleaves	8.82	330.74	0.41	15.57	0.03
Norway spruce	124.25	24.73	–9.07	–1.81	0.85
Rowan	2.69	341.02	0.11	14.53	0.50

3.3. ABA

The number of nearest neighbors was set to three, although the volumes of the majority species did not substantially change using one or two neighbors. The accuracy assessment and visualization of the volume predictions using the *k*MSN approach appear in Table 6 and Figure 5. The RMSE of the total volume (Table 6) was within the standard deviation of the observed volumes except for the other broadleaves volume. The Wilcoxon signed rank test showed that the differences between the predicted and observed volumes were not statistically significant ($p > 0.05$).

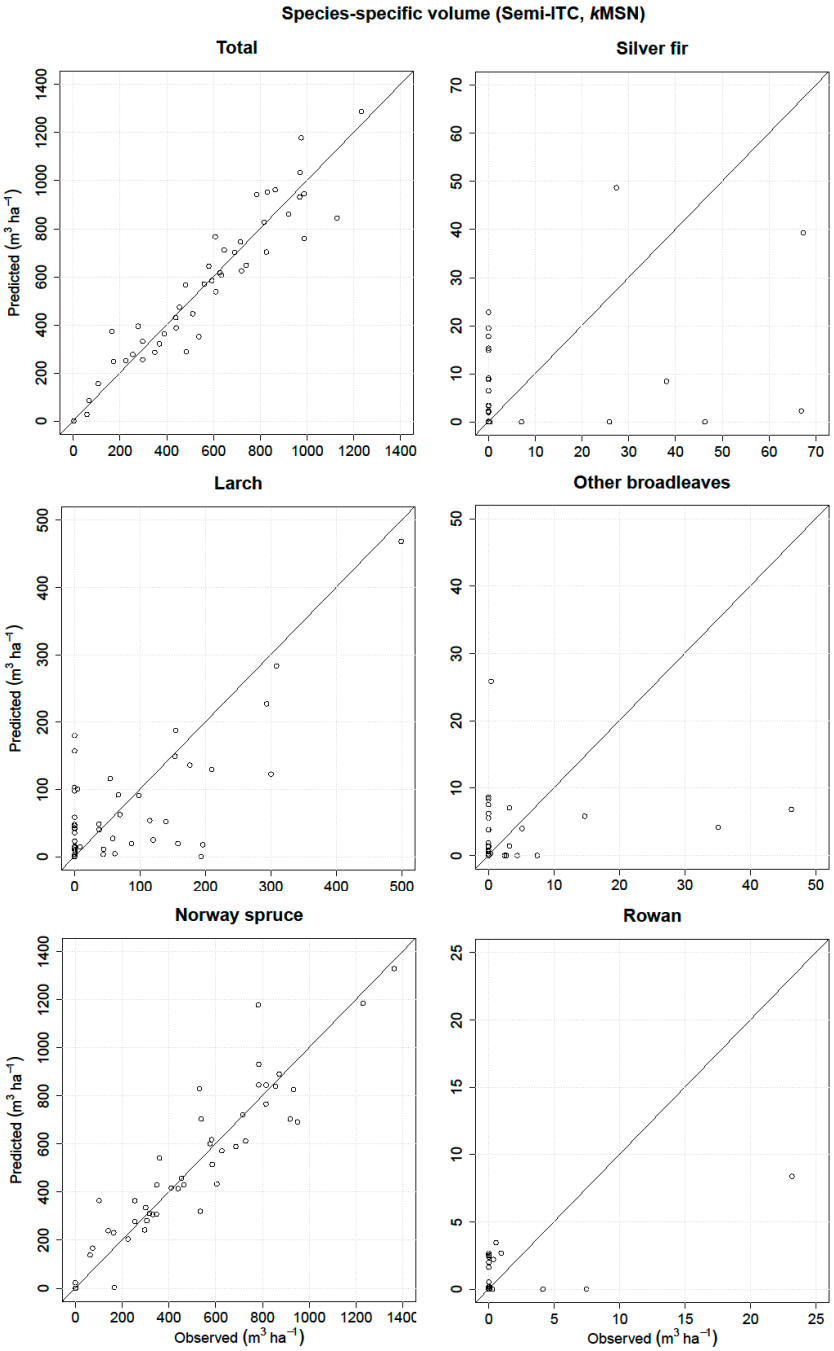

Figure 4. Observed versus predicted species-specific volumes at the plot level derived from the semi-ITC method.

Table 6. Results of the predicted volumes using the k-nearest neighbor approach derived from ABA at the plot level.

Volume	RMSE (m^3 ha^{-1})	Relative RMSE (%)	MD (m^3 ha^{-1})	Relative MD (%)	r^2
Total	182.75	30.95	−15.88	−2.69	0.67
Silver fir	18.01	303.25	−0.49	−8.26	0.01
Larch	69.36	88.44	10.00	12.76	0.60
Other broadleaves	8.20	306.02	1.74	65.02	0.12
Norway spruce	183.54	36.52	−27.77	−5.53	0.68
Rowan	3.76	465.42	0.63	78.56	0

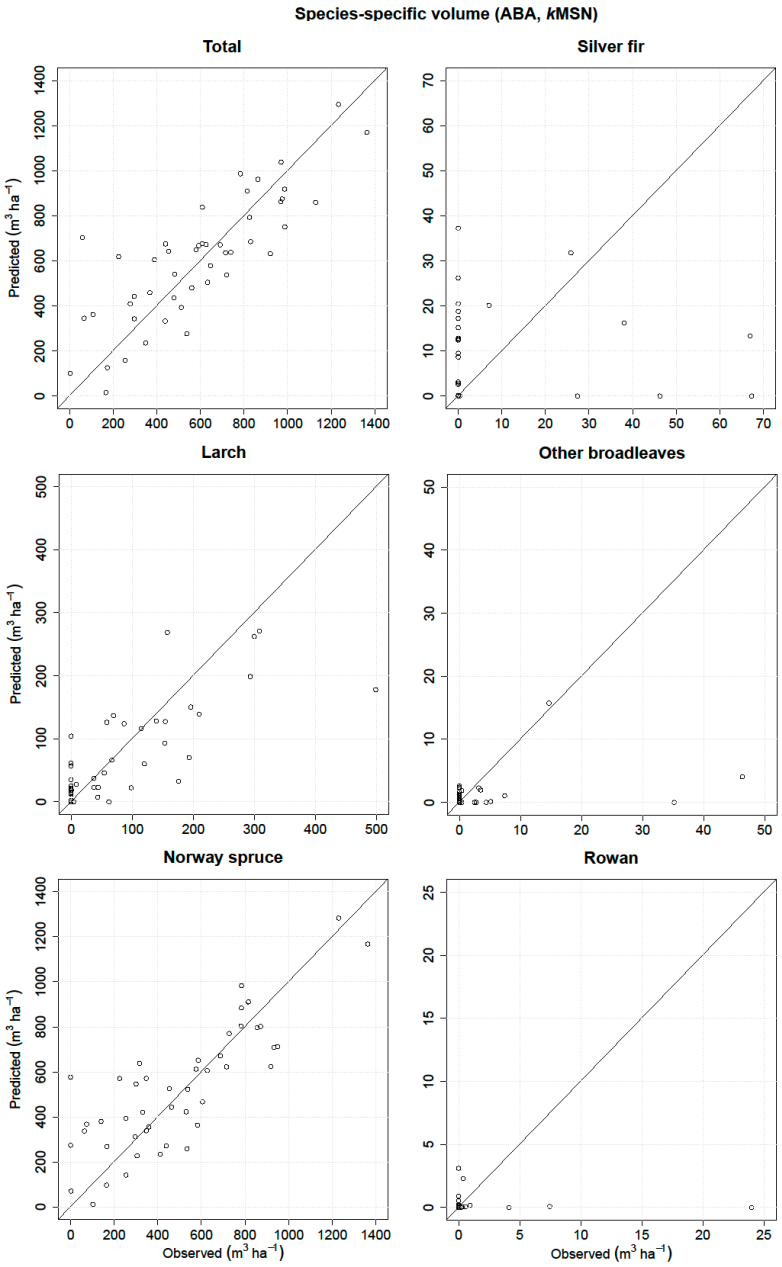

Figure 5. Observed versus predicted species-specific volumes at the plot level derived from the area based approach (ABA) method.

3.4. Comparison of the Different Inventory Approaches

For all three inventory approaches, the RMSEs and MDs of the total and five species-specific volumes were compared (Figure 6). The lowest relative RMSEs of the volumes were achieved by the ITC approach, except for the total and Norway spruce volumes where the semi-ITC resulted in the greatest accuracies. The ABA and semi-ITC approaches resulted in quite large RMSEs for the minority species, like silver fir, rowan, and other broadleaves. The accuracies for the total volume and majority species (Norway spruce) were in the same range for all three inventory approaches. Regarding the relative MDs, the smallest values were obtained by the semi-ITC approach, except for the silver fir which resulted in smaller systematic error by ABA. The ITC approach resulted in the largest MDs, except for the rowan where the ABA resulted in a larger MD. The Friedman test showed that the three inventory approaches had statistically significant different median of the differences between

the observed and predicted volumes per plot for all species classes, except for the larch. Furthermore, we performed post-hoc analysis for the Friedman's Test, which demonstrated that the pairs of the inventory approaches (ITC vs. semi-ITC, ITC vs. ABA, semi-ITC vs. ABA) were significantly different ($p \leq 0.05$) from each other for the total, silver fir, other broadleaves, and rowan volumes. For the pairs of ITC vs. semi-ITC and ITC vs. ABA, the differences between the larch and Norway spruce volumes were also statistically significant but not for the pair of semi-ITC vs. ABA ($p > 0.05$). Overall, the greatest balance between the RMSEs and MDs for all volumes was achieved by the semi-ITC approach.

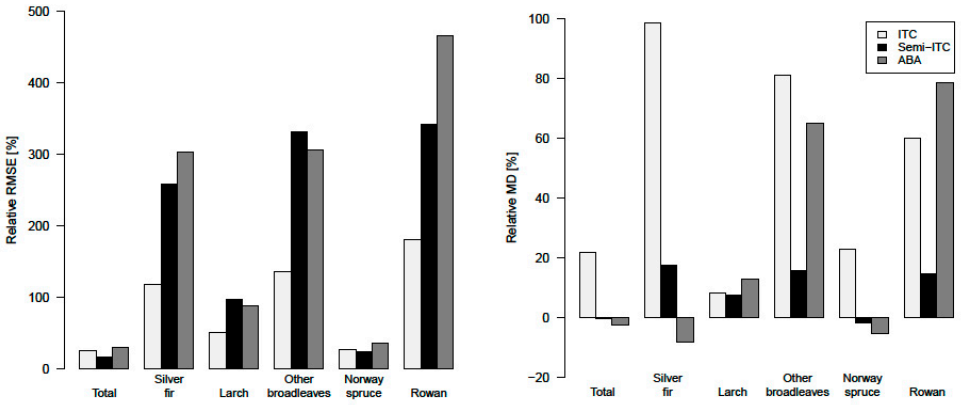

(**a**) (**b**)

Figure 6. (**a**) Relative RMSEs and (**b**) relative MDs of the total and five species classes' volumes obtained by the three inventory approaches: ITC, semi-ITC, and ABA.

4. Discussion

Many methods have been proposed for fusing ALS data with stereo or airborne multispectral or hyperspectral images in order to achieve a more accurate species recognition [23,56,57]. In this study, we showed that the fusion of ALS and hyperspectral data enabled the prediction of volumes at good accuracy levels. Moreover, hyperspectral variables were not only used for species classification, but they were also incorporated in the common ALS framework as they were selected as important variables for volume modeling. At the moment, hyperspectral data are the most powerful tool for species identification [6] and consequently they can improve the accuracy of the predicted biophysical attributes [31]. Forest inventories can be improved by the use of these combined data as they can increase the spatial detail, coverage, and accuracy of forest biophysical attributes. Thus, the combined data also helps forest managers to develop a broad and detailed database of forestry information to be coupled with a decision support system [58].

The accuracies of the species-specific volumes of the minority species obtained by the ITC approach were relatively higher compared to the semi-ITC and ABA approaches, but the accuracies of the more frequent species, i.e., the Norway spruce, were very much alike. The semi-ITC approach had slightly smaller RMSEs compared to the ABA, except for the larch and other broadleaves where the RMSEs were similar for both approaches. The largest systematic errors occurred in the ITC approach, caused by non-detected trees. Although all delineated crown segments were used for the volume modeling, a large underprediction due to omission errors of the ITC delineation still appeared in the ITC approach, mainly due to the forest structure [14]. The semi-ITC approach underpredicted all volumes, except for the Norway spruce volume, which was negligibly overpredicted. Even though, the semi-ITC is compensating the problem related to the omission error, it is not able to eliminate it completely. On average, the species-specific volumes were achieved with the smallest systematic errors with the semi-ITC approach. The ABA approach also underpredicted all volumes, but overpredicted the Norway spruce and silver fir volumes. The overprediction in ABA can be the result of species

presence of the nearest sample plots. As the volumes were predicted based on selected nearest neighbors, the *k*MSN method can predict small volumes for tree species classes that do not really occur in a sample plot. Since the *k*NN method was used, the predicted values will have a smaller range than the observed because of an averaging effect, which can caused the underprediction for the ABA and semi-ITC approach. We have to consider that the systematic error of the semi-ITC approach is the result of the combination of the delineation and *k*NN method's characteristics. In most cases, the systematic errors obtained with the semi-ITC approach were smaller compared to the ABA. A similar observation was also found in the study of Breidenbach et al. [37].

In the literature, there are no similar studies comparing the species-specific attributes obtained by the ITC and semi-ITC approaches, except for Ørka et al. [23]. In general, the main problem of the ITC methods is the quite large omission error, caused by undetected understory and suppressed trees [59], mostly resulting in underprediction [12] of biophysical attributes when aggregated at the plot level [60]. This systematic error can be considerably reduced with the semi-ITC approach as demonstrated in our study. Comparing the semi-ITC and ABA inventory approaches, Breidenbach et al. and Rahlf et al. [37,61] showed that the semi-ITC approach provided prediction accuracies that were higher or similar to the ABA, while in the study of Ørka et al. [23], the ABA performed better than the semi-ITC approach. Based on a trade-off between the goodness of fit and the systematic error, the compared total and species-specific results suggest that the semi-ITC approach in total outperformed the other approaches.

For the *k*NN methods, a sufficient number of sample plots is required for the ABA in order to have a sufficient number of neighbors available for the calculation of the distance matrix. For example, 300–500 sample plots are usually applied in operational forest inventories. On the other hand, many studies showed that nonparametric models were in line with parametric models also with a lower number of observations (e.g., 200 sample plots) [44,62]. However, we assumed that 94 subsample plots using three nearest neighbors were sufficient to achieve good results. The reason to not apply a parametric method was that the field-observed species-specific volumes contained many values close to zero or zeros due to the absence of minority tree species in the sample plots. Moreover, in complex stands with a wide variety of tree sizes and species, the nonparametric methods might be preferred to avoid implausible (e.g., negative) predictions and to obtain a reasonable extrapolation beyond the range of calibration data. In fact, among the nonparametric methods, the *k*NN, in particular the *k*MSN method, have been shown to be efficient in providing simultaneous multivariate predictions at a satisfactory accuracy level [17,37,54,63,64].

The volumes of the minor species were always predicted with smaller accuracies than the volumes of the majority species. The reason could be the small share of some tree species, especially broadleaves, and thus it was difficult to obtain accurate results. Moreover, a large share of only one species is the typical situation of the European forests. This phenomenon of small accuracy of the minor species is typical also for other studies [23,37], but despite the small RMSEs, the information on the existence of the minority species in stands can be valuable information, for example in tree-oriented silvicultural practices. Looking at the problem from an economical perspective, minority species are of secondary interest as the majority of the harvested volume is coming from Norway spruce and larch. Other species are mainly used for energy wood, as is the case of the broadleaves volume, or for very specific uses (e.g., high quality furniture). Minority species are important from the ecological perspective and thus, the use of ITC or semi-ITCs approaches is essential in this case as it is difficult to monitor such species with the ABA approach [23]. The ITC and semi-ITC approaches can also be used to detect and report the presence and spread of non-native invasive species that can irreversibly alter the productivity of the systems they invade. The semi-ITC approach is overall quite good for predicting volumes of the minority and majority species. However, in studies where the volume of majority species is of high interest, the ABA is recommended, as the field data collection (e.g., tree positions) is less demanding and less costly compared to what is required for the semi-ITC approach.

5. Conclusions

The ITC approach reached high accuracies for the volumes of minority species but in general large systematic errors and the ABA approach resulted in small systematic errors and relatively high accuracies for the dominant species. Considering the systematic errors and accuracies for the total and species-specific volumes, the semi-ITC approach achieved the greatest balance. Eventually, we found that the ITC approach is important for applications in which information on the minority species is needed, such as for biodiversity studies and silviculture treatments. The ABA is recommended where the dominant species are a key value for management purposes, due to a less demanding collection of field data, relatively high accuracy, and minor systematic error for the dominant species. Overall, the semi-ITC approach has the potential to become competitive with the ABA, as it achieved more accurate results with negligible systematic error for the dominant species. Additionally, when the minor species volumes are requested, the semi-ITC approach might be preferred over the ITC approach as it resulted in small differences with the field measured values. In addition, when the ITC or semi-ITC approaches are applied, they could always be supplemented with the results of the ABA as its computation time is fast. We also suggest selecting the approach according to the application's tolerance to systematic errors. To conclude, the results of the semi-ITC approach are promising in providing accurate total and species-specific volumes. Further studies are needed to examine the accuracies of such an approach for other biophysical attributes and its use at the operational level over larger areas.

Acknowledgments: This work was mainly supported by the Edmund Mach Foundation. The acquisition of the remote sensing data and the collection of part of the field data were funded by the European Commission (project Alpine Space 2-3-2-FR NEWFOR) within the European Territorial Cooperation program "Alpine Space." This work was also partially supported by the hyperBio project (project 244599), financed by the BIONÆR program of the Research Council of Norway and TerraTec AS, Norway.

Author Contributions: K.K. as the main author processed the remote sensing data, performed the experiments and data analysis, and wrote the manuscript. K.K., M.D., and H.O.Ø. conceived and designed the experiments. L.F. planned, collected, and prepared the field data. M.D. and H.O.Ø. supervised and advised all the research work that led to this paper. M.D., H.O.Ø, and E.N. reviewed the manuscript and conducted the English editing.

Conflicts of Interest: The authors declare no conflict of interest.

References

1. Scrinzi, G.; Galvagni, D.; Marzullo, L. *I Nuovi Modelli Dendrometrici Per La Stima Delle Masse Assestamentali in Provincia di Trento*; Provincia Autonoma di Trento-Servizio Foreste e Fauna: Trento, Italy, 2010.
2. Næsset, E.; Gobakken, T.; Holmgren, J.; Hyyppä, H.; Hyyppä, J.; Maltamo, M.; Nilsson, M.; Olsson, H.; Persson, Å.; Söderman, U. Laser scanning of forest resources: The nordic experience. *Scand. J. For. Res.* **2004**, *19*, 482–499. [CrossRef]
3. Tomppo, E. The Finish multi-Source National Forest Inventory-Small area estimation and map production. In *Forest Inventory: Methodology and Applications*; Managing Forest Ecosystems; Kangas, A., Maltamo, M., Eds.; Springer: Dordrecht, The Netherlands, 2006; Volume 10, pp. 195–224.
4. Eid, T.; Gobakken, T.; Næsset, E. Comparing stand inventories for large areas based on photo-Interpretation and laser scanning by means of cost-Plus-Loss analyses. *Scand. J. For. Res.* **2004**, *19*, 512–523. [CrossRef]
5. Holmgren, J.; Persson, Å. Identifying species of individual trees using airborne laser scanner. *Remote Sens. Environ.* **2004**, *90*, 415–423. [CrossRef]
6. Dalponte, M.; Bruzzone, L.; Gianelle, D. Tree species classification in the southern Alps based on the fusion of very high geometrical resolution multispectral/hyperspectral images and LiDAR data. *Remote Sens. Environ.* **2012**, *123*, 258–270. [CrossRef]
7. Baltsavias, E.P. Airborne laser scanning: Basic relations and formulas. *ISPRS J. Photogramm. Remote Sens.* **1999**, *54*, 199–214. [CrossRef]
8. Wehr, A.; Lohr, U. Airborne laser scanning–An introduction and overview. *ISPRS J. Photogramm. Remote Sens.* **1999**, *54*, 68–82. [CrossRef]
9. Næsset, E. Predicting forest stand characteristics with airborne scanning laser using a practical two-Stage procedure and field data. *Remote Sens. Environ.* **2002**, *80*, 88–99. [CrossRef]

10. Popescu, S.C.; Wynne, R.H.; Nelson, R.F. Estimating plot-Level tree heights with lidar: Local filtering with a canopy-Height based variable window size. *Comput. Electron. Agric.* **2002**, *37*, 71–95. [CrossRef]
11. Maltamo, M.; Suvanto, A.; Packalén, P. Comparison of basal area and stem frequency diameter distribution modelling using airborne laser scanner data and calibration estimation. *For. Ecol. Manag.* **2007**, *247*, 26–34. [CrossRef]
12. Peuhkurinen, J.; Mehtätalo, L.; Maltamo, M. Comparing individual tree detection and the area-based statistical approach for the retrieval of forest stand characteristics using airborne laser scanning in Scots pine stands. *Can. J. For. Res.* **2011**, *41*, 583–598. [CrossRef]
13. Vauhkonen, J.; Ene, L.; Gupta, S.; Heinzel, J.; Holmgren, J.; Pitkanen, J.; Solberg, S.; Wang, Y.; Weinacker, H.; Hauglin, K.M.; et al. Comparative testing of single-tree detection algorithms under different types of forest. *Forestry* **2011**, *85*, 27–40. [CrossRef]
14. Kandare, K.; Ørka, H.O.; Chan, J.C.; Dalponte, M. Effects of forest structure and airborne laser scanning point cloud density on 3D delineation of individual tree crowns. *Eur. J. Remote Sens.* **2016**, *49*, 337–359. [CrossRef]
15. Ørka, H.O.; Næsset, E.; Bollandsås, O.M. Classifying species of individual trees by intensity and structure features derived from airborne laser scanner data. *Remote Sens. Environ.* **2009**, *113*, 1163–1174. [CrossRef]
16. Packalén, P.; Maltamo, M. Predicting the plot volume by tree species using airborne laser scanning and aerial photographs. *For. Sci.* **2006**, *52*, 611–622.
17. Packalén, P.; Maltamo, M. The k-MSN method for the prediction of species-specific stand attributes using airborne laser scanning and aerial photographs. *Remote Sens. Environ.* **2007**, *109*, 328–341. [CrossRef]
18. Niska, H.; Skon, J.-P.; Packalen, P.; Tokola, T.; Maltamo, M.; Kolehmainen, M. Neural networks for the prediction of species-Specific plot volumes using airborne laser scanning and aerial photographs. *IEEE Trans. Geosci. Remote Sens.* **2010**, *48*, 1076–1085. [CrossRef]
19. Popescu, S.C.; Wynne, R.H.; Scrivani, J.A. Fusion of small-Footprint lidar and multispectral data to estimate plot-Level volume and biomass in deciduous and pine forests in Virginia, USA. *For. Sci.* **2004**, *50*, 551–565.
20. Tonolli, S.; Dalponte, M.; Neteler, M.; Rodeghiero, M.; Vescovo, L.; Gianelle, D. Fusion of airborne LiDAR and satellite multispectral data for the estimation of timber volume in the Southern Alps. *Remote Sens. Environ.* **2011**, *115*, 2486–2498. [CrossRef]
21. Dalponte, M.; Ørka, H.O.; Gobakken, T.; Gianelle, D.; Næsset, E. Tree species classification in boreal forests with hyperspectral data. *IEEE Trans. Geosci. Remote Sens.* **2013**, *51*, 2632–2645. [CrossRef]
22. Hill, R.A.; Thomson, A.G. Mapping woodland species composition and structure using airborne spectral and LiDAR data. *Int. J. Remote Sens.* **2005**, *26*, 3763–3779. [CrossRef]
23. Ørka, H.O.; Dalponte, M.; Gobakken, T.; Næsset, E.; Ene, L.T. Characterizing forest species composition using multiple remote sensing data sources and inventory approaches. *Scand. J. For. Res.* **2013**, *28*, 677–688. [CrossRef]
24. Sarrazin, M.J.D.; Van Aardt, J.A.N.; Asner, G.P.; Mcglinchy, J.; Messinger, D.W.; Wu, J. Fusing small-Footprint waveform LiDAR and hyper spectral data for canopy-Level species classification and herbaceous biomass modeling in savanna ecosystems. *Can. J. Remote Sens.* **2011**, *37*, 653–665. [CrossRef]
25. Ahokas, E.; Hyyppä, J.; Yu, X.; Liang, X.; Matikainen, L.; Karila, K.; Litkey, P.; Kukko, A.; Jaakkola, A.; Kaartinen, H.; et al. Towards automatic single-Sensor mapping by multispectral airborne laser scanning. *Int. Arch. Photogramm. Remote Sens. Spat. Inf. Sci.* **2016**, *41*, 155–162. [CrossRef]
26. Yu, X.; Hyyppä, J.; Litkey, P.; Kaartinen, H.; Vastaranta, M.; Holopainen, M. Single-Sensor Solution to Tree Species Classification Using Multispectral Airborne Laser Scanning. *Remote Sens.* **2017**, *9*, 108. [CrossRef]
27. Junttila, S.; Kaasalainen, S.; Vastaranta, M.; Hakala, T.; Nevalainen, O.; Holopainen, M. Investigating bi-temporal hyperspectral lidar measurements from declined trees-Experiences from laboratory test. *Remote Sens.* **2015**, *7*, 13863–13877. [CrossRef]
28. Clark, M.L.; Roberts, D.A.; Clark, D.B. Hyperspectral discrimination of tropical rain forest tree species at leaf to crown scales. *Remote Sens. Environ.* **2005**, *96*, 375–398. [CrossRef]
29. Ferreira, M.P.; Zortea, M.; Zanotta, D.C.; Shimabukuro, Y.E.; De Souza Filho, C.R. Mapping tree species in tropical seasonal semi-Deciduous forests with hyperspectral and multispectral data. *Remote Sens. Environ.* **2016**, *179*, 66–78. [CrossRef]
30. Asner, G.P.; Knapp, D.E.; Boardman, J.; Green, R.O.; Kennedy-Bowdoin, T.; Eastwood, M.; Martin, R.E.; Anderson, C.; Field, C.B. Carnegie Airborne Observatory-2: Increasing science data dimensionality via high-Fidelity multi-Sensor fusion. *Remote Sens. Environ.* **2012**, *124*, 454–465. [CrossRef]

31. Luo, S.; Wang, C.; Xi, X.; Pan, F.; Peng, D.; Zou, J.; Nie, S.; Qin, H. Fusion of airborne LiDAR data and hyperspectral imagery for aboveground and belowground forest biomass estimation. *Ecol. Indic.* **2017**, *73*, 378–387. [CrossRef]
32. Næsset, E. Estimating timber volume of forest stands using airborne laser scanner data. *Remote Sens. Environ.* **1997**, *61*, 246–253. [CrossRef]
33. Hyyppä, J.; Inkinen, M. Detecting and estimating attributes for single trees using laser scanner. *Photogramm. J. Finl.* **1999**, *16*, 27–42.
34. Wang, Y.; Hyyppä, J.; Liang, X.; Kaartinen, H.; Yu, X.; Lindberg, E.; Holmgren, J.; Qin, Y.; Mallet, C.; Ferraz, A.; et al. International benchmarking of the individual tree detection methods for modeling 3-D canopy structure for silviculture and forest ecology using airborne laser scanning. *IEEE Trans. Geosci. Remote Sens.* **2016**, *54*, 5011–5027. [CrossRef]
35. Hyyppä, J.; Kelle, O.; Lehikoinen, M.; Inkinen, M. A segmentation-Based method to retrieve stem volume estimates from 3-D tree height models produced by laser scanners. *IEEE Trans. Geosci. Remote Sens.* **2001**, *39*, 969–975. [CrossRef]
36. Persson, Å.; Holmgren, J.; Soderman, U. Detecting and measuring individual trees using an airborne laser scanner. *Photogramm. Eng. Remote Sens.* **2002**, *68*, 925–932.
37. Breidenbach, J.; Næsset, E.; Lien, V.; Gobakken, T.; Solberg, S. Prediction of species specific forest inventory attributes using a nonparametric semi-Individual tree crown approach based on fused airborne laser scanning and multispectral data. *Remote Sens. Environ.* **2010**, *114*, 911–924. [CrossRef]
38. Vauhkonen, J.; Seppänen, A.; Packalén, P.; Tokola, T. Improving species-Specific plot volume estimates based on airborne laser scanning and image data using alpha shape metrics and balanced field data. *Remote Sens. Environ.* **2012**, *124*, 534–541. [CrossRef]
39. Moeur, M.; Stage, A.R. Most similar neighbor: An improved sampling inference procedure for natural resource planning. *For. Sci.* **1995**, *41*, 337–359.
40. Ørka, H.O.; Gobakken, T.; Næsset, E.; Ene, L.; Lien, V. Simultaneously acquired airborne laser scanning and multispectral imagery for individual tree species identification. *Can. J. Remote Sens.* **2012**, *38*, 125–138. [CrossRef]
41. McRoberts, R.; Nelson, M.; Wendt, D. Stratified estimation of forest area using satellite imagery, inventory data, and the k-Nearest Neighbors technique. *Remote Sens. Environ.* **2002**, *82*, 457–468. [CrossRef]
42. Yu, B.; Ostland, I.M.; Gong, P.; Pu, R.L. Penalized discriminant analysis of in situ hyperspectral data for conifer species recognition. *IEEE Trans. Geosci. Remote Sens.* **1999**, *37*, 2569–2577. [CrossRef]
43. Falkowski, M.J.; Hudak, A.T.; Crookston, N.L.; Gessler, P.E.; Uebler, E.H.; Smith, A.M.S. Landscape-Scale parameterization of a tree-Level forest growth model: A k-Nearest neighbor imputation approach incorporating LiDAR data. *Can. J. For. Res.* **2010**, *40*, 184–199. [CrossRef]
44. Pippuri, I.; Maltamo, M.; Packalen, P.; Mäkitalo, J. Predicting species-Specific basal areas in urban forests using airborne laser scanning and existing stand register data. *Eur. J. For. Res.* **2013**, *132*, 999–1012. [CrossRef]
45. Räty, J.; Vauhkonen, J.; Maltamo, M.; Tokola, T. On the potential to predetermine dominant tree species based on sparse-Density airborne laser scanning data for improving subsequent predictions of species-Specific timber volumes. *For. Ecosyst.* **2016**, *3*, 1–17. [CrossRef]
46. R Development Core Team R: A Language and Environment for Statistical Computing. Available online: http://www.r-project.org (accessed on 22 September 2016).
47. Kaartinen, H.; Hyyppä, J.; Yu, X.; Vastaranta, M.; Hyyppä, H.; Kukko, A.; Holopainen, M.; Heipke, C.; Hirschmugl, M.; Morsdorf, F.; et al. An international comparison of individual tree detection and extraction using airborne laser scanning. *Remote Sens.* **2012**, *4*, 950–974. [CrossRef]
48. Karatzoglou, A.; Smola, A.; Hornik, K. The Kernlab Package. Available online: https://cran.r-project.org/web/packages/kernlab/index.html (accessed on 16 February 2017).
49. Dalponte, M.; Coomes, D.A. Tree-Centric mapping of forest carbon density from airborne laser scanning and hyperspectral data. *Methods Ecol. Evol.* **2016**, *7*, 1236–1245. [CrossRef]
50. Crookston, N.L.; Finley, A.O. YaImpute: An R Package for kNN Imputation. *J. Stat. Softw.* **2008**, *23*, 1–16. [CrossRef]
51. McRoberts, R.E.; Gobakken, T.; Næsset, E. Post-Stratified estimation of forest area and growing stock volume using lidar-Based stratifications. *Remote Sens. Environ.* **2012**, *125*, 157–166. [CrossRef]

52. Nilsson, M. Estimation of tree heights and stand volume using an airborne lidar system. *Remote Sens. Environ.* **1996**, *56*, 1–7. [CrossRef]
53. Mohammadi, J.; Joibary, S.S.; Yaghmaee, F.; Mahiny, A.S. Modelling forest stand volume and tree density using Landsat ETM+data. *Int. J. Remote Sens.* **2010**, *31*, 2959–2975. [CrossRef]
54. Mäkelä, H.; Pekkarinen, A. Estimation of forest stand volumes by Landsat TM imagery and stand-Level field-Inventory data. *For. Ecol. Manag.* **2004**, *196*, 245–255. [CrossRef]
55. Packalén, P.; Temesgen, H.; Maltamo, M. Variable selection strategies for nearest neighbor imputation methods used in remote sensing based forest inventory. *Can. J. Remote Sens.* **2012**, *38*, 557–569. [CrossRef]
56. Packalén, P.; Suvanto, A.; Maltamo, M. A two stage method to estimate species-specific growing stock. *Photogramm. Eng. Remote Sens.* **2009**, *75*, 1451–1460. [CrossRef]
57. Puliti, S.; Gobakken, T.; Ørka, H.O.; Næsset, E. Assessing 3D point clouds from aerial photographs for species-Specific forest inventories. *Scand. J. For. Res.* **2017**, *32*, 68–79. [CrossRef]
58. Wikström, P.; Edenius, L.; Elfving, B.; Eriksson, L.O.; LäMåS, T.; Sonesson, J.; ÖHMAN, K.; Wallerman, J.; Waller, C.; Klintebäck, F. The Heureka forestry decision support system: An overview. *Math. Comput. For. Nat. Sci.* **2011**, *3*, 87–95.
59. Latifi, H.; Fassnacht, F.E.; Müller, J.; Tharani, A.; Dech, S.; Heurich, M. Forest inventories by LiDAR data: A comparison of single tree segmentation and metric-Based methods for inventories of a heterogeneous temperate forest. *Int. J. Appl. Earth Obs. Geoinf.* **2015**, *42*, 162–174. [CrossRef]
60. Yu, X.; Hyyppä, J.; Holopainen, M.; Vastaranta, M. Comparison of area-Based and individual tree-Based methods for predicting plot-Level forest attributes. *Remote Sens.* **2010**, *2*, 1481–1495. [CrossRef]
61. Rahlf, J.; Breidenbach, J.; Solberg, S.; Astrup, R. Forest parameter prediction using an image-Based point cloud: A comparison of semi-ITC with ABA. *Forests* **2015**, *6*, 4059–4071. [CrossRef]
62. Bollandsås, O.M.; Maltamo, M.; Gobakken, T.; Næsset, E. Comparing parametric and non-Parametric modelling of diameter distributions on independent data using airborne laser scanning in a boreal conifer forest. *Forestry* **2013**, *86*, 493–501. [CrossRef]
63. Hudak, A.T.; Crookston, N.L.; Evans, J.S.; Hall, D.E.; Falkowski, M.J. Nearest neighbor imputation of species-Level, plot-Scale forest structure attributes from LiDAR data. *Remote Sens. Environ.* **2008**, *112*, 2232–2245. [CrossRef]
64. Penner, M.; Pitt, D.G.; Woods, M.E. Parametric vs. nonparametric LiDAR models for operational forest inventory in boreal Ontario. *Can. J. Remote Sens.* **2013**, *39*, 426–443.

Paper IV

Fusion of airborne laser scanning and hyperspectral data for assessing forest structural diversity indices

Kaja Kandare[1, 2]*, Samantha Riccadonna[3], Pietro Franceschi[3], Hans Ole Ørka[2], Michele Dalponte[3]

[1] FoxLab, Joint CNR-FEM Initiative, Fondazione Edmund Mach (FEM), Via E. Mach 1, 38010 San Michele all'Adige (TN), Italy.
[2] Faculty of Environmental Sciences and Natural Resource Management, Norwegian University of Life Sciences, P.O. Box 5003, N-1432 Ås, Norway; E-Mail: hans.ole.orka@nmbu.no
[3] Research and Innovation Centre, Fondazione Edmund Mach (FEM), Via E. Mach 1, 38010 San Michele all'Adige (TN), Italy; E-Mails: samantha.riccadonna@fmach.it, pietro.franceschi@fmach.it, michele.dalponte@fmach.it
* Author to whom correspondence should be addressed; E-Mail: kaja.kandare@fmach.it; Tel.: +386-41-292-200.

Abstract

In this paper, airborne laser scanning (ALS) and hyperspectral (HS) data, were explored for the prediction of structural diversity indices in a structurally complex temperate Alpine forest. We considered three types of measures of forest structural diversity that describes the variability of tree sizes (Gini coefficient of basal area and diameter differentiation index), the spatial distribution of tree positions (mean nearest neighbor distance and uniform angle index), and the tree species diversity (Shannon's index and species mingling index). We computed 1st and 2nd order image statistics on HS data to check if the encoded information may be useful for prediction purposes when considered neither alone or fused with ALS variables, such as height percentiles, 1st order statistics on ALS heights, and canopy densities. None of the structural diversity indices' models based on HS data passed the permutation test meaning that the predictions were not different from a random prediction. The uniform angle index was the only one that was not predictable with any remote sensing data combination. Fused data improved the prediction performances of the model built for the diameter differentiation index only, when obtained as a combination of ALS and 2nd order image statistics on HS data. The fusion of ALS and HS data did not improve any other indices' models, but produced accuracy levels comparable to the models built on ALS data alone. In our experiments, ALS data showed the better predictions for the majority of the structural diversity indices taken into account.

Introduction

Quantification of forest structural diversity has been integrated into forest management to support decision making (Lexerød and Eid, 2006; Valbuena et al., 2016), to provide a measure of biodiversity (McElhinny et al., 2005; Nagendra et al., 2013; Sarkar and Margules, 2002), to determine forest dynamics (Valbuena et al., 2013a) and successional stages (Spies and Franklin, 1991), and to analyze forest ecosystems (Sterba, 2008; Vihervaara et al., 2015). Different growth patterns are associated with species composition and tree sizes distribution in a forest stand and can affect species productivity (Ngo Bieng et al., 2013). Moreover, forest structural diversity is described by variability in spatial distribution of tree positions, mingling of different tree species, and distribution of tree dimensions (Aguirre et al., 2003; McElhinny et al., 2005; Pommerening, 2002). These characteristics can be quantified through different indices, such as uniform angle index, diameter differentiation index, species mingling index, Shannon's index, or Gini coefficient of basal area for listing a few (Falkowski et al., 2009; Hill and Thomson, 2005; Ozdemir et al., 2008). These indices enable the classification of stands into structural classes, the improvement of growth predictions, and the quantification of biodiversity and ecological indicators for ecosystem management (Clawges et al., 2008; Guo et al., 2017; Lo and Lin, 2013; van Ewijk et al., 2011).

The structure of mountain forests is continuously changing (Bachofen and Zingg, 2001; Dobbertin et al., 2001; Schulze et al., 2007). Remotely sensed data could be a tool for rapid assessment of highly dynamic and spatially complex landscapes, and over large geographic areas (Hill and Thomson, 2005; Nagendra et al., 2013). The use of remotely sensed data for obtaining forest information has become a widely used approach to describe forest structural diversity, in particular using airborne laser scanning (ALS) data (Hernández-Stefanoni et al., 2014; Listopad et al., 2015; Ozdemir and Donoghue, 2013; Vaglio Laurin et al., 2016), airborne hyperspectral images (Schäfer et al., 2016), and airborne or spaceborne multispectral images (Akbari and Kalbi, 2017; Beguet et al., 2014; Kayitakire et al., 2006; Meng et al., 2016; Ozdemir and Karnieli, 2011; Zhang and Franklin, 2002). Indeed, ALS technology can accurately measure three-dimensional vegetation structure and provide important forest attributes, such as forest gaps, volume, DBH (diameter at breast height) (Maltamo et al., 2014). Differently, optical data, such as multispectral and hyperspectral images were

demonstrated to be effective in providing tree species information (Dalponte et al., 2012; Ørka et al., 2012) and in improving the biophysical attributes predictions (Breidenbach et al., 2010). A synergistic use of hyperspectral and ALS data was demonstrated effective in many forestry applications (Luo et al., 2017; Tompalski et al., 2015; Tonolli et al., 2011; Torabzadeh et al., 2014; Yang et al., 2015), while the domain of forest diversity structural indices estimation has been less explored (Schäfer et al., 2016). Thus, a data analysis approach combining hyperspectral and ALS data could offer a novel and sophisticated solution for predicting various forest structural indices.

Here we explore and evaluate the performances of ALS and hyperspectral data, both alone and combined, to model and predict forest structural diversity indices in a temperate forest in the Alps. In particular, we consider three types of measures of forest structural diversity that describes (a) the variability of tree sizes (Gini coefficient of basal area and diameter differentiation index); (b) the spatial distribution of tree positions (mean nearest neighbor distance and uniform angle index); (c) tree species diversity (Simpson's index and species mingling index). The sub-objective was to explore if the first and second order image statistics, computed from the hyperspectral bands, carry information that may also be useful for prediction purposes.

Materials and methods

Study area description

The study area is an Alpine forest located in the Province of Trento (Italy), in the municipality of Pellizzano (46°17'22''N, 10°46'05''E), with altitude ranging between 850 m and 2700 m above sea level. The dominant tree species are Norway spruce (*Picea abies* (L.) Karst.), European larch (*Larix decidua* Mill.) and the remaining consists of other conifers (i.e. Silver fir (*Abies alba* Mill.), Swiss stone pine (*Pinus cembra* L.) and broadleaves (i.e. Rowan (*Sorbus aucuparia* (L.) Crantz), Silver birch (*Betula pendula* Roth), Common alder (*Alnus glutinosa* (L.) Gaertn.), Sycamore maple (*Acer pseudoplatanus* L.)), with a tree volume composition of 65%, 25% and 10%, respectively. The forest structure is complex, with patches of mixed and pure tree species composition (Dalponte and Coomes, 2016). Vegetation varies from meadows at higher altitude to very dense

forest in the lower altitudes. The area has been managed since 1950 with silvicultural plans carried out every 10 years. Selective logging is done with the help of cableway focusing on productive wood. The harvesting methods are different depending on the forest structure and species present.

Field data

Field data were collected in summer time in 2013 and 2015, comprising 47 circular plots of 15 m radius, which were randomly selected among the areas that represents diverse forest structure. For this study, we discarded nine plots due to species homogeneity or low number of trees (at least 5 trees per plot are needed to compute nearest neighbor-based indices; see section "Structural diversity indices"). The center of each plot was measured with a GPS/GLONASS system resulting in a position error of less than 1 m. For all trees the location was recorded in polar coordinates with respect to the center of the plot (azimuth and range). In addition, the tree species and the DBH along two orthogonal directions, were recorded. Tree heights were measured on two-thirds of the trees using a Vertex III hypsometer. In each plot, we considered only living trees, while no DBH thresholding was applied in the analyses. In all plots, 17 different tree species were recorded among which the dominants were Norway spruce (73%), followed by rowan (9%) and larch (8%). Statistic of the field trees are summarized in Table 1.

Table 1: Statistics of the field-observed trees per plot (mean values).

	DBH [cm]	**Basal area [m^2]**	**Height [m]**
Range	6.4 – 70.0	0.01 – 0.40	5.1 – 34.4
Mean	31.2	0.12	20.5
Standard deviation	17.6	0.10	9.0

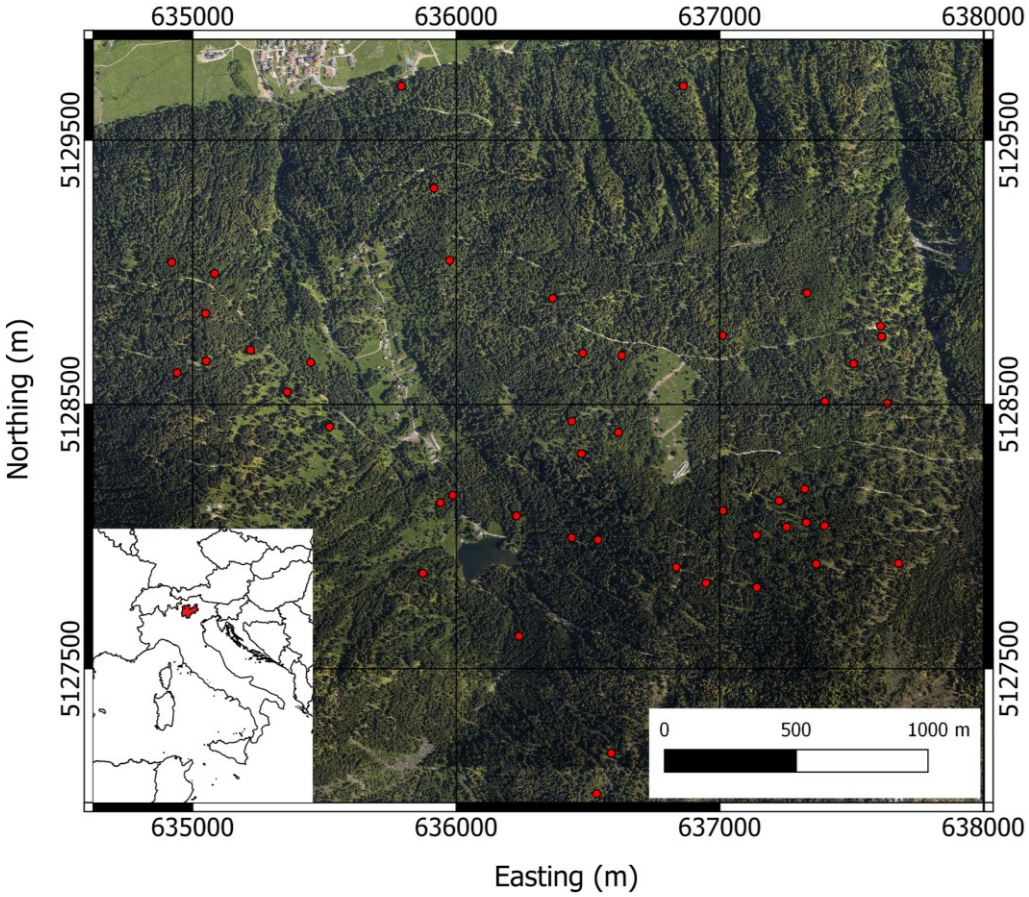

Figure 1: Location of the study area and the field plots (red dots in the image).

Remote sensing data description and pre-processing

ALS data were acquired from the 7th to the 9th September 2012 with a Riegl LMS-Q680i laser scanner. The system mounted on a Multi Mission Aircraft was optimized to measure canopy structure with a flying speed of about 51 m/s at an altitude of 660 m above ground level. The pulse repetition frequency was 400 kHz with a 60° field of view, and the overlap for each stripe was at least 30%. The result of the scanning was an ALS point cloud (X, Y, Z) with a mean point density of 48 pulses m^{-2} for the first returns. The scanner recorded up to four returns for each laser pulse. The company that acquired the data generated a digital terrain model (DTM) with TerraScan software, with a spatial resolution of 0.5 m. Furthermore, ALS point cloud was normalized to obtain a canopy height above ground by subtracting the DTM elevations from the Z values of the ALS pulses.

HS data were acquired on the 13th June 2013 with an AISA Eagle II sensor. Twenty-one images were

acquired and mosaicked in order to create a uniform image. The minimum overlap among the images was 20%. Each image was characterized by 65 spectral bands acquired between 400 nm and 990 nm, with a spatial resolution of 1 m. Non-forested areas were removed filtering out pixels with NDVI<0.5. To reduce minor differences in reflectance occurring between different images, the value of each pixel was normalized dividing it by the sum of the (original) values of the same pixel along all the bands (Yu et al., 1999).

Structural diversity indices

Six structural diversity indices were calculated for each sample plot on the basis of the field-observed tree species, tree coordinates (X, Y) and DBH:

- GiniBA: Gini coefficient of basal area (Valbuena et al., 2016, 2013b);
- MNND: mean nearest neighbour distance;
- DDI: diameter differentiation index (Equation 1) (Pommerening, 2002);
- UAI: uniform angle index (Equation 2) (Gangying et al., 2007),
- SHAN: Shannon-Wiener index (Shannon et al., 1950),
- SMI: Species Mingling Index (Equation 3) (Pommerening, 2002).

DDI, UAI, and SMI were computed for each tree based on four nearest neighbors and then averaged over each sample plot. We refer to the number of trees in the sample plot as n, while m is the number of nearest neighbors j around a reference tree i.

$$SMI = \frac{1}{nm}\sum_{i=1}^{n}\sum_{j=1}^{m} species_j \,, where\ v_j = \begin{cases} 1, if\ species_j = species_i \\ 0, if\ species_j \neq species_i \end{cases} and\ 0 \leq SMI \leq 1; \quad (1)$$

$$DDI = \frac{1}{nm}\sum_{i=1}^{n}\sum_{j=1}^{m} 1 - \frac{\min(DBH_i, DBH_j)}{\max(DBH_i, DBH_j)}\ and\ 0 \leq DDI \leq 1; \quad (2)$$

$$DDomI = \frac{1}{nm}\sum_{i=1}^{n}\sum_{j=1}^{m} d_{ij} \,, where\ v_j = \begin{cases} 1, if\ DBH_i < DBH_j \\ 0, if\ DBH_i \geq DBH_j \end{cases} and\ 0 \leq DDomI \leq 1; \quad (3)$$

$$UAI = \frac{1}{nm}\sum_{i=1}^{n}\sum_{j=1}^{m} v_{ij}\,, where\ v_{ij} = \begin{cases} 1, if\ angle_{ij} < \dfrac{360°}{m} \\ 0, if\ angle_{ij} > \dfrac{360°}{m} \end{cases} and\ 0 \le UAI \le 1; \quad (4)$$

The DDI refers to the diameter homogeneity in the close proximity: values close to 0 means that neighboring trees have an equal size, while values approaching 1 indicates high differentiation in the size of neighboring trees. UAI is reflecting the pattern of spatial distribution of neighboring trees around a reference, which could be regular ($UAI < 0.475$), random ($0.475 \le UAI < 0.517$), or clumped ($UAI \ge 0.517$) (Gangying et al., 2007). The SMI quantifies the degree of species mixing, where 0 means species segregation, and 1 correspond to a high degree of different tree species. The number of nearest neighbors was set to four, as in other studies this number was found appropriate (Aguirre et al., 2003; Gangying et al., 2007; Meng et al., 2016; Pommerening, 2002). Nearest neighbour-based indices could be affected by the edge effect as neighboring trees will fall out of the sample plots, thus an edge effect correction is very important to obtain unbiased results (Li and Zhang, 2007; Pommerening and Stoyan, 2006). Therefore, we accounted for an edge effect for all nearest neighbor-based indices applying a buffer zone of 10 m width from the plot center. Only trees within this buffer zone were used as reference trees.

Modeling and statistical analysis

In order to predict the six structural diversity indices, five different sets of predictor variables were used: i) ALS (67 variables described in Table 2), ii) HS 1st order statistics, which we will indicate as HS-1 (325 variables, see Table iii), HS 2nd order statistics, which we will label as HS-2 (1301 variables), and the "fusion" of iv) both ALS and HS-1, labelled as ALS+HS-1 (392 variables), and of v) both ALS and HS-2, referred to as ALS+HS-2 (1368 variables). The 2nd order statistics computed on the HS data are textural features originally developed for classification purposes (Haralick et al., 1973). We calculated them in R 3.3.2 ("R: The R Project for Statistical Computing," n.d.), using the *radiomics* package. The textural features were computed from gray-level co-occurrence matrices (GLCM), , as the average of 16 gray values in all directions (0°, 45°, 90° and 135°), using lag distances of 2 m (2 pixels) as this setting worked well based on empirical testing. The following features were computed: mean, variance, autocorrelation, cluster prominence, cluster shared, cluster

tendency, contrast, difference entropy, dissimilarity, energy, entropy, homogeneity, normalized inverse difference moment, normalized Inverse difference, inverse variance, maximum probability, sum average, sum entropy, and sum variance. For all ALS variables, except for the canopy volume variable, returns below 1 m were removed in order to avoid rocks and low vegetation.

Table 2: ALS variables calculated per sample plot unit.

Variable	Description
$\mathbf{CVol}$	Canopy volume calculated as the difference between first and last returns multiplied by the number of first returns
$\boldsymbol{H_{mean\_r}}$	Mean height of the *r-th* return
$\boldsymbol{H_{\max\_r}}$	Maximum height of the *r-th* return
$\boldsymbol{H_{sk\_r}}$	Skewness of height of the *r-th* return
$\boldsymbol{H_{ku\_r}}$	Kurtosis of height of the *r-th* return
$\boldsymbol{H_{cv\_r}}$	Coefficient of variation of height of the *r-th* return
$\boldsymbol{H_{q10\%-90\%\_r}}$	Quantile of height of the *r-th* return,
$\boldsymbol{CD_{1-8\_r}}$	Cumulative canopy densities calculated for the fixed bin of 5 m, starting from 1 m up to 41 m, for the r-th return

$*$ refers to first, intermediate, and last returns.

Table 3: HS-1 variables calculated per sample plot unit.

Variable	Description
$\boldsymbol{B_{mean\_nb}}$	Mean of the nb-th band
$\boldsymbol{B_{ske\_nb}}$	Skewness of the nb-th band
$\boldsymbol{B_{kur\_nb}}$	Kurtosis of the nb-th band
$\boldsymbol{B_{cv\_nb}}$	Coefficient of variation of the nb-th band
$\boldsymbol{B_{var\_nb}}$	Variance of the nb-th band

*nb refers to hyperspectral bands ranging from 1 to 65.

A partial least square (PLS) regression model, whose aim is to maximize the covariance between the predictor and response blocks was applied to a modified version of each predictor variable group listed above. Indeed, since the number of both ALS and HS variables is much larger than the number of samples, we filtered highly correlated variables selecting only one representative for highly correlated ones. Thus, in order to obtain a number of variables comparable between the ALS, HS-1, and HS-2 datasets, we set the correlation threshold to 0.99 and to 0.75 for HS-2, obtaining 46 variables respectively. In principle, filtering out highly correlated features is not required in PLS models but this step allows us to obtain a "balanced" fused dataset, having similar number of ALS and HS variables, thus, equally weighting the impact of both kind of variables on the PLS model. We performed all the analysis in R (R Development Core Team, 2008) using the *pls* package (Mevik and Wehrens, 2007). There data were centered and scaled before building the model.

The optimal number of latent variables was selected by minimizing the root mean square error in prediction based on a 5-fold cross-validation (CV).

A permutation test was applied to test each model reliability: the model was run 1,000 times on the same data used in the building phase with a randomly shuffled response variable . We evaluated how well the observed data correspond to the fitted model with the relative root mean square error (rRMSE) and the adjusted coefficient of determination (q^2) indicating the amount of variance explained by the model. The systematic error was measured with the relative mean differences (rMD) between the observed and predicted structural diversity indices.

Results

The goodness of fit was performed with the rRMSE and q^2, the rMD and the permutation test are for all combination of data shown in Tables 5-6. An example of a model that did not passed and did passed the permutation test is shown in Figure 2. As the structural diversity indices of each group performed quite similar, we choose one of each for plotting field-observed versus predicted values for all data combinations (Figure 3-5).

The models aiming at predicting indices describing the variability of tree sizes (GiniBA and DDI) always passed the permutation test, except for the one constructed only with HS features (Tables 5-6). The rRMSE and q^2 for the GiniBA were similar for the ALS and fused models. While for the DDI, the fused model ALS+HS-1 reached higher accuracy and variance explained for cca. 5% and 30%, respectively, compared to ALS and ALS+HS-2 models (Figure 3). The models of the indices describing the spatial distribution of the tree positions (MNND and UAI) were not doing better than random chance except for MNND in the case of ALS and ALS+HS-2 models, where accuracies were similar. Both models explained 21% and 17% of the variance, with rRMSE of 39.4% and 39.8%, respectively. Figure 4 shows the observed versus predicted MNND values for all model combinations. Tree species diversity indices (SHAN and SMI) did not passed the permutation test for the hyperspectral models (Table 5). In addition, the SHAN did not performed better than random chance also for the fused models. With the ALS model the SHAN explained 20% of the model's variability with 60.6% of rRMSE. SMI obtained similar results with ALS and ALS+HS-2 models with rRMSE of 53.4% and 54.2%, and q^2

of 38% and 34%, respectively. The fused model ALS+HS-1 reached lower accuracies (Figure 5). The rMD were negligibly small, with maximum value of 4.2% and minimum value of -3.0%, in all the abovementioned cases.

*Table 5: Accuracy measures in terms of rRMSE, q^2, rMD and permutation test (marked with * if passed) of structural diversity indices' models based on ALS, HS-1, and HS-2 data.*

	ALS			**HS-1**			**HS-2**		
	rRMSE [%]	**q2 [%]**	**rMD [%]**	**rRMSE [%]**	**q2 [%]**	**rMD [%]**	**rRMSE [%]**	**q2 [%]**	**rMD [%]**
GiniBA	22.9	52*	-1.6	37.9	-27	-0.9	35.3	-7	0.2
DDI	20.0	31*	-0.4	24.7	-2	0.1	25.6	-8	1.0
MNND	39.4	21*	-0.5	46.2	-9	-1.6	48.1	-18	1.8
UAI	6.70	-4	0.1	7.2	-20	-0.2	6.5	3	-0.1
SHAN	60.6	20*	0.5	63.4	14	-0.6	65.4	11	-0.7
SMI	53.4	38*	1.3	65.9	7	2.2	66.2	9	2.7

*Table 6: Accuracy measures in terms of RMSE, q^2, MD and permutation test (marked with * if passed) of structural diversity indices' models based on fused data, ALS + HS-1 and ALS + HS-2 data.*

	ALS + HS-1			**ALS + HS-2**		
	rRMSE [%]	**Q2 [%]**	**rMD [%]**	**rRMSE [%]**	**q2 [%]**	**rMD [%]**
GiniBA	24.6	44*	1.8	23.6	51*	-2.2
DDI	15.2	59*	0	19.8	27*	1.1
MNND	45.0	-1	-0.4	39.8	17*	4.2
UAI	6.7	-4	0.1	6.7	-4	0.1
SHAN	65.4	10	0.8	65.0	11	0.3
SMI	59.0	20*	-3.0	54.2	34*	1.3

a) UAI - ALS+HS1 data

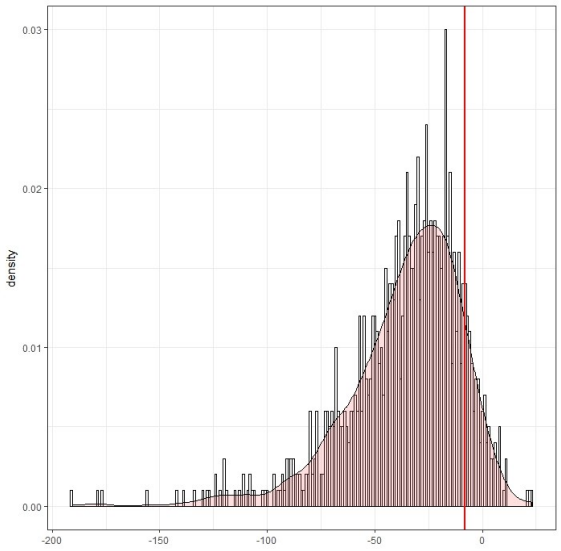

b) GiniBA - ALS data

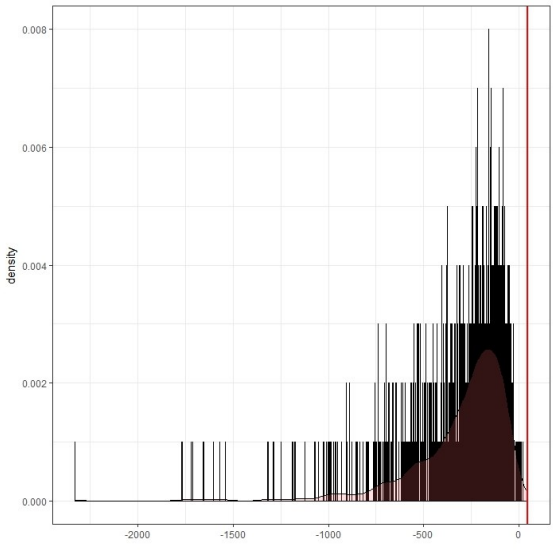

Figure 2: Examples of passing and not passing the permutation test, respectively: a) the model is not performing better than random chance; b) the model is performing better than random chance.

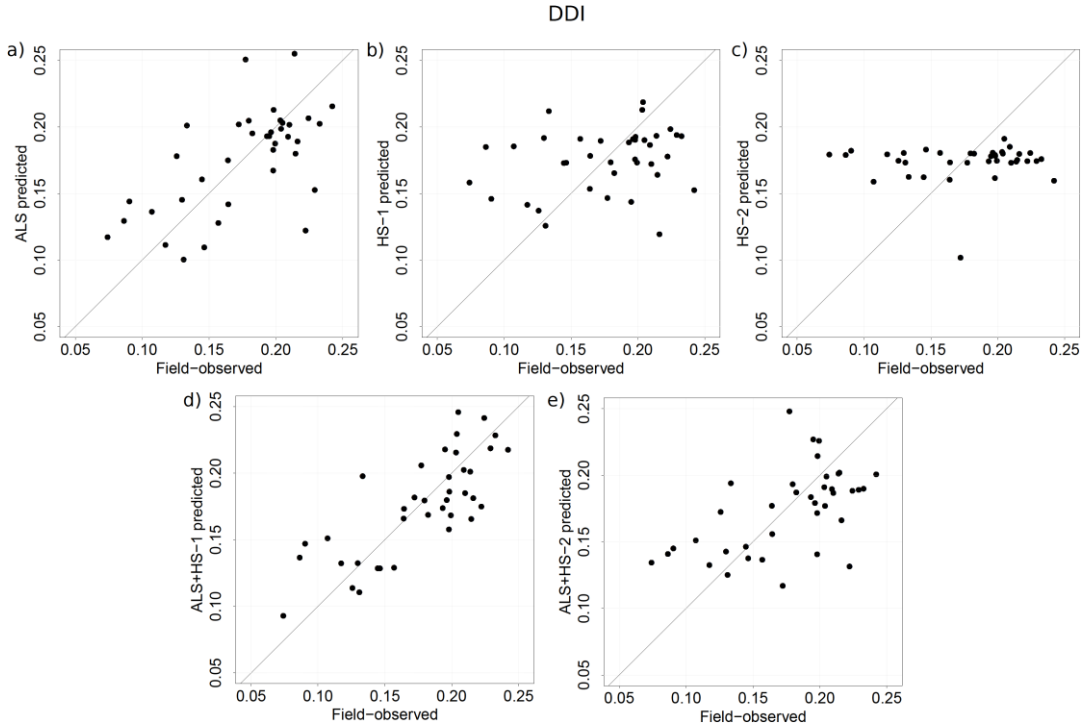

Figure 3: Field-observed versus predicted DDI obtained by a) ALS, b) HS-1, c) HS-2, and the fused data d) ALS+HS-1 and e) ALS+HS-2.

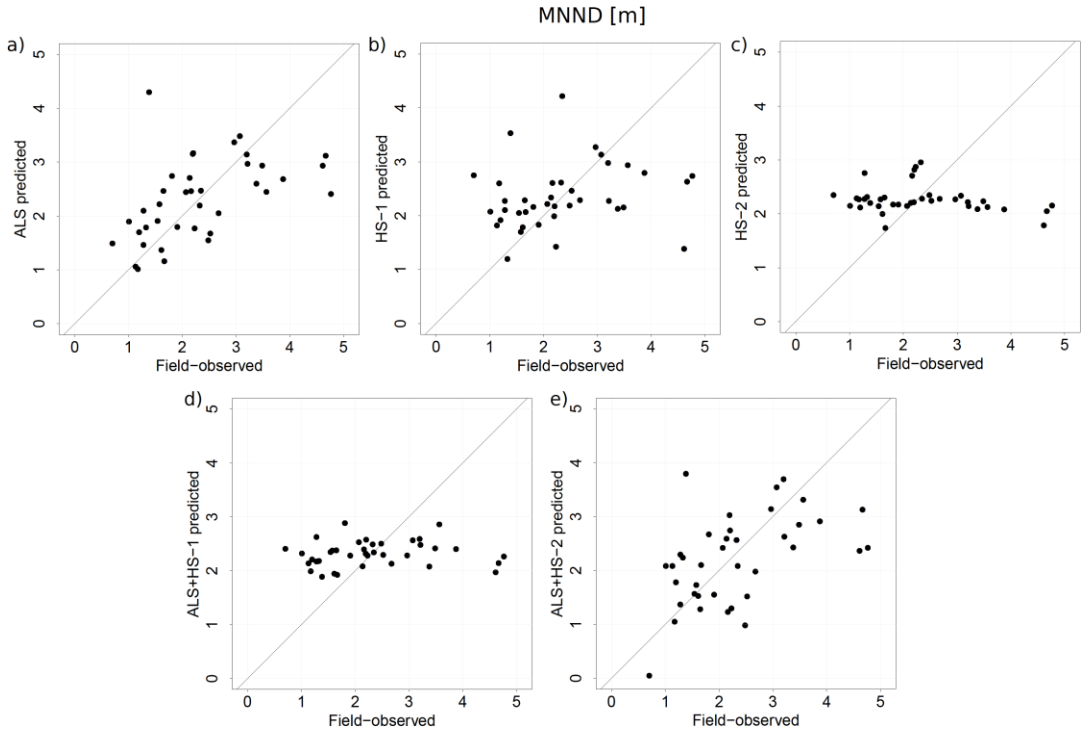

Figure 4: Field-observed versus predicted MNND obtained by a) ALS, b) HS-1, c) HS-2, and the fused data d) ALS+HS-1 and e) ALS+HS-2.

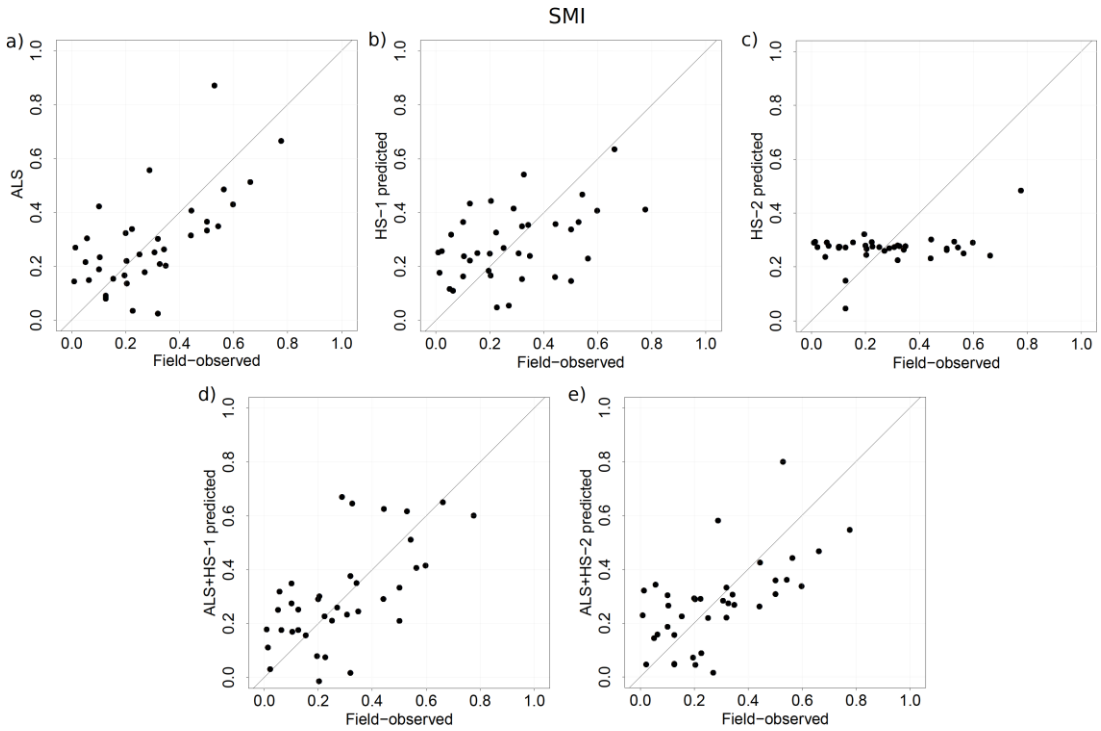

Figure 5: Field-observed versus predicted SMI obtained by a) ALS, b) HS-1, c) HS-2, and the fused data d) ALS+HS-1 and e) ALS+HS-2.

Discussion

Variability of tree size indices

GiniBA reached similar accuracies using ALS or fused data for modeling, thus the data fusion did not contribute to improve the accuracies. In the study of Valbuena et al. (2016), the ALS variables were shown as good predictors for such index and reached similar accuracies to our results. Thus, we could say that the ALS data alone could offer a good solution for reliable predictions of GiniBA. The DDI model reached the most accurate predictions fusing ALS and HS-1 data. This indicates that the fusion of ALS and HS data really contributed to an increase of prediction accuracy of the DDI compared to the model based only on ALS data. Ozdemir and Karnieli (2011) predicted GiniBA and DDI using 2nd order textural statistics computed on a multispectral image. The GiniBA resulted in similar accuracies respect to our results while the DDI in much lower accuracies. In a similar study of Meng et al. (2016), the predictive models of the GiniBA and DDI, based on the 1st and 2nd order statistics computed on multispectral images, resulted in similar accuracies compared to our results.

Spatial distribution of tree positions indices

The models predicting the UAI were found unreliable for any combination of ALS and hyperspectral data, while for the MNND both the ALS and ALS+HS-2 models passed the permutation test. Both models' accuracies were similar, thus the fusion of ALS and HS data did not contribute to any improvement. Moreover, for both models the variance explained was 21% or below. The predictability for such indices explaining distribution pattern of trees was found unreliable applied on satellite multispectral images (Meng et al., 2016; Ozdemir and Karnieli, 2011). We assume that such indices require larger sample plots to recognize and distinguish different pattern of tree positions, especially when the range of the index is small.

Tree species diversity indices

SHAN models did not pass the permutation test using any HS data or their combination with the ALS data. Surprisingly, the only model that passed the permutation test was based on ALS data. For the SMI, the only models that passed the test were based on ALS and ALS+HS-2, where the fusion of data did not improve the model's accuracy. However, both indices resulted in low accuracies. Other studies reported much higher accuracies for both indices using satellite multispectral images (Akbari and Kalbi, 2017; Meng et al., 2016). In other studies, ALS data, such as canopy cover, were found highly correlated with species indices (Listopad et al., 2015). Low accuracies for both indices could be correlated with the small sized sample plots (700 m^2), which were not able to capture the local variability of the landscape. Moreover, also other studies reported that the larger the sampling unit is, greater the spectral and ecological complexity is (Oldeland et al., 2010; Palmer et al., 2002; Rocchini et al., 2011). Thus, larger sample sizes improve the indices prediction accuracy (Marignani et al., 2007; Oldeland et al., 2010). It is worth noting that increasing the size of the plot increases also the field work cost, especially if tree positions needs to be measured.

Hyperspectral variables 1st and 2nd order image statistics

The 1st order statistics express the variability within the plot with one value (e.g. skewness, variance) calculated based on a group of pixel. In this study, HS variables calculated based on 1st order statistics were

not able to provide any useful information for modeling forest structural diversity indices. The 2nd order statistics derived from the grey level co-occurrence matrix are the most used textural variables in forestry remote sensing literature and were shown to provide good results for predicting forest structure based on satellite multispectral images for classification and modeling purposes (Beguet et al., 2014; Franklin, 2009; Gallardo-Cruz et al., 2012; Wunderle et al., 2007). From our preliminary investigation, it seems that none of the HS variables were useful variables in distinguishing spatial pattern. This could be attributed to how the data were pre-processed or the specificity of the study area, and thus it should be further explored.

Conclusion

All structural diversity indices could be predicted with ALS data, except for the UAI. Models based on 1st and 2nd order image statistics computed on the HS bands did not resulted in high accuracies and in many cases they did not pass the permutation test. The fusion of ALS and HS-1 variables reached high accuracies for DDI. Other indices did not benefit from the fused data as they obtained similar accuracies using only ALS variables. In the future, more studies should be conducted on the fused ALS and HS data, in order to explore better their capabilities, especially for predicting spatial distribution of trees and species diversity using larger sample plots. Moreover more analyses should be done on the HS data exploring other pre-processing options.

Acknowledgements

This work is a part of Kaja Kandare PhD thesis and was mainly supported by the Edmund Mach Foundation in Italy. The acquisition of the remote sensing data and the collection of part of the field data were funded by the European Commission (project Alpine Space 2-3-2-FR NEWFOR) within the European Territorial Cooperation program “Alpine Space.” This work was also supported by the hyperBio project (project 244599), financed by the BIONÆR program of the Research Council of Norway and TerraTec AS, Norway. The authors would like to thank Dr. Lorenzo Frizzera for his help in the field data collection.

References

Aguirre, O., Hui, G., von Gadow, K., Jiménez, J., 2003. An analysis of spatial forest structure using neighbourhood-based variables. For. Ecol. Manage. 183, 137–145.

Akbari, H., Kalbi, S., 2017. Determining Pleiades satellite data capability for tree diversity modeling. iForest - Biogeosciences and Forestry 10, 348–352.

Bachofen, H., Zingg, A., 2001. Effectiveness of structure improvement thinning on stand structure in subalpine Norway spruce (Picea abies (L.) Karst.) stands. For. Ecol. Manage. 145, 137–149.

Beguet, B., Guyon, D., Boukir, S., Chehata, N., 2014. Automated retrieval of forest structure variables based on multi-scale texture analysis of VHR satellite imagery. ISPRS J. Photogramm. Remote Sens. 96, 164–178.

Breidenbach, J., Næsset, E., Lien, V., Gobakken, T., Solberg, S., 2010. Prediction of species specific forest inventory attributes using a nonparametric semi-individual tree crown approach based on fused airborne laser scanning and multispectral data. Remote Sens. Environ. 114, 911–924.

Clawges, R., Vierling, K., Vierling, L., Rowell, E., 2008. The use of airborne lidar to assess avian species diversity, density, and occurrence in a pine/aspen forest. Remote Sens. Environ. 112, 2064–2073.

Dalponte, M., Bruzzone, L., Gianelle, D., 2012. Tree species classification in the Southern Alps based on the fusion of very high geometrical resolution multispectral/hyperspectral images and LiDAR data. Remote Sens. Environ. 123, 258–270.

Dobbertin, M., Baltensweiler, A., Rigling, D., 2001. Tree mortality in an unmanaged mountain pine (Pinus mugo var. uncinata) stand in the Swiss National Park impacted by root rot fungi. For. Ecol. Manage. 145, 79–89.

Falkowski, M.J., Evans, J.S., Martinuzzi, S., Gessler, P.E., Hudak, A.T., 2009. Characterizing forest succession with lidar data: An evaluation for the Inland Northwest, USA. Remote Sens. Environ. 113, 946–956.

Franklin, S.E., 2009. Remote sensing for biodiversity and wildlife management: synthesis and applications. McGraw-Hill Professional.

Gallardo-Cruz, J.A., Meave, J.A., González, E.J., Lebrija-Trejos, E.E., Romero-Romero, M.A., Pérez-García, E.A., Gallardo-Cruz, R., Hernández-Stefanoni, J.L., Martorell, C., 2012. Predicting tropical dry forest successional attributes from space: is the key hidden in image texture? PLoS One 7, e30506.

Gangying, H., Li, L., Zhonghua, Z., Puxing, D., 2007. Comparison of methods in analysis of the tree spatial distribution pattern. Acta Ecol. Sin. 27, 4717–4728.

Guo, X., Coops, N.C., Tompalski, P., Nielsen, S.E., Bater, C.W., John Stadt, J., 2017. Regional mapping of vegetation structure for biodiversity monitoring using airborne lidar data. Ecol. Inform. 38, 50–61.

Haralick, R.M., Shanmugam, K., Dinstein, I. 'hak, 1973. Textural Features for Image Classification. IEEE Trans. Syst. Man Cybern. SMC-3, 610–621.

Hernández-Stefanoni, J., Dupuy, J., Johnson, K., Birdsey, R., Tun-Dzul, F., Peduzzi, A., Caamal-Sosa, J., Sánchez-Santos, G., López-Merlín, D., 2014. Improving Species Diversity and Biomass Estimates of Tropical Dry Forests Using Airborne LiDAR. Remote Sensing 6, 4741–4763.

Hill, R.A., Thomson, A.G., 2005. Mapping woodland species composition and structure using airborne spectral and LiDAR data. Int. J. Remote Sens. 26, 3763–3779.

Kayitakire, F., Hamel, C., Defourny, P., 2006. Retrieving forest structure variables based on image texture analysis and IKONOS-2 imagery. Remote Sens. Environ. 102, 390–401.

Lexerød, N.L., Eid, T., 2006. An evaluation of different diameter diversity indices based on criteria related to forest management planning. For. Ecol. Manage. 222, 17–28.

Li, F., Zhang, L., 2007. Comparison of point pattern analysis methods for classifying the spatial distributions of spruce-fir stands in the north-east USA. Forestry 80, 337–349.

Listopad, C.M.C.S., Masters, R.E., Drake, J., Weishampel, J., Branquinho, C., 2015. Structural diversity indices based on airborne LiDAR as ecological indicators for managing highly dynamic landscapes. Ecol. Indic. 57, 268–279.

Lo, C.-S., Lin, C., 2013. Growth-Competition-Based Stem Diameter and Volume Modeling for Tree-Level Forest Inventory Using Airborne LiDAR Data. IEEE Trans. Geosci. Remote Sens. 51, 2216–2226.

Luo, S., Wang, C., Xi, X., Pan, F., Peng, D., Zou, J., Nie, S., Qin, H., 2017. Fusion of airborne LiDAR data and hyperspectral imagery for aboveground and belowground forest biomass estimation. Ecol. Indic. 73, 378–387.

Maltamo, M., Næsset, E., Vauhkonen, J., 2014. Forestry Applications of Airborne Laser Scanning: Concepts and Case Studies. Springer Science & Business Media.

Marignani, M., Del Vico, E., Maccherini, S., 2007. Spatial scale and sampling size affect the concordance between remotely sensed information and plant community discrimination in restoration monitoring. Biodivers. Conserv. 16, 3851–3861.

Bollandsås, O.M., Næsset, E., 2007. Estimating percentile-based diameter distributions in uneven-sized Norway spruce stands using airborne laser scanner data. Scand. J. For. Res. 22, 33–47.

McElhinny, C., Gibbons, P., Brack, C., Bauhus, J., 2005. Forest and woodland stand structural complexity: Its definition and measurement. For. Ecol. Manage. 218, 1–24.

Meng, J., Li, S., Wang, W., Liu, Q., Xie, S., Ma, W., 2016. Estimation of Forest Structural Diversity Using the Spectral and Textural Information Derived from SPOT-5 Satellite Images. Remote Sensing, Managing Forests as Complex Adaptive Systems: Building Resilience to the Challenge of Global Change 8, 125.

Mevik, B.-H., Wehrens, R., 2007. ThepIsPackage: Principal Component and Partial Least Squares Regression inR. J. Stat. Softw. 18. doi:10.18637/jss.v018.i02

Nagendra, H., Lucas, R., Honrado, J.P., Jongman, R.H.G., Tarantino, C., Adamo, M., Mairota, P., 2013. Remote sensing for conservation monitoring: Assessing protected areas, habitat extent, habitat condition, species diversity, and threats. Ecol. Indic. 33, 45–59.

Ngo Bieng, M.A., Bieng, M.A.N., Perot, T., de Coligny, F., Goreaud, F., 2013. Spatial pattern of trees influences species productivity in a mature oak–pine mixed forest. Eur. J. For. Res. 132, 841–850.

Oldeland, J., Wesuls, D., Rocchini, D., Schmidt, M., Jürgens, N., 2010. Does using species abundance data improve estimates of species diversity from remotely sensed spectral heterogeneity? Ecol. Indic. 10, 390–396.

Ørka, H.O., Gobakken, T., Næsset, E., Ene, L., Lien, V., 2012. Simultaneously acquired airborne laser scanning and multispectral imagery for individual tree species identification. Can. J. Remote Sens. 38, 125–138.

Ozdemir, I., Donoghue, D.N.M., 2013. Modelling tree size diversity from airborne laser scanning using canopy height models with image texture measures. For. Ecol. Manage. 295, 28–37.

Ozdemir, I., Karnieli, A., 2011. Predicting forest structural parameters using the image texture derived from WorldView-2 multispectral imagery in a dryland forest, Israel. Int. J. Appl. Earth Obs. Geoinf. 13, 701–710.

Ozdemir, I., Norton, D.A., Ozkan, U.Y., Mert, A., Senturk, O., 2008. Estimation of Tree Size Diversity Using Object Oriented Texture Analysis and Aster Imagery. Sensors 8, 4709–4724.

Palmer, M.W., Earls, P.G., Hoagland, B.W., White, P.S., Wohlgemuth, T., 2002. Quantitative tools for perfecting species lists. Environmetrics 13, 121–137.

Pommerening, A., 2002. Approaches to quantifying forest structures. Forestry 75, 305–324.

Pommerening, A., Stoyan, D., 2006. Edge-correction needs in estimating indices of spatial forest structure. Can. J. For. Res. 36, 1723–1739.

Rocchini, D., McGlinn, D., Ricotta, C., Neteler, M., Wohlgemuth, T., 2011. Landscape complexity and spatial scale influence the relationship between remotely sensed spectral diversity and survey-based plant species richness. J. Veg. Sci. 22, 688–698.

R Development Core Team, 2008. R: A language and environment for statistical computing [WWW Document]. R Found. Stat. Comput. Vienna, Austria. ISBN 3-900051-07-0. URL http://www.r-project.org (accessed 9.22.16).

R: The R Project for Statistical Computing [WWW Document], n.d. URL https://www.R-project.org/ (accessed 5.8.17).

Sarkar, S., Margules, C., 2002. Operationalizing biodiversity for conservation planning. J. Biosci. 27, 299–308.

Schäfer, E., Heiskanen, J., Heikinheimo, V., Pellikka, P., 2016. Mapping tree species diversity of a tropical montane forest by unsupervised clustering of airborne imaging spectroscopy data. Ecol. Indic. 64, 49–58.

Schulze, E.-D., Mischì, G., Asche, G., Börner, A., 2007. Land-use history and succession of Larix decidua in the Southern Alps of Italy–An essay based on a cultural history study of Roswitha Asche. Flora - Morphology, Distribution, Functional Ecology of Plants 202, 705–713.

Shannon, C.E., Weaver, W., Wiener, N., 1950. The Mathematical Theory of Communication. Phys. Today 3, 31–32.

Spies, T.A., Franklin, J.F., 1991. The structure of natural young,mature, and old-growth douglas-fir forests in Oregon and Washington, USDA Forest Service General Technical Report PNW-GTR-285. Portland, OR, US.

Sterba, H., 2008. Diversity indices based on angle count sampling and their interrelationships when used in forest inventories. Forestry 81, 587–597.

Tompalski, P., Coops, N.C., White, J.C., Wulder, M.A., Pickell, P.D., 2015. Estimating Forest Site Productivity Using Airborne Laser Scanning Data and Landsat Time Series. Can. J. Remote Sens. 41, 232–245.

Tonolli, S., Dalponte, M., Neteler, M., Rodeghiero, M., Vescovo, L., Gianelle, D., 2011. Fusion of airborne LiDAR and satellite multispectral data for the estimation of timber volume in the Southern Alps. Remote Sens. Environ. 115, 2486–2498.

Torabzadeh, H., Morsdorf, F., Schaepman, M.E., 2014. Fusion of imaging spectroscopy and airborne laser scanning data for characterization of forest ecosystems – A review. ISPRS J. Photogramm. Remote Sens. 97, 25–35.

Vaglio Laurin, G., Laurin, G.V., Puletti, N., Chen, Q., Corona, P., Papale, D., Valentini, R., 2016. Above ground biomass and tree species richness estimation with airborne lidar in tropical Ghana forests. Int. J. Appl. Earth Obs. Geoinf. 52, 371–379.

Valbuena, R., Eerikäinen, K., Packalen, P., Maltamo, M., 2016. Gini coefficient predictions from airborne lidar remote sensing display the effect of management intensity on forest structure. Ecol. Indic. 60, 574–585.

Valbuena, R., Maltamo, M., Martín-Fernández, S., Packalen, P., Pascual, C., Nabuurs, G.-J., 2013a. Patterns of covariance between airborne laser scanning metrics and Lorenz curve descriptors of tree size inequality. Can. J. Remote Sens. 39, S18–S31.

Valbuena, R., Packalen, P., Mehtätalo, L., García-Abril, A., Maltamo, M., 2013b. Characterizing forest structural types and shelterwood dynamics from Lorenz-based indicators predicted by airborne laser scanning. Can. J. For. Res. 43, 1063–1074.

van Ewijk, K.Y., Treitz, P.M., Scott, N.A., 2011. Characterizing Forest Succession in Central Ontario using Lidar-derived Indices. Photogrammetric Engineering & Remote Sensing 77, 261–269.

Vihervaara, P., Mononen, L., Auvinen, A.-P., Virkkala, R., Lü, Y., Pippuri, I., Packalen, P., Valbuena, R., Valkama, J., 2015. How to integrate remotely sensed data and biodiversity for ecosystem assessments at landscape scale. Landsc. Ecol. 30, 501–516.

Wunderle, A.L., Franklin, S.E., Guo, X.G., 2007. Regenerating boreal forest structure estimation using SPOT-5 pan-sharpened imagery. Int. J. Remote Sens. 28, 4351–4364.

Yang, J., Jones, T., Caspersen, J., He, Y., 2015. Object-Based Canopy Gap Segmentation and Classification: Quantifying the Pros and Cons of Integrating Optical and LiDAR Data. Remote Sensing 7, 15917–15932.

Yu, B., Ostland, M., Gong, P., Pu, R., 1999. Penalized discriminant analysis of in situ hyperspectral data for conifer species recognition. IEEE Trans. Geosci. Remote Sens. 37, 2569–2577.

Zhang, C., Franklin, S.E., 2002. Forest structure classification using airborne multispectral image texture and kriging analysis, in: IEEE International Geoscience and Remote Sensing Symposium. doi:10.1109/igarss.2002.1026598